



TECHNISCHE
UNIVERSITÄT
WIEN

DISSERTATION

COMBINED MODELS OF PULSE WAVE AND ECG ANALYSIS FOR RISK PREDICTION IN END-STAGE RENAL DISEASE PATIENTS

ausgeführt zum Zwecke der Erlangung des akademischen Grades eines
Doktors der technischen Wissenschaften unter der Leitung von

Ao.Univ.Prof.i.R. Dipl.-Ing. Dr.techn. Felix Breitenecker

E101 - Institut für Analysis und Scientific Computing

eingereicht an der Technischen Universität Wien
bei der Fakultät für Mathematik und Geoinformation

von

Dipl.-Ing. Stefan Hagmair, BSc

0825976

Flachgasse. 24/33

1150 Wien

Ort, Datum

Unterschrift

Abstract

Cardiovascular diseases are the main cause of death worldwide. Noninvasively measured biomedical recordings such as electrocardiography and pulse wave yield important information about the status of the cardiovascular system. As a result, clinical practice guidelines recommend the evaluation of several parameters of those signals. Especially individuals receiving hemodialysis are in the highest risk group for the evaluation and management of cardiovascular disease according to established guidelines. Given the high morbidity and mortality of individuals with end-stage renal disease (ESRD), there is need for improved risk prediction in dialysis patients.

Therefore, the purpose of this work was to investigate, improve and further develop risk models including parameters describing the cardiovascular system. Particularly, simultaneously recorded 12-lead electrocardiogram (ECG) and ambulatory blood pressure recordings for 24 hours were analyzed. Throughout this thesis, all data was from the ISAR (rISk strATification in end-stage Renal disease) study, which is a prospective, longitudinal, observational cohort study.

First, an algorithm for automatic obtained RR-intervals of the multi-lead ECG was developed in order to quantify heart rate variability (HRV). The results demonstrate good agreement between the time series gained by the algorithm and the manual reviewed reference time series. Additionally, standard time- and frequency domain HRV parameters were calculated in the subgroup of patients without atrial fibrillation. The HRV indicators show high similarity with indices obtained from the reference series. Exemplarily, the limits of agreement of the index root mean square of successive differences (RMSSD) between both time series range from -2.7 ms to 2.2 ms with a mean difference of 0.22 ms.

Together with standard HRV parameters, nonlinear entropy measures were used for risk assessment by means of Cox regression analysis. With recently published parameter sets, fuzzy entropy and corrected approximate entropy predict mortality significantly and remained significant after adjustment for common risk factors. Exemplarily, after adjustment, one absolute unit increase of fuzzy entropy results in a hazard ratio of 0.58 with a 95% confidence interval ranging from 0.37 to 0.92. However, only a small time interval during the night was used to ensure standardized condition of ECG data.

Finally, 24 hour parameters from both biosignals were included in a multivariable survival tree model. Synchronous measurements of 234 ISAR study patients were available. Beside comorbid conditions, tree-based survival analysis clearly indicated that decreased HRV triangular index ($HRVTI < 18$ ms) and increased augmented pressure ($AP \geq 10$ mmHg) a parameter gained from pulse wave analysis (PWA) are associated with all-cause mortality in the hemodialysis cohort.

Overall, the synchronous measurement and assessment of both recordings, i.e., ambulatory blood pressure and multi-lead ECG, with their derived PWA and HRV parameters could serve as important tools in event prediction of this very high-risk patient population. These results warrant further investigations.

Kurzfassung

Herz-Kreislauf-Erkrankungen stellen weltweit die Haupttodesursache dar. Nichtinvasiv gemessene biomedizinische Aufzeichnungen, wie Elektrokardiographie und Pulswelle, liefern wichtige Informationen über den Zustand des Herz-Kreislauf-Systems. Daher empfehlen ärztliche Behandlungsleitlinien die Auswertung mehrerer Parameter dieser Biosignale. Personen die sich einer Hämodialyse unterziehen, gehören zur Hochrisikogruppe für Erkrankungen, die das Herz oder die Blutgefäße betreffen und erfordern daher eine Bewertung und Behandlung nach festgelegten Richtlinien. Angesichts der hohen Morbidität und Mortalität von Patienten mit terminaler Niereninsuffizienz ist außerdem eine verbesserte Risikostratifizierung für Dialysepatienten vonnöten.

Daher ist das Ziel dieser Arbeit, bestehende kardiovaskuläre Risikomodelle zu untersuchen, zu verbessern und mit Parameter die das Herz-Kreislauf-System beschreiben, weiterzuentwickeln. Die verwendete Biosignale sind einerseits ein 12-Kanal-Elektrokardiogramm (EKG) und desweiteren eine ambulante Blutdruckmessung - jeweils mit einer Aufzeichnungsdauer von 24 Stunden. Alle verwendete Daten dieser Arbeit stammen aus der ISAR (rISK strAtification in end-stage Renal disease) Dialyse-Studie, einer prospektiven Beobachtungskohortenstudie.

Zunächst wurde ein Algorithmus entwickelt, welcher automatisch RR-Intervalle vom Mehrkanal-EKG ableitet, um damit die Herzratenvariabilität (HRV) quantifizieren zu können. Die Ergebnisse zeigen eine gute Übereinstimmung zwischen den durch den Algorithmus gewonnenen Zeitreihen und den manuell von Medizinern überprüften Referenzzeitreihen. Zusätzlich wurden HRV-Parameter im Zeit- sowie Frequenzbereich berechnet, nachdem Patienten mit Vorhofflimmern ausgeschlossen wurden. Die HRV-Indikatoren weisen eine hohe Ähnlichkeit mit den aus den Referenzreihen erhaltenen Parametern auf. Beispielsweise zeigt der statistische Zeitparameter RMSSD eine mit-

tlere Differenz von 0.22 ms zwischen beiden Zeitreihen bei einer Schwankungsbreite von -2.7 ms bis 2.2 ms.

Zur Risikobewertung mittels Cox-Regressionsanalyse wurden, neben Standard-HRV-Parametern, nichtlineare Entropiemaße verwendet. Zwei Entropiemaße (Fuzzy entropy und Corrected approximate entropy) waren signifikante Risikoprädiktoren für Mortalität und blieben signifikant nach multivariabler Adjustierung für bekannte Risikofaktoren. Die Ergebnisse zeigen beispielsweise, dass bei einer Erhöhung des Parameters Fuzzy entropy (um 1), das Sterberisiko um 42% gesenkt wird (Hazard Ratio 0.58; 95%-Konfidenzintervall [0.37,0.92]). Es wurde allerdings nur ein kleines Zeitintervall während der Nacht der 24-Stunden EKG Aufzeichnung verwendet, um einheitliche Verhältnisse sicherzustellen.

Schließlich wurde ein multivariablen Überlebenszeitmodell, basierend auf Entscheidungsbäumen, mithilfe der 24-Stunden-Parameter beider Biosignale erstellt. Hierfür lagen synchrone Messungen von 234 Patienten der ISAR-Studie vor. Neben den komorbiden Zuständen zeigte die baumbasierte Überlebenszeitanalyse eindeutig, dass eine reduzierte Herzratenvariabilität (triangular index; HRVTI < 18 ms) und ein erhöhter Reflexionsparameter der Pulswellenanalyse (augmented pressure; $AP \geq 10$ mmHg) mit der Gesamtmortalität in der Hämodialysekohorte assoziiert sind.

Zusammenfassend kann festgehalten werden, dass die synchrone Messung und Auswertung, sowohl des ambulanten Blutdrucks, als auch des Mehrkanal-EKGs als wichtiges Instrument in der Überlebenszeitanalyse dienen kann. Die bisherigen Ergebnisse der Pulswellen- und EKG-Parameter rechtfertigen weitere Untersuchungen.

Contents

1	Introduction	1
1.1	Background and motivation	1
1.2	Aim of the thesis	2
1.3	Outline	3
1.4	End-stage renal disease	3
1.4.1	History	3
1.4.2	Definition	4
1.4.3	Incidence and prevalence	4
2	ISAR Study and Cardiovascular Parameters	8
2.1	ISAR study	8
2.1.1	Hemodialysis	11
2.1.2	Treatment parameters	12
2.2	Electrocardiography	14
2.3	Heart rate variability	15
2.3.1	Background	16
2.3.2	Time-domain methods	16
2.3.3	Frequency-domain methods	18
2.3.4	Nonlinear methods	21
2.4	Ambulatory blood pressure monitoring and pulse wave analysis	21
2.4.1	History of blood pressure measurement	22
2.4.2	Pulse wave analysis	23
2.4.3	Ambulatory hemodynamic monitoring	36

3	Multi-Lead RR-Interval Computation	38
3.1	State of the art	38
3.2	Aim of the study	39
3.3	Methods	40
3.3.1	Study population	40
3.3.2	Single-lead annotation	41
3.3.3	Multi-lead correction	42
3.3.4	RR-interval computation	45
3.3.5	Difference between two RR-series	47
3.3.6	Agreement indicators	49
3.4	Results	51
3.5	Discussion	53
4	HRV Parameters for Risk Prediction	57
4.1	State of the art	57
4.2	Aim of the study	59
4.3	Methods	59
4.3.1	Study Population	59
4.3.2	HRV indices and entropy measures	60
4.3.3	Statistics	65
4.4	Results	66
4.5	Discussion	69
5	Combined Pulse Wave and ECG Analysis	75
5.1	State of the art	75
5.2	Aim of the study	77
5.3	Methods	77
5.3.1	Study population	77
5.3.2	Classification and survival trees	77
5.3.3	Statistics	83
5.3.4	Implementation	84
5.4	Results	85
5.5	Discussion	87
6	Summary and Conclusions	93
A	Supplementary material	95

<i>CONTENTS</i>	vii
List of Figures	97
List of Tables	99
Acronyms	100
Nomenclature	103
Bibliography	105
Curriculum Vitæ	127

1.1 Background and motivation

Estimates of the Global Burden of Disease Study 2015 attributed 1.2 million deaths in 2015 to chronic kidney disease (CKD) [186]. The percentage change of 32% from 2005 to 2015 is among the highest of all noncommunicable diseases between these ten years. In comparison, around 18 million deaths are contributed to cardiovascular disease (CVD), which is the main cause of all-cause mortality, with a relative change from 2005 to 2015 by 12.5% [186].

Current guidelines consider CKD patients in the highest risk group for CVD [133]. Especially in end-stage renal disease (ESRD) patients, CVD is the major cause of morbidity and mortality [60]. At initiation of renal replacement therapy (RRT), which includes dialysis and transplantation, the burden of CVD is manifested. A systematic review calculated the estimated gap between needed and actual RRT worldwide. In 2010, more than 2.6 million people received RRT, but more than 4 million were in need of RRT [104]. Furthermore, the number of patients undergoing RRT will be more than double in 2030 with highest increase in developing regions, such as Asia. Though, the number of patients without access to RRT, mainly in low-income countries, will remain substantial [104].

The excess risk of CVD is caused by a higher prevalence of conditions recognized as risk factors in the general population, such as hypertension, diabetes, and older age [50]. Furthermore, arterial stiffness increases with those risk factors and ESRD [19]. Expected remaining lifetime for dialysis patients is disconcerting. Compared to the age-matched

counterparts in the general population patients around 60 years are expected to live only a quarter (see figure 1.1) [79].

The 2018 European Society of Cardiology (ESC)/European Society of Hypertension (ESH) guidelines recommended ambulatory blood pressure monitoring (ABPM) rather than home blood pressure (BP) monitoring for CKD patients, due to its ability to measure nocturnal BP [197]. Additional pulse wave analysis (PWA) parameters allow to assess aortic stiffness.

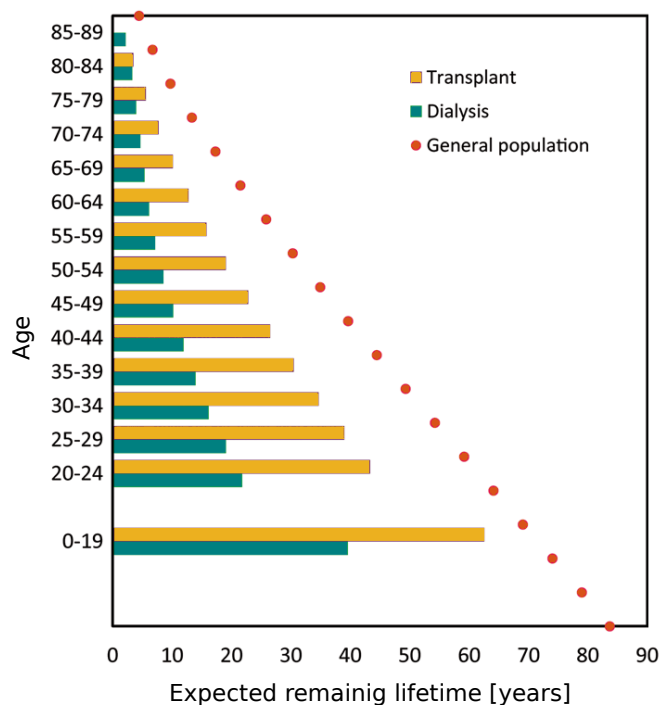


Figure 1.1: Expected remaining lifetime for dialysis patients, patients living with a kidney transplant compared to general population. Data of prevalent dialysis and transplant patients (cohort 2011-2015) from European registries of 12 countries. Adapted from [79].

1.2 Aim of the thesis

The aim of this thesis is on the longitudinal analysis of clinical endpoints in end-stage renal disease (ESRD) patients. Therefore, heart rate variability (HRV) parameters are calculated from a multi-lead time series. An algorithm to obtain these series from the 24-hour electrocardiogram (ECG) is presented. By combining HRV parameters and indices of the cardiovascular system obtained from PWA, this work aims for an improved risk stratification in hemodialysis patients.

1.3 Outline

This thesis is composed of six chapters. In chapter 1, a brief overview of the history of cardiovascular diseases is given. Furthermore, an introduction to end-stage renal disease (ESRD) and its definition is given. Chapter 2 lays out the rISk strATification in end-stage Renal disease (ISAR) study and the dimension for dialysis patients. The different parameters derived from electrocardiogram (ECG) and pressure waves are also defined in this chapter.

The third chapter deals with the automatic determination of an RR-interval series from a multi-lead ECG. This interval series combines the single-lead annotations and can be computed on long-term recordings. Chapter 4 evaluates nonlinear heart rate variability (HRV) parameters obtained from the multi-lead ECG for risk prediction of the ISAR cohort.

In chapter 5, a comprehensive survival analysis of 234 hemodialysis patients from the ISAR study is performed. For this purpose parameters derived from 24 h recordings of the pulse wave and ECG, as defined in chapter 2, are combined together with clinical data in multivariable risk models. Finally, chapter 6 summarizes the findings of this thesis and concludes with possible future implications of this work.

1.4 End-stage renal disease

End-stage renal disease (ESRD), also known as end-stage kidney disease, is CKD that is treated by dialysis or kidney transplant. Kidney failure is a medical condition in which the kidneys function is severely limited. The best test to measure the level of kidney function is the estimated glomerular filtration rate (GFR).

1.4.1 History

In 1990, CKD was included in the list of noncommunicable diseases investigated by the Global Burden of Disease study. This study, in fact a global research program of disease burden, assesses mortality and disability from major diseases, injuries and risk factors. Five CKD classes (see table 1.1) were proposed in the clinical practice guidelines 2002 by the National Kidney Foundation [133]. The classification system has become internationally widely accepted [123]. After a “Kidney Disease: Improving Global Outcomes (KDIGO) controversies conference” the classification was revised in 2009 to a two-dimensional grid by adding albuminuria stages (see figure 1.2)[98].

Stage	Description	GFR [ml/min/1.73m ²]
1	Kidney damage with normal or relative high GFR	≥ 90
2	Mild GFR reduction	60 – 89
3	Moderate GFR reduction	30 – 59
4	Severe GFR reduction	15 – 29
5	Kidney failure	< 15 (or dialysis)

Table 1.1: The five stages of chronic kidney disease (CKD) according to glomerular filtration rate (GFR) level.

		A1	A2	A3
		< 30	30-299	> 300
G1	> 90	Green	Yellow	Orange
G2	60-89	Green	Yellow	Orange
G3a	45-59	Yellow	Orange	Red
G3b	30-44	Orange	Red	Red
G4	15-29	Red	Red	Red
G5	< 15	Red	Red	Red

Figure 1.2: Prognosis of chronic kidney disease (CKD) by glomerular filtration rate (GFR) and Albuminuria categories. GFR categories (G1, ..., G5) in ml/min/1.73m²; Albuminuria category (A1, A2, A3) in mg/g. Green: low risk; Yellow: moderately increased risk; Orange: high risk; Red: very high risk. Reproduced from [99].

1.4.2 Definition

According to table 1.1, kidney failure is defined either with a GFR level less than 15 ml/min/1.73m² or a need for RRT (dialysis or transplantation). The administrative term ESRD does not exactly match with the definition of kidney failure, as ESRD patients are treated by dialysis or transplantation which is not the case for all individuals in CKD stage 5 [133]. Usually, RRT commences in stage 5 CKD and many do not begin treatment until the estimated GFR is much lower than 15. Among treated patients, kidney transplant recipients have increased levels of GFR and superior health outcomes than dialysis patients [133]. However, in this work ESRD subjects are only hemodialysis patients.

1.4.3 Incidence and prevalence

The United States Renal Data System (USRDS) is a national data system that collects, analyzes, and distributes information about CKD and ESRD in the United States. An annual data report is available in two volumes [163]. Volume 2 examines ESRD in the United States, though one chapter is dedicated to international comparisons. Since 2018,

the number of contributing countries to the USRDS annual data report has increased to 79. Austria is part of the contributing countries as well as all other contributors of the ERA-EDTA (European Renal Association-European Dialysis and Transplant Association). Unfortunately, Germany is not contributing data.

In figure 1.3, incident cases in the US and Austria are shown. Incidence refers to the number of new cases in a given time period. The ESRD incidence is calculated as the number of incident cases in one year. In both countries and over all years, hemodialysis was the predominant form of initial therapy among incident cases.

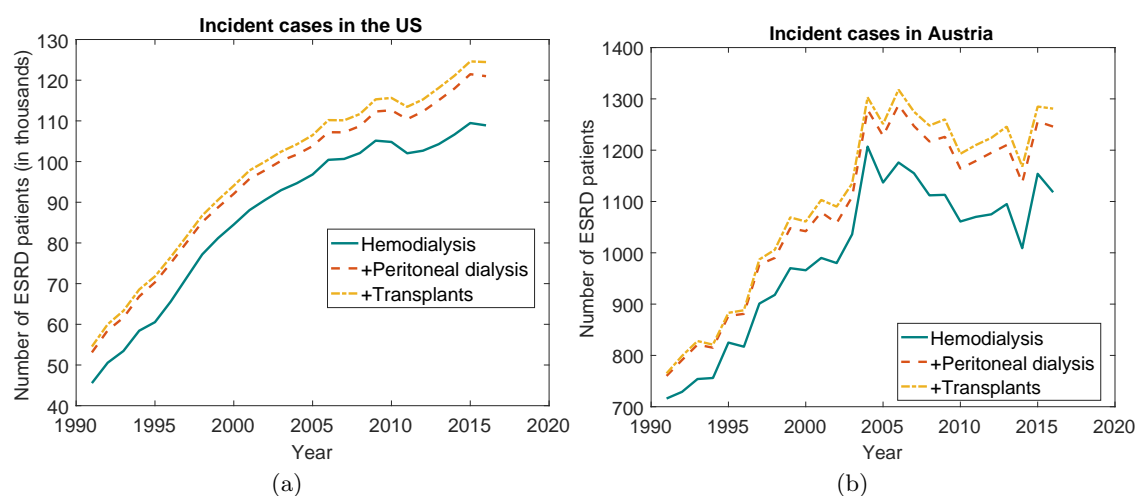


Figure 1.3: Incident cases in the (a) US and (b) Austria by treatment modality. Solid (teal) line represents hemodialysis incidence cases, additional peritoneal dialysis cases are plotted dashed (red). Finally, the dash-dotted (yellow) line represents all ESRD incidence cases by adding the transplant incident cases.

Prevalence refers to the presence of existing cases of a disease at a given time. ESRD prevalence in a population depends on the ESRD incidence and the duration of the disease from start of RRT to death or loss to follow-up. In the US, hemodialysis is the most common therapy among prevalent cases, see figure 1.4 (a). Nevertheless, the prevalent peritoneal dialysis population is slightly increasing and the transplant population almost doubled from 2000 to 2016. In figure 1.4 (b), the modality of ESRD prevalent cases in Austria is shown. Since 2000 more prevalent patients with kidney transplants than patients on hemodialysis were counted.

The situation in Germany is complex. Due to arising conflicts, such as a new data protection law in former West-Germany, tedious paperwork and delayed feedback of the EDTA registry, the response rate in Germany dropped to approximately 50% for the dialysis centers in the beginning of the 90s [52]. A national registry for RRT, namely QuaSi-Niere, was constituted in 1992 [52]. In their first annual report in English 1998, Frei and Schober-Halstenberg mentioned that after 3 years an acceptable observance to

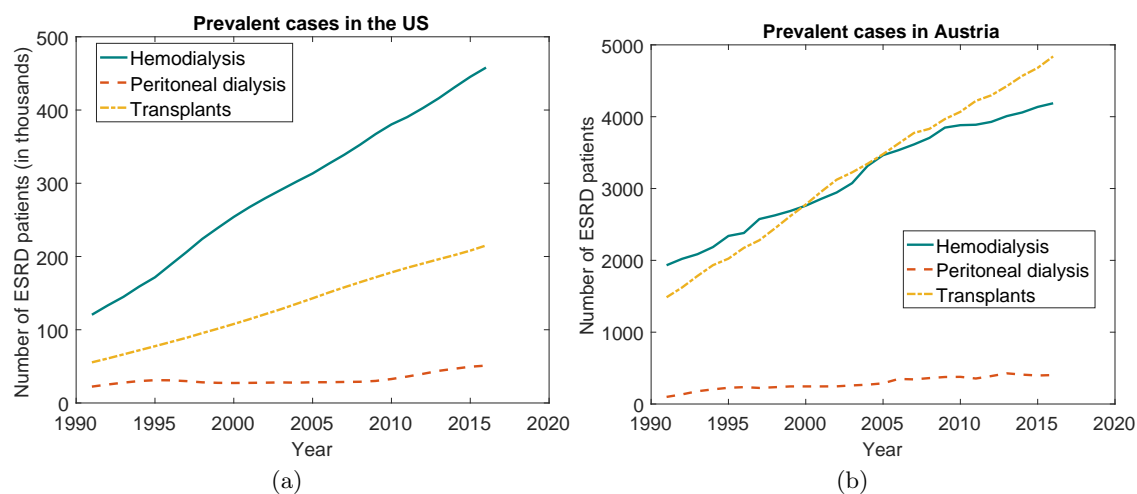


Figure 1.4: Prevalent cases in the (a) US and (b) Austria by modality. Hemodialysis patients are visualized with solid (teal) lines, peritoneal dialysis patients represented by dashed (red) lines, and transplant patients plotted dash-dotted (yellow).

provide data voluntarily was achieved [53]. Nevertheless, a mandatory reporting seems to be necessary to achieve complete data within an acceptable time frame [53]. Annual reports from 1994-2007 in German, made by the nonprofit-making organization QuaSi-Niere, are available online [54]. Since 2007, Medical Netcare GmbH creates annual reports on behalf of the Federal Joint Committee in Germany [125]. Germany is not contributing data to the ERA-EDTA report since 2007 [172].

The network of the largest dialysis care company worldwide provides a global overview of ESRD patients from 120 countries in the year 2001 [128]. Three years later another global overview of 122 countries was published [65]. At the end of 2004, approximately 1.8 million people worldwide were undergoing treatment for ESRD [65]. According to Grassmann et al., there was a rough 70/30 % split of dialysis and transplant patients for North America and Europe. Strong variations in the prevalence between regions and countries was reported [65, 128].

Figure 1.5 visualizes the dialysis prevalence for Austria, the US, and Germany. Dividing the number of dialysis patients treated in a county by the country population yield values per million population (p.m.p.). Population data sources are the U.S. Census Bureau and Eurostat, respectively [201]. Dialysis data for the US is taken from the USRDS annual data report [163]. Data for Austria can be obtained from the national dialysis and transplant register (annual reports online) [138]. Dialysis prevalence data for Germany for the years 2001 and 2004 is specified in global overviews [65, 128]. In the German annual data report 2016, a total number of 93103 prevalent dialysis cases is reported [126]. Furthermore, 4756 dialysis incident cases with a mean age of 67 years

are mentioned [126].

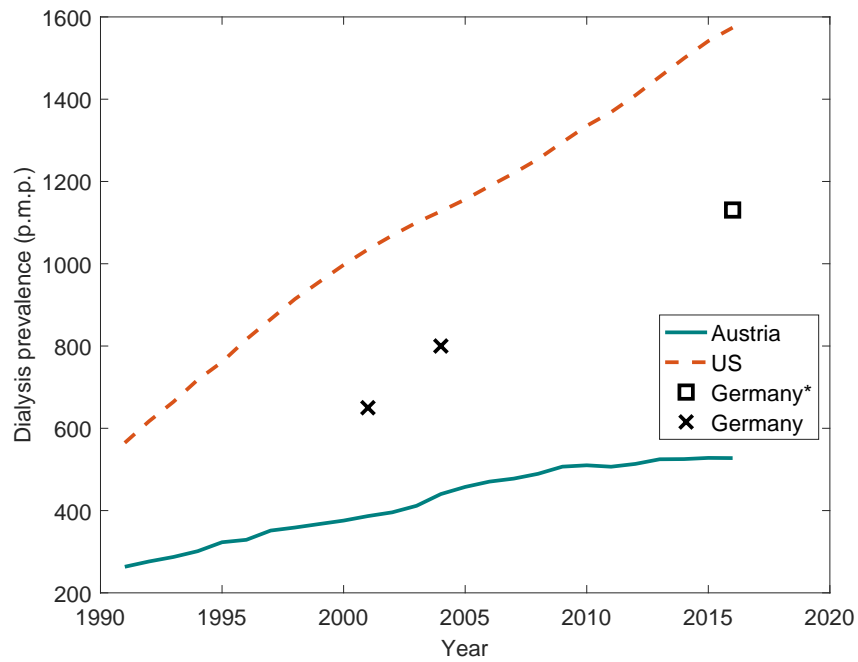


Figure 1.5: Dialysis patients divided by country population in the US, Austria, and Germany. Values specified as per million population (p.m.p.). Data for Germany for the years 2001 and 2004 from [65, 128]. The point prevalence for Germany* in 2016 is computed as $93103/82.3$ [126].

ISAR Study and Cardiovascular Parameters

This chapter describes the data used in all following chapters of this work: The ISAR cohort. Furthermore, parameters gained from electrocardiograms, heart rate variability, and measured pressure waves and their background will be described.

2.1 ISAR study

The ISAR study (ClinicalTrials.gov; identifier number: NCT01152892) is a prospective, longitudinal, observational cohort study carried out in 17 dialysis center in Munich and the surrounding area. The aim of the study is to improve cardiovascular risk stratification in an ESRD cohort [168]. The study protocol was approved by the ethic comitees of the Klinikum rechts der Isar of the Technical University Munich and of the Bavarian State Board of Physicians. Patients were included between 2010 and 2013 if the following conditions were fulfilled [168]:

- 18 years or older,
- 90 days of dialysis vintage or more,
- willingness to participate in at least one technical examination (24 h ABPM or 24 h ECG), and
- written and informed consent.

Exclusion criteria for the study were:

- ongoing infection,

- pregnancy, or
- malignant disease having a life expectancy of less than 24 months.

The cohort included in total 519 patients. After measurement of basic clinical data, blood samples were taken before the midweek dialysis session. Furthermore, the start of a 24 h Holter ECG measurement and a 24 h ABPM were performed in each dialysis center shortly before a midweek dialysis session [168]. Out of the 519 patients, 381 underwent 24 h Holter ECG measurement [69]. Noninvasive 24h ABPM and pulse wave analysis was performed in 414 subjects [122].

At inclusion in the study, patient characteristics, comorbidities, medical history and medication were assessed from medical records in the dialysis centers. Regular blood tests for dialysis patients were also taken. They comprise, e. g., the concentration of the protein albumin. Although albumin is synthesized in the liver and low serum albumin levels may indicate liver failure, hypoalbuminemia can be an indicator that protein is lost in the urine due to kidney damage. Another protein produced in the liver and determined in the blood screens is the C-reactive protein (CRP). It is used as marker of inflammation, hence it is not a very specific prognostic indicator. Nevertheless, CRP is a powerful indicator of mortality in hemodialysis patients [187]. A cumulative comorbidity score was computed by means of the adapted Charlson comorbidity index (CCI) for dialysis patients [103]. Weights (integer points) were assigned to eleven comorbid conditions, such as congestive heart failure (CHF), cancer or diabetes. The final score for each subject is the sum of the weights based on presence of conditions [103].

Dialysis prescription was also provided by the contributing dialysis centers. It included e. g. the dialysis session duration, ultrafiltration, and clearance of urea (Kt/V). These parameters are described in section 2.1.2. Baseline data for all 519 patients is shown in table 2.1

The 24 h 12-lead ECG data were recorded using the Lifecard CF digital Holter recorder (Delmar Reynolds/Spacelabs Healthcare, Nuremberg, Germany) [130]. Reference ECG annotation and RR-interval determination were performed using evaluated commercial equipment (Pathfinder, Delmar Reynolds/Spacelabs Healthcare, Nuremberg, Germany; v.9.027) [130]. An experienced physician blinded to the patient's clinical status manually reviewed and processed all recordings to obtain the sequence of individual RR-intervals together with beat classifications (sinus beat, premature ventricular contraction, artifact) [168]. Additionally, ECGs were analyzed with the Pathfinder algorithm to detect atrial fibrillation (AF). They were classified into individuals with paroxysmal (60% or less AF of the 24 h ECG) or permanent AF (more than 60%). Every ECG was manually

Variable	ISAR cohort, $n = 519$
Age (years)	65.3 (15.1 SD)
Sex—male, n (%)	358 (69 %)
Body weight (kg)	74.5 [65,86]
Height (m)	1.71 (0.09 SD)
Body mass index (kg/m ²)	25.2 [22.6,28.7]
Presence of diabetes, n (%)	209 (40 %)
Presence of hypertension, n (%)	489 (94 %)
Atrial fibrillation, n (%)	109 (21 %)
Heart failure, n (%)	99 (19 %)
Adapted CCI (-)	3 [1,6]
Dialysis vintage (mo)	42.6 [22.4,78.9]
Dialysis duration per session (h)	4.27 [4.02,4.55]
UFV (ml)	2239 (1155 SD)
Kt/V (-)	1.47 [1.25,1.67]
Serum albumin (g/dl)	4 [3.72,4.2]
hsCRP (mg/dl)	0.44 [0.19,0.97]
Total cholesterol (mg/dl)	177 (44.4 SD)
Calcium \times phosphate (mmol ² /l ²)	3.95 (1.23 SD)
Antihypertensive drugs, n (%)	472 (91 %)
Statins, n (%)	196 (38 %)
Anticoagulant, n (%)	83 (16 %)

Table 2.1: Baseline data of the entire ISAR cohort. Data given as number (%) for categorical. Continuous data is presented as mean (SD) or median [IQR]. CCI = Charlson comorbidity index; mo = months; UFV = ultrafiltration volume; hsCRP = high-sensitivity C-reactive protein; Kt/V = dialyzer clearance of urea \cdot dialysis time/volume of distribution of urea.

reviewed by one rater for the presence of permanent AF.

All BP and PWA measurements were obtained with the Mobil-O-Graph 24 h PWA monitor (I.E.M. GmbH, Stolberg, Germany) using validated ARCSolver algorithms (AIT Austrian Institute of Technology GmbH, Vienna, Austria) [159, 191]. The Mobil-O-Graph is a ABPM device with a validated brachial BP measurement unit [51, 193]. By means of a generalized transfer function an aortic pulse wave is generated from the brachial reading [189]. Furthermore, the pulse wave velocity (PWV), as a surrogate for arterial stiffness, is determined by the Mobil-O-Graph. This noninvasive measurements have been compared and validated with intra-aortic catheter measurements [70] and across all age groups close PWV values to the invasive gold standard were determined [192]. BP measurements and PWA parameters were automatically measured every 15 minutes at daytime (8 am-9 pm) and every 30 minutes at night (9 pm-8 am) by the Mobil-O-Graph.

The ISAR Endpoint Committee, a panel of a nephrologist and a cardiologist and a physician independently adjudicated all end points based on medical documentation or interviews with the dialysis centers [168]. Patients were censored at time of transplantation or loss to follow-up. Otherwise, followed up until death occurred. The latest follow-up took place in 2016. All-cause mortality was defined as the primary study end point. Furthermore, major cardiovascular events (sudden cardiac death, myocardial infarction (MI), CHF, stroke) or other cardiovascular procedure leading to death were grouped to the secondary end point: cardiovascular mortality [168].

2.1.1 Hemodialysis

As all ESRD patients of the ISAR study are hemodialysis patients, this RRT is described in more detail in this section. This section is based on chapter 10 of the “Handbook of Dialysis Therapy” by Ward [188].

During hemodialysis, the patient’s blood is pumped through a filter, called dialyzer (see figure 2.1). This dialyzer basically filters waste and water from the blood, as a healthy kidney does. It is composed of tiny hollow synthetic fibers. As illustrated in figure 2.1, the dialysis solution passes the fibers in the opposite direction as blood does (and on the outside of the fibers). Waste products from the blood move into the dialysis solution. Filtered blood is returned through the extracorporeal circuit to the patient. Heparin is infused into the arterial blood line between the blood pump and dialyzer to prevent clotting. The dialysate is prepared by the addition of electrolyte concentrate to purified water. Current machines allow the variation of the dialysate composition as well as a change of the fluid removal rate during treatment. Arterial and venous blood pressure

are monitored and an air-foam detector monitors blood in the venous tubing.

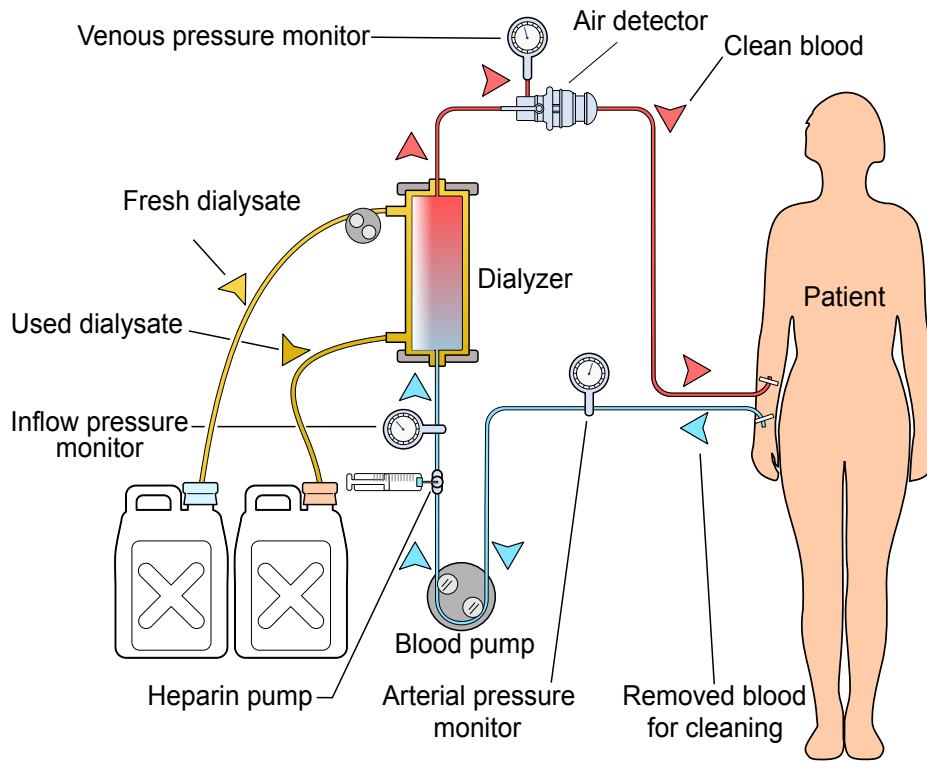


Figure 2.1: Schematic representation of hemodialysis circuit. Adapted from [195].

The most prominent parameter to quantify hemodialysis adequacy is Kt/V . It is a dimensionless ratio representing the fractional urea clearance. Urea clearance, and therefore the delivered Kt/V for urea depends in large part on the effective blood flow rate through the extracorporeal circuit.

2.1.2 Treatment parameters

Measuring the urea of the dialysate would be the most accurate method to determine dialysis delivery to a patient [169]. Because this would be time consuming and difficult to perform, mathematical methods to model the urea balance have been developed.

In 1991, Lowrie introduced the simple urea reduction ratio (URR) to measure the dialysis dose [107]. It is defined by means of the blood urea nitrogen (BUN), i. e., the amount of urea nitrogen in the blood as

$$URR := \frac{BUN_{pre} - BUN_{post}}{BUN_{pre}}. \quad (2.1)$$

BUN_{pre} and BUN_{post} are blood samples obtained immediately before and after dialysis.

The dimensionless parameter Kt/V is defined as

$$Kt/V := \frac{K \cdot t}{V}, \quad (2.2)$$

where K denotes the clearance, t is the dialysis treatment time, and V the distribution volume of urea. As the clearance is expressed in mL/min or L/h, the treatment length is given in min or h, the units of the numerator and denominator (L or mL) cancel each other out. For $Kt/V = 1$, the volume of blood cleared during dialysis treatment is equal to the distribution volume of urea. The relationship between URR and Kt/V can be modeled by neglecting the fluid removal (ultrafiltration) and the urea generation during dialysis. Assuming this simplifications, dialysis results in a simple exponential decline of urea concentration during the treatment process as

$$URR = 1 - e^{-Kt/V}. \quad (2.3)$$

Rearranging this formula and by means of equation (2.1), the following equation holds

$$Kt/V = -\ln(1 - URR) = -\ln(1 - 1 + BUN_{\text{post}}/BUN_{\text{pre}}) =: -\ln(R), \quad (2.4)$$

where R is defined as the ratio of the postdialysis to the predialysis BUN.

Kt/V values computed from the simple model with equation (2.4) were overestimated. Hence, Daugirdas developed a more precise formula by adding a term for the urea generation and another term to account for ultrafiltration. The more reliable relationship was defined in [44] as

$$Kt/V = -\ln(R - 0.008 \cdot t - f \cdot UF/W), \quad \text{where} \quad (2.5)$$

UF denotes the ultrafiltrate volume, W the postdialysis weight, and the “fudge factor” represented as f . By means of a three-times a week dialysis population, the second generation formula was established [44]

$$Kt/V = -\ln(R - 0.008 \cdot t) + (4 - 3.5 \cdot R) \cdot UF/W. \quad (2.6)$$

This equation was also used for the ISAR cohort, since the requirements of a thrice-weekly dialysis for 2.5-5 hours are fulfilled.

2.2 Electrocardiography

An electrocardiogram (ECG) records the electrical activity of the heart via electrodes attached to the human body. To be more precise, skin electrodes measure electrical potential differences between corresponding locations of attachment. The resulting voltage of such a pair is called lead.

A standard 12-lead ECG is obtained by ten electrodes (see figure 2.2): four on the limbs and six on the chest. Resulting leads can be divided in three types: limb leads, augmented limb leads, and precordial leads. Limb leads are measured directly between two electrodes. E. g., lead II is the voltage between the left leg and the right arm. The augmented leads were introduced by Goldberger and are calculated with a central terminal [61]. This central terminal is based on Wilson's indifferent electrode [198], which is also used for the calculation of the six precordial leads. Hence, the whole cardiac cycle is recorded from twelve different perspectives.

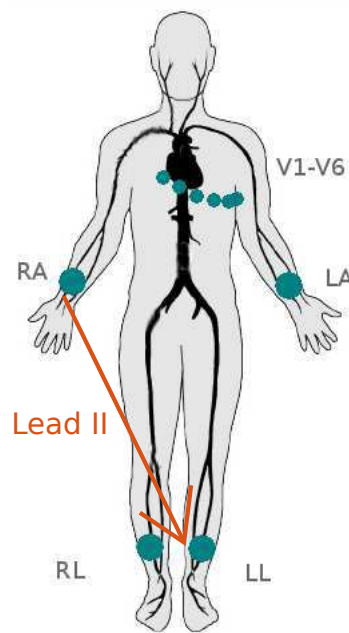


Figure 2.2: Electrode placement of a standard 12-lead electrocardiogram (ECG) consisting of ten electrodes: four limb electrodes and six precordial electrodes (V_1 - V_6) on the surface of the chest. Exemplarily, limb lead II between the right arm (RA) and left leg (LL) is visualized.

The following section describes the electrical conduction system of the heart and is based on chapters 9-10 of the textbook of medical physiology of Guyton & Hall [67]. Historical background of the ECG including a few annotation algorithms is provided in section 3.1.

The normal rhythmical impulse of the heart is generated in the sinus node (also named sinoatrial node). This so-called normal pacemaker is located in the wall of the right atrium. With a rhythmical discharge around 70 times per minute the impulse travels via internodal pathways to the atrioventricular (AV) node. The AV node delays this cardiac impulse from the atria into the ventricles. Hence, it is ensured that the atria can empty their blood into the ventricles before they contract. Via the AV bundle, the signal is conducted to the left and right bundle branch. Finally, the impulse reaches the ends of the Purkinje fibers and is transmitted through the ventricular muscle fibers themselves.

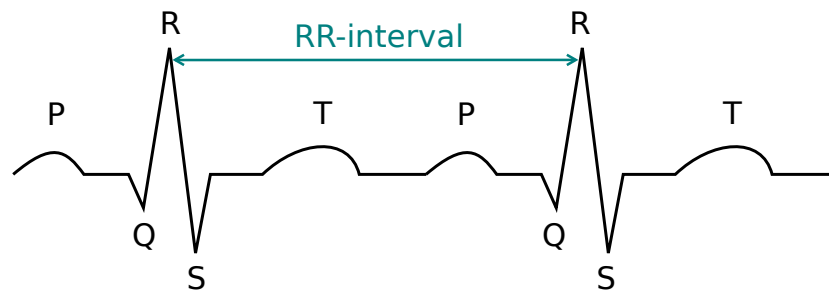


Figure 2.3: Electrocardiogram (ECG) of two normal heartbeats with representation of the main components: P-wave, QRS-complex, T-wave, and the RR-interval obtained from two consecutive R-peaks.

Figure 2.3 illustrates an ECG signal with fiducial points. Two heartbeats of a healthy subject are plotted. The P-wave represents the polarization of the atria followed by the delay of the AV node (time segment between end of P-wave and before Q-peak dip). The QRS complex represents the depolarization of the ventricles (most prominent the rapid slope to the R-peak with a high amplitude due to large muscle mass). Afterwards, an electrically neutral delay (the ST segment) occurs, before the T-wave represents the repolarization of the ventricles.

Rarely, some other parts of the heart becomes the pacemaker. E. g., the AV node with a lower intrinsic rhythmical rate of 40-60 times per minute. Other pacemakers, except the sinus node, are called ectopic pacemakers. They cause an abnormal sequence of contraction, thus can lead to several problems.

2.3 Heart rate variability

Heart rate variability (HRV) is the variation of RR-intervals, i. e., intervals between consecutive heartbeats (see figure 2.3).

The set of RR-intervals for all parameters defined in this section are presented as

$$\mathcal{RR} := \{RR(1), \dots, RR(N)\}. \quad (2.7)$$

In order to obtain useful and comparable results, data has to be preprocessed and filtered before calculating the indices. A deeper look into various filtering methods and artifact detection and removal techniques are out of scope of this work. In section 3.3.5, the robust impulse rejection filter (IRF) is presented since it is used in this work. Further widely accepted data preprocessing steps are described at the beginning of section 4.3.2.

However, for the calculation of HRV the series of normal-to-normal intervals is needed which is denoted as

$$\mathcal{NN} := \{NN(1), \dots, NN(N)\} = \{x_1, \dots, x_N\} =: X. \quad (2.8)$$

The ESC and the North American Society of Pacing and Electrophysiology advise to standardize the recordings either to a duration of five minutes (short-term) or 24 hours (long-term) [135].

2.3.1 Background

HRV analysis became a significant tool for assessing the cardiac health. The first clinical relevance was dated in 1965 when fetal distress was detected in the consecutive RR-series before the heart rate itself showed any notable change [76].

HRV is an important tool to investigate the autonomic nervous system (ANS) [150]. Its two branches, sympathetic and parasympathetic (vagus) nervous system, modify and regulate the heart rate in opposition to each other. Sympathetic stimulations accelerate the heart rate by release of neuropeptide as well as norepinephrine [202]. In contrast, parasympathetic stimulation reduces the heart rate by inhibition of the sympathetic nervous system via the release of acetylcholine [136]. Additionally, sinus nodal cells are directly hyperpolarized by vagus stimulations [136].

2.3.2 Time-domain methods

Based on the guidelines [135], statistical measures on the NN-interval series and those on their difference are presented. Furthermore, a geometrical method the triangular interpolation of NN-interval histogram (*TINN*) will be used in this thesis.

The simple standard deviation of NN-intervals (*SDNN*) to quantify the variability is

defined as

$$SDNN := \sqrt{\frac{1}{N} \sum_{i=1}^N (x_i - \text{mean}(X))^2}. \quad (2.9)$$

The total variance of HRV and therefore the $SDNN$ increases with the length of the recording. Hence, same data lengths have to be considered in order to compare $SDNN$ measures between studies [135].

For the following measures, we consider the differences in the NN-series, i. e., $\Delta X := \{x_2 - x_1, \dots, x_N - x_{N-1}\}$. Precisely, the root mean square of successive differences ($RMSSD$) is calculated as

$$RMSSD := \sqrt{\frac{1}{N-1} \sum_{i=1}^{N-1} (x_{i+1} - x_i)^2}. \quad (2.10)$$

The number of interval differences of successive NN-intervals greater than 50 ms ($NN50$) and the percentage of interval differences of successive NN-intervals greater than 50 ms ($pNN50$) have the following definitions

$$NN50 := \#(|\Delta X| > 50 \text{ ms}), \quad (2.11)$$

$$pNN50 := \frac{NN50}{N} \cdot 100. \quad (2.12)$$

Geometrical methods

As a geometrical measure, the $TINN$ is shown. It is defined as baseline width of a triangle fitted to the NN-distribution, i. e., $TINN := B - A$. Furthermore, its approximation HRV triangular index ($HRVTI$) is presented, which is dependent on the choice of the bin width of the NN-data histogram.

In order to obtain the two points A and B on the x-axis of the interval histogram, a piecewise continuous linear function $T(t)$ is fitted in a least-squares sense to the NN-histogram data. Hence, the essential start is to bin the data. $D(j)$ represents the number of equally long NN-intervals at each bin (see figure 2.4). D_{\max} denotes the maximum of the histogram data, which is the most frequent interval length. The triangular (linear) function is finally defined as

$$T(t) := \begin{cases} T_1, & A \leq t \leq D_{\max} \\ T_2, & D_{\max} \leq t \leq B \\ 0, & \text{otherwise, such that} \end{cases} \quad (2.13)$$

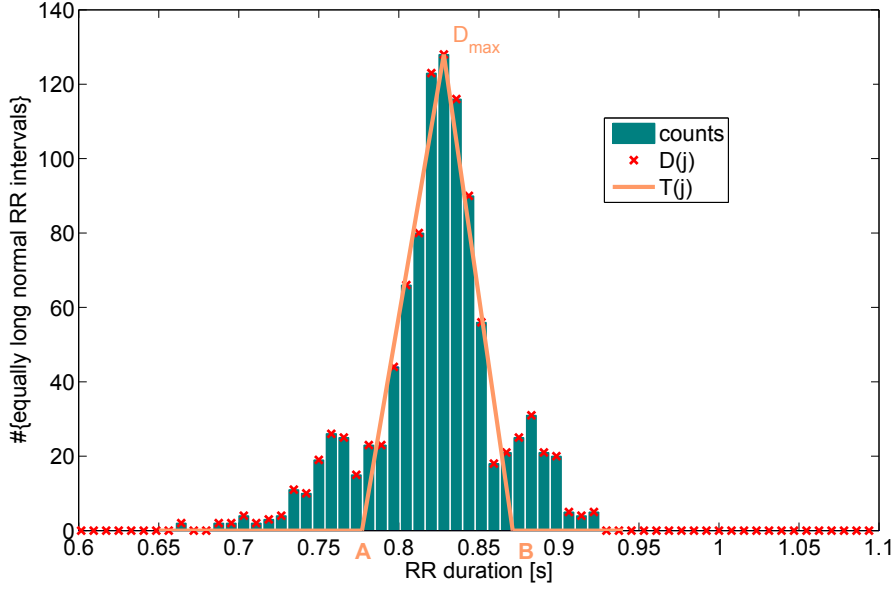


Figure 2.4: Calculation of the geometrical index triangular interpolation of NN-interval histogram ($TINN$). Red crosses ($D(j)$) represent the number of equally long RR-intervals in corresponding bin width. Parameters A and B are derived by optimization with a linear fitting function $T(j)$. $TINN=B-A$.

$$\int (D(t) - T(t))^2 dt \rightarrow \min. \quad (2.14)$$

An approximation of the $TINN$ is given with the $HRVTI$, which is defined as

$$HRVTI := \frac{N}{D_{\max}}. \quad (2.15)$$

As most of the NN-intervals are surrounded by the triangle, the area of the triangle matches approximately the number of NN-intervals, i. e., $TINN \cdot D_{\max}/2 \approx N \cdot h$.

2.3.3 Frequency-domain methods

The power spectral density (PSD) describes how power of the time series is distributed over frequency. In practice, the PSD is usually obtained by Fourier transformation with fast Fourier transformation (FFT) algorithms. These algorithms operate on samples of the signal, hence evenly sampled discrete time series are a precondition for this methods. Inherently, RR-series are unevenly sampled as the time between heartbeats varies.

Before the applied method to obtain a PSD is presented, the spectral components used for HRV frequency domain analysis are defined. These measures are independent of the PSD algorithm and standardized by the HRV Guidelines [135]. Table 2.2 provides a comprehensive list of the frequency domain measures (short-term and long-term) used

in this work. Furthermore, an exemplary PSD with the frequency bands is plotted in figure 2.5.

In most clinical studies, a strong association between the high frequency (HF) component and vagal activity was demonstrated [17, 135]. More controversial is the link between the low frequency (LF) component and sympathetic activity as previously assumed [111]. In a review about the sympatho-vagal balance of low frequency to high frequency ratio (LF/HF), Billman stated that a link of low frequency (LF) power to cardiac sympathetic and a connection of high frequency (HF) power to parasympathetic activity oversimplifies the complex nonlinear interactions [18].

Variable	Units	Description	Frequency range
VLF	ms^2	Power in very low frequency range	0.003 – 0.04 Hz
LF	ms^2	Power in low frequency range	0.04 – 0.15 Hz
HF	ms^2	Power in high frequency range	0.15 – 0.4 Hz
LF/HF		Low frequency to high frequency ratio	
$totalP$	ms^2	Total power of entire spectrum	0 – 0.4 Hz

Table 2.2: Frequency domain measures used in this work. The upper measure (VLF) has to be excluded in the analysis of short-term recordings. Adapted from [135]

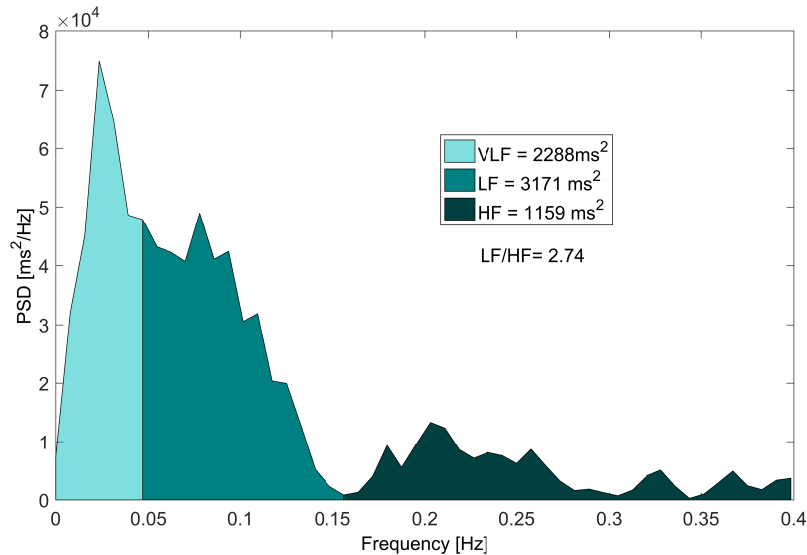


Figure 2.5: Power spectral density (PSD) estimate of a healthy subject. The left area corresponds to the very low frequency (VLF), the area in the middle to the low frequency (LF) and the rightmost area to the high frequency (HF). low frequency to high frequency ratio (LF/HF) is also specified.

There are several methods for the calculation of PSD to overcome issues related to unevenly sampled RR-data. E. g., interpolation leads to a discrete event series. Thus, Fourier transformation can be applied and the PSD can be estimated for instance by Welch's method. This method reduces the variance of the estimated PSD by computing many periodograms on overlapping data segments [173]. The Lomb-Scargle method can directly applied on irregularly sampled data (see section 2.3.3) [105, 166]. Parametric methods, such as autoregressive models, have the disadvantage of prior information of the functional form of the model [135, 173]. In contrast, a better spectral resolution for short frames is determined [114] and post-processing of spectrum is straightforward [135]. Studies have shown that an order around $p = 16$ is suitable for an accurate estimate of the power spectrum of RR-time series [21].

Lomb-Scargle periodogram

The benefit of the Lomb-Scargle method is that it can directly be applied to unequally sampled data. Furthermore, there is no choice of parameters. Hence, this method is used throughout in this work for the calculation of HRV frequency parameters.

The Lomb-Scargle periodogram P_{LS} at frequency ω for the (already filtered) discrete time series $(x_n)_{n=1}^N$, see equation (2.8), is defined by Scargle in [166] as

$$P_{LS}(\omega) = 1/2 \left\{ \frac{[\sum_n x_n \cos \omega(t_n - \tau)]^2}{\sum_n \cos^2 \omega(t_n - \tau)} + \frac{[\sum_n x_n \sin \omega(t_n - \tau)]^2}{\sum_n \sin^2 \omega(t_n - \tau)} \right\}, \quad (2.16)$$

where the time offset τ is defined to ensure the time-shift invariance by

$$\tan 2\omega\tau = \frac{\sum_n \sin 2\omega t_n}{\sum_n \cos 2\omega t_n}. \quad (2.17)$$

The classical periodogram P_{Clas} for the evenly sampled discrete time series $(y_n)_{n=1}^N$ is written as

$$P_{Clas} = \frac{1}{N} \left| \sum_n y_n \exp(-i\omega t_n) \right|^2 = \frac{1}{N} \left(\sum_n y_n \cos \omega t_n \right)^2 + \frac{1}{N} \left(\sum_n y_n \sin \omega t_n \right)^2. \quad (2.18)$$

A generalized discrete Fourier transform for $(x_n)_{n=1}^N$ can be written as

$$FT_G(\omega) = C \sum_n x(t_n) [A \cos \omega t_n + iB \sin \omega t_n], \quad (2.19)$$

where A and B may depend on the sampling t_n , but not on the data $\{x_n = x(t_n)\}_{n=1}^N$.

Hence, the corresponding periodogram is

$$P_G(\omega) = \frac{1}{N} |FT_G(\omega)|^2 = \frac{A^2}{2} \left(\sum_n x(t_n) \cos \omega t_n \right)^2 + \frac{B^2}{2} \left(\sum_n x(t_n) \sin \omega t_n \right)^2, \quad (2.20)$$

for an arbitrary $C := \sqrt{N/2}$. For $A = B = \sqrt{N/2}$, the generalized periodogram reduces to the classical form, i. e., equally spaced observations.

Further conditions have to be deployed, to determine A and B of the generalized periodogram. Scargle stated that the statistical distribution of the generalized periodogram should be as close as possible to the evenly sampled case [166]. Hence, the properties and statistics of the least-squares spectrum investigated by Lomb have been deployed [105]. The resulting least-squares Lomb-Scargle periodogram is defined in equation (2.16).

2.3.4 Nonlinear methods

Since complex mechanisms contribute to the generation of the heart rate, nonlinear techniques to quantify these gained interest over the past 40 years. These methods are based on the fractal behaviour of the heart rate time series (e. g., Hurst exponent, fractal dimension, detrended fluctuation analysis) or developed from chaos theory (e. g., correlation dimension, entropy, Poincare plot) [150]. In 2015, Sassi et al. emphasized the gap between complex signal processing algorithms and the so far limited clinical validation [165].

Notwithstanding, nonlinear methods increasingly finding their way in clinical studies. In this work, chapter 4 is dedicated to risk prediction with nonlinear HRV parameters, namely entropies.

2.4 Ambulatory blood pressure monitoring and pulse wave analysis

Each heart beat generates a pulsatile blood flow, which is conducted into the vascular system. This fluctuation of the arterial pulse is visible in a maximum (systolic) and a minimum (diastolic) pressure. Numerous parameters to identify risk for cardiovascular disease can be obtained from measured pressure/flow waves.

With mathematical tools, the pulse wave can be analyzed and transformed along the arterial tree. In particular, the examination of waves proximal to the heart, i. e., central arterial pressure wave, is of great interest. Sophisticated parameters, such as pulse wave velocity (PWV) and augmentation index, are able to assess differences in the pressure wave between periphery and aorta caused by elasticity of the vessels and wave reflections

originated from bifurcations in the arterial tree. Therefore, hemodynamic monitoring plays an important role in risk prevention now and in the future.

2.4.1 History of blood pressure measurement

The first blood pressure measurements date back to in the middle of the 18th century with the experiments of Hales¹ [22]. He inserted a fine tube into a horse's artery and fixed a vertical glass tube of nearly the same diameter. Hence, he was able to measure the level of blood in the tube. Almost a century later, Poiseuille² invented a mercury manometer for the measurement of arterial blood pressure. Therefore - actually it was his dissertation - he was awarded the gold medal of the Royal Academy of Medicine in 1828 [22].

Up to 1854, puncture of an artery was necessary to measure arterial pressure. The first sphygmograph, a device using weights and levers to estimate blood pressure noninvasively, was created by Vierordt³. Marey⁴ improved the cumbersome apparatus by making a portable device (see figure 2.6). Great contribution was also made by Mahomed⁵, who developed the first quantitative sohygmograph, while he was a medical student. The first sphygmomanometer was invented in 1881 by von Basch⁶. The simplicity of the new device and a better accuracy made it possible that van Basch's sphygmomanometer was accepted in clinical use [22].

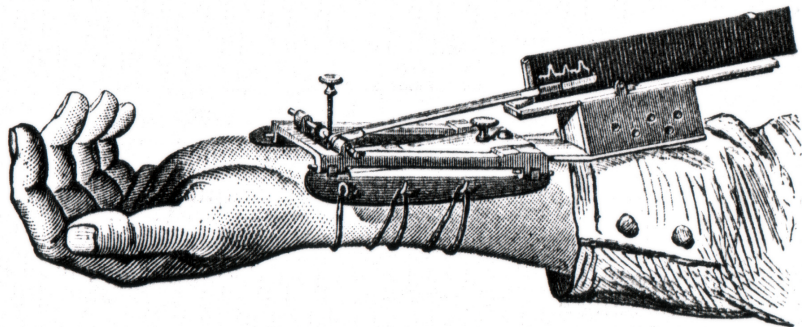


Figure 2.6: Marey's sphygmograph with a registration unit, where blood pressure waveforms are obtained [113, p. 281].

Present-day technique of blood pressure measurement is based on methods introduced

¹Stephen Hales (1677–1761), English clergyman

²Jean Léonard Marie Poiseuille (1797–1869), French physicist and physiologist

³Karl von Vierordt (1818–1884), German physiologist

⁴Étienne-Jules Marey (1830–1904), French scientist, physiologist and chronophotographer

⁵Frederick Akbar Mahomed (1849–1884), British physician

⁶Samuel Siegfried Karl von Basch (1837–1905), Austrian-Jewish physician

by Riva-Rocci⁷ and Korotkov⁸. Riva-Rocci used a pressure cuff around the upper arm, which can be inflated with air. With an usual mercury manometer measuring the pressure in the cuff, the systolic blood pressure (SBP) could be obtained as follows. First, the pressure in the cuff was increased until the radial pulse could no longer be palpated. By slowly releasing the pressure of the cuff, the pulse reappears and the pressure value can be read. The pressure at reappearance relates to SBP. In the beginning of the 20th century, Korotkov reported a method to estimate diastolic blood pressure (DBP) as well. Placing a stethoscope over the brachial artery, tapping sounds were audible as the cuff was deflated. This auscultatory method, using the Korotkov sounds has been used for more than 100 years without any substantial improvement [143].

In 1954, SBP was measured oscillometric and compared to intra-arterial pressure [180]. The oscillometric method uses the amplitude of cuff-pressure oscillations when the cuff pressure is reduced from above systolic to below diastolic pressure. Ramsey developed an automatic device which measures the mean arterial pressure (MAP), as it appears to correspond to the maximal oscillations [151]. Furthermore, a theoretical study investigated this coincidence and identified conditions under which the relationship holds [119]. Systolic and diastolic levels can be obtained using fixed fractions of the maximal amplitude [59]. In figure 2.7, noninvasive oscillometric brachial blood pressure measurement is illustrated.

2.4.2 Pulse wave analysis

Although the ECG, a measured waveform of the electric heart activity, was accepted before long, solely single pressure values were still in use for a long time. Two extreme values, the diastolic (minimum) and systolic (maximum) blood pressure measured at the brachial artery were most commonly used. The predominance of simple sphygmomanometric values was due to a missing theory to analyze the pulse contour and sensitivity to artifacts of the mechanical instruments [85]. Even if Marey's sphygmograph already obtained entire pulse waveforms one-hundred years ago (see figure 2.6), with noninvasive technologies such as applanation tonometry pulse-contour recordings gained interest. This measurement technique uses a pencil-shaped probe which flattens the artery. Hence, tangential pressures are eliminated and the sensor detects the intra-arterial pressure.

In the late 1940s, human diagnostic cardiac catheterization was introduced [134]. Subsequently, central and peripheral arterial pulse pressure countours were studied [157]. The

⁷Scipione Riva-Rocci (1863–1937, Italian internist, pathologist and pediatrician

⁸Nikolai Korotkov (1974–1920), Russian surgeon

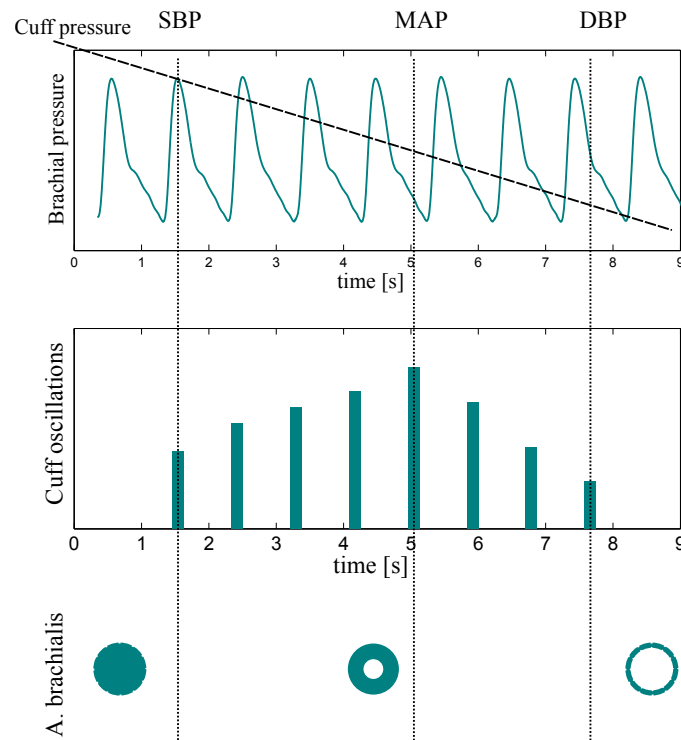


Figure 2.7: Noninvasive brachial blood pressure measurement with an oscillometric pressure cuff. Bottom image sketches the compression of arteria brachialis. Systolic blood pressure (SBP), mean arterial pressure (MAP), and diastolic blood pressure (DBP).

collaboration of McDonald⁹ and Womersley¹⁰, who applied mathematical techniques to the analysis of blood flow and hemodynamics, originated essential work in this field. McDonald described that differences between peripheral and aortic pulse wave are based on reflections. Possible reflection spots are branching points, areas of alteration in arterial stiffness, and high-resistance arterioles [134]. In figure 2.8, different shapes of the pressure waveform in dependence of location and age are shown. In young individuals, the shape of the pressure wave changes apparently between the heart and periphery. With decreasing elasticity of the arteries, as a result of aging or hypertension, the pressure wave close to the heart (ascending aorta) is similar to recorded pressure waves in a peripheral artery (see figure 2.8).

The analysis of the central aortic pulse wave allows to assess accurately the pressure against the heart must eject [82]. Furthermore, indices related to arterial stiffness and augmentation can be derived from the aortic pressure wave. In a meta-analysis the slightly better predictive ability of central pulse pressure (PP) compared with brachial PP was reported [184].

⁹Donald Arthur McDonald (1917–1973, British physician

¹⁰John Ronald Womersley (1907–1958), British mathematician

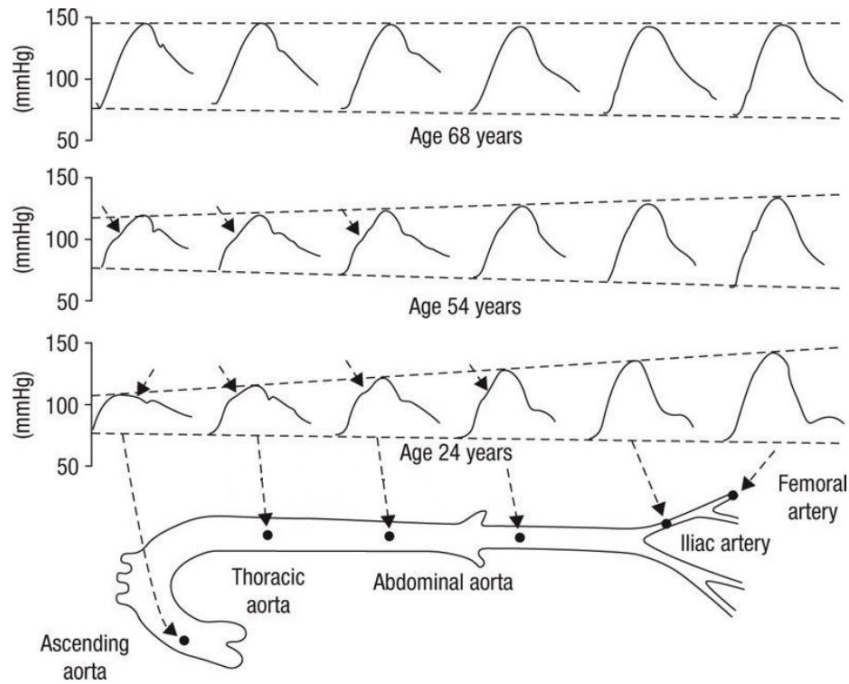


Figure 2.8: Comparison of arterial pressure waveforms based on location and age. Reprinted from [134].

Pressure-flow relation

This section deals with the formulas describing the blood flow. By means of the Navier-Stokes^{11,12} equations the motion of viscous fluid can be described. First, the pulsatile behavior of arterial flow is neglected and the well-known Poiseuille equation are obtained. Womersley was able to describe the flow related to a periodic pressure gradient by the use of Fourier series.

At the beginning, a steady, laminar flow (in one direction) and a constant pressure gradient ($\frac{\partial p}{\partial z} = \frac{\Delta p}{L}$) reduces the third momentum equation from the Navier-Stokes equation to

$$\frac{1}{r} \frac{\partial}{\partial r} \left(r \frac{\partial u_z}{\partial r} \right) = \frac{1}{\mu} \frac{\Delta p}{L}, \quad (2.21)$$

with u_z representing the longitudinal flow velocity, Δp the pressure drop along the tube of length L , μ the dynamic viscosity of the liquid, and radius r . With a no-slip boundary condition ($u_z(R) = 0$), the solution is the following parabolic velocity profile

$$u_z(r) = \frac{\Delta p}{4\mu L} (R^2 - r^2), \quad (2.22)$$

¹¹Claude-Louis Navier (1785–1836), French engineer and physicist

¹²George Gabriel Stokes (1819–1903), Irish physicist and mathematician

with internal radius R . Finally, the Poiseuille equation for the volume flow Q is written as

$$Q = \int_0^R 2\pi u_z r \, dr = \frac{2\pi\Delta p}{4\mu L} \int_0^R r(R^2 - r^2) \, dr = \frac{\pi R^4 \Delta p}{8\mu L}. \quad (2.23)$$

As blood flow in arteries is not steady ($\frac{\partial u_z}{\partial t} \neq 0$), one main assumption of the Poiseuille flow is not fulfilled. To model a pulsatile flow, the incompressible Navier-Stokes equation is considered. It is defined as

$$\frac{\partial^2 w}{\partial r^2} + \frac{1}{r^2} \frac{\partial w}{\partial r} + \frac{1}{\mu} \frac{\partial p}{\partial z} = \frac{1}{\nu} \frac{\partial w}{\partial t}, \quad (2.24)$$

where $\nu = \frac{\mu}{\rho}$ denotes the kinematic viscosity and ρ the density. Womersley introduced the pressure gradient as a periodic function, argued that the pulse itself is a periodic phenomenon [200]. By defining the gradient as

$$\frac{\partial p}{\partial z} = A \cdot e^{i\omega t}, \quad (2.25)$$

and substituting the velocity as $w(r) = u(r) \cdot e^{i\omega t}$, the Navier-Stokes equation reads

$$\frac{d^2 u}{dr^2} + \frac{1}{r} \frac{du}{dr} + i^3 \frac{\omega}{\nu} u = -\frac{A}{\mu}. \quad (2.26)$$

A solution of this equation is written as

$$u = \frac{A}{i \omega \rho} \left\{ 1 - \frac{J_0(r\sqrt{\omega/\nu} i^{3/2})}{J_0(R\sqrt{\omega/\nu} i^{3/2})} \right\}, \quad (2.27)$$

where $J_0(x i^{3/2})$ are (well-known) first kind Bessel functions of order zero. Womersley introduced the nondimensional parameter [199]

$$\alpha := R\sqrt{\omega/\nu}, \quad (2.28)$$

which is named Womersley number and substituted the fractional radius $y = r/R$. Finally, the solution of equation (2.24), i. e., the flow velocity w is given as

$$w = \frac{A}{i \omega \rho} \left\{ 1 - \frac{J_0(\alpha y i^{3/2})}{J_0(\alpha i^{3/2})} \right\} e^{i\omega t}. \quad (2.29)$$

Integration gives the volume flow by

$$Q = 2\pi \int_0^R wr \, dr = 2\pi R^2 \int_0^1 wy \, dy \quad (2.30)$$

$$= \frac{2R^2\pi A}{\rho i\omega} \left\{ \frac{1}{2} - \frac{1}{J_0(\alpha i^{3/2})} \int_0^1 J_0(\alpha y i^{3/2}) y \, dy \right\} e^{i\omega t}. \quad (2.31)$$

With the property of Bessel functions $\int x J_0(x) \, dx = x J_1(x)$ it follows

$$Q = \frac{\pi R^2 A}{\rho i\omega} \left\{ 1 - \frac{2\alpha i^{3/2} J_1(\alpha i^{3/2})}{i^3 \alpha^2 J_0(\alpha i^{3/2})} \right\} e^{i\omega t}. \quad (2.32)$$

Moreover, if just real parts are considered and the real part of the pressure gradient is defined with the modulus M and the argument ϕ as

$$\frac{\partial p}{\partial z} = M \cos \omega t - \phi, \quad (2.33)$$

the velocity may be written as

$$w = \frac{MR^2}{\mu} \frac{M'_0}{\alpha^2} \sin(\omega t - \phi + \epsilon_0). \quad (2.34)$$

The terms M'_0 and ϵ_0 are defined in [200] and the zero subscript indicates that only Bessel functions of zero order are involved.

The volume flow can be written with terms M'_{10} and ϵ_{10} , which are tabulated in [200] as

$$Q = \frac{\pi R^4 M}{\mu} \frac{M'_{10}}{\alpha^2} \sin(\omega t + \phi + \epsilon_{10}). \quad (2.35)$$

For $\alpha \rightarrow 0$, the Poiseuille equation (see equation (2.23)) is resembled, since $M'_{10}/\alpha^2 \rightarrow 1/8$ and $\epsilon_{10} \rightarrow \pi/2$ [199]. Hence, $\sin(\omega t + \phi + \pi/2) = \cos(\omega t + \phi) = \frac{\partial p}{\partial z} = \Delta p/L$.

In summary, with an oscillating pressure the formula obtained by Womersley approximates Poiseuille's law in small vessels ($\alpha \leq 0.5$). In large vessels, the oscillating flow deviates greatly from Poiseuille formula and can be expressed as a sum of harmonic components of the pressure gradient. Experimental results in 1965 compared measured and calculated values of Womersley flow and velocity and showed good agreement [100].

Impedance analysis

Based on the concept of Fourier analysis, both flow and pressure wave can be decomposed into harmonics. Their relation is manifested in the input impedance. To be more precise, the input impedance is the ratio of oscillatory pressure to flow at a particular

region of the arterial system. In contrast to the characteristic impedance (Z_c), which is used for the determination of the PWV, the input impedance (Z_{in}) is influenced by wave reflections.

A T -periodic, continuously differentiable function $f(t) = f(t + T)$ can be defined by its Fourier series

$$f(t) = \frac{a_0}{2} + \sum_{n=1}^{\infty} [a_n \cos(\omega_n t) + b_n \sin(\omega_n t)], \text{ with} \quad (2.36)$$

$$a_n = \frac{2}{T} \int_{T/2}^{T/2} f(t) \cos(\omega_n t) dt \quad n = 0, 1, \dots \quad (2.37)$$

$$b_n = \frac{2}{T} \int_{T/2}^{T/2} f(t) \sin(\omega_n t) dt \quad n = 1, 2, \dots \quad (2.38)$$

The angular frequency is given as reciprocal of the period by $\omega_n = n \frac{2\pi}{T}$.

Furthermore, if f is real valued, the following compact form can be obtained¹³

$$f(t) = \frac{a_0}{2} + \sum_{n=1}^{\infty} A_n \cos(\omega_n t - \phi_n), \text{ with} \quad (2.39)$$

$$A_n^2 = a_n^2 + b_n^2 \quad \text{and} \quad \phi_n = \tan^{-1} \left(\frac{b_n}{a_n} \right). \quad (2.40)$$

Hence, the pressure wave $P(t)$ and flow wave $Q(t)$ can be represented as

$$P(t) = \bar{P} + \sum_{n=1}^{\infty} P_n \cos(\omega_n t - \phi_n), \quad (2.41)$$

$$Q(t) = \bar{Q} + \sum_{n=1}^{\infty} Q_n \cos(\omega_n t - \psi_n) \quad (2.42)$$

with the zero-frequency coefficients \bar{P} and \bar{Q} , i. e., the mean components

$$\bar{P} := \frac{1}{T} \int_0^T P(t) dt, \quad (2.43)$$

$$\bar{Q} := \frac{1}{T} \int_0^T Q(t) dt. \quad (2.44)$$

Further coefficients are calculated with equation (2.40), e. g.,

$$P_n^2 = \left(\frac{2}{T} \int_0^T P(t) \cos(\omega_n t) dt \right)^2 + \left(\frac{2}{T} \int_0^T P(t) \sin(\omega_n t) dt \right)^2. \quad (2.45)$$

¹³Follows directly from cosine difference formula: $\cos(\omega_n t - \phi_n) = \cos(\omega_n t) \cos(\phi_n) + \sin(\omega_n t) \sin(\phi_n)$.

Figure 2.9 shows the Fourier decomposition of a pressure wave for the first six harmonics. Furthermore, the reconstructed wave by summation of the individual harmonics is visualized.

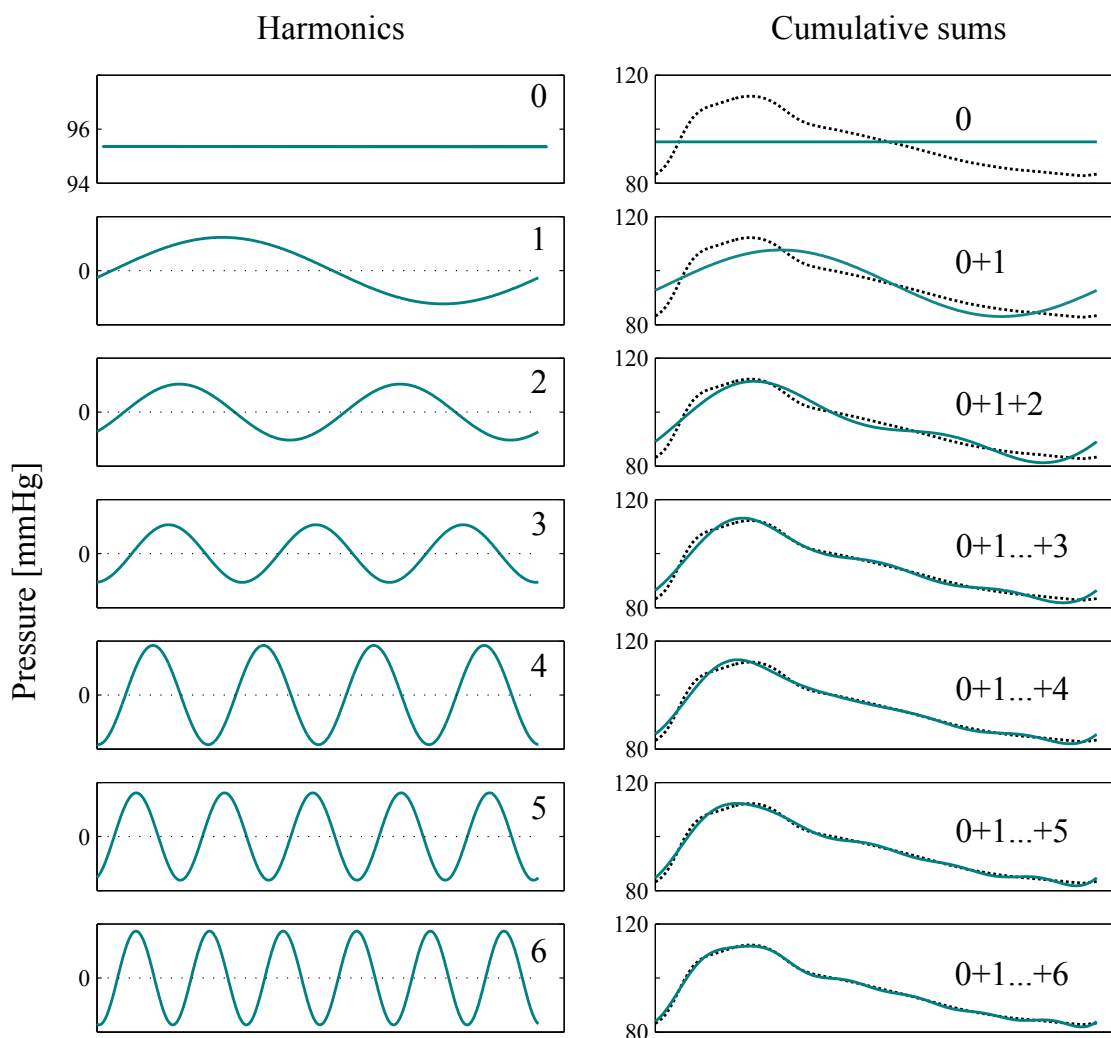


Figure 2.9: Fourier decomposition of a pressure wave. On the left side the harmonics 0-6 are shown. The right panel shows the original pressure wave (black dotted) and the reconstructed wave by cumulative summation of the harmonics. The 0 harmonics (mean term) captures the offset (see axis of top images).

The input impedance (Z_{in}) is defined as the pressure-flow relationship for each harmonic

$$Z_{in}(\omega_n) = \frac{P_n}{Q_n}, \quad n \geq 0. \quad (2.46)$$

With reference to signal processing theory, Z_{in} can be interpreted as transfer function, as P_n and Q_n in the frequency domain can easily be obtained by Fourier transformation.

At zero frequency, the magnitude of the input impedance is maximal and corresponds to the peripheral resistance [194]. Higher frequency components of the input impedance (> 2 Hz) can be used to estimate the characteristic impedance (Z_c), another important index of arterial stiffness. An appropriate frequency range for the calculation of the characteristic impedance is 2 – 16 Hz [109]. More precisely, Z_c can be estimated by averaging the input impedance moduli from 2 – 16 Hz [109]. Figure 2.10 illustrates the modulus of the input impedance, with its peak at frequency $f = 1$ Hz. After a steep drop $|Z_{in}|$ fluctuates around an approximate value, which corresponds to the estimated characteristic impedance Z_c .

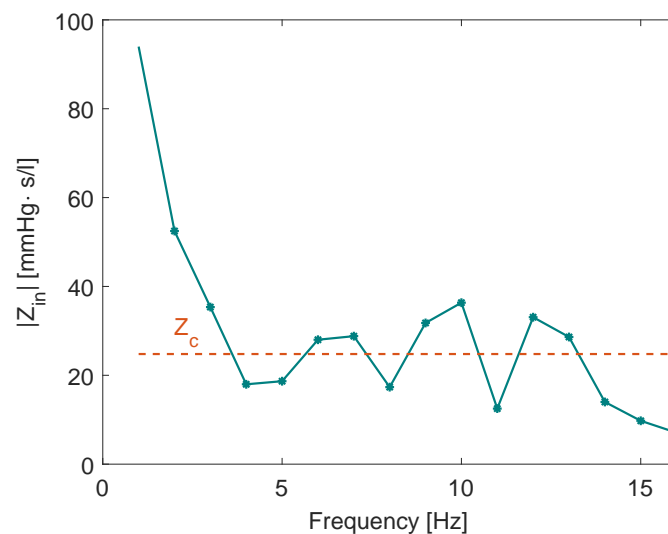


Figure 2.10: Estimation of characteristic Impedance Z_c from moduli of the input impedance $|Z_{in}|$. The frequency region used for taking the mean (2-16 Hz) is indicated by dots.

Arterial wall and elasticity

In all models of the previous section, the vessels are treated as (thin-walled) cylindrical tubes of constant diameter. In fact, arterial vessels have viscoelastic properties and their diameter varies with pulsating pressure [134]. Furthermore, the elastic properties change along the arterial tree with stiffer arteries in distal direction (away from the heart) [95]. The ESC/ESH guidelines defined carotid-femoral PWV as gold standard to measure arterial stiffness [95, 197].

In 1809, Young¹⁴ examined the functions of the heart and arteries and inquired his own hydraulic investigations [204]. The relation of the arterial stiffness and PWV was formulated independently by the Dutch Korteweg¹⁵ and Moens¹⁶ in 1878 [90, 129]. They

¹⁴Thomas Young (1773–1829), British physician

¹⁵Diederik Johannes Korteweg (1848–1941), Dutch mathematician

¹⁶Adriaan Isebree Moens (1846–1891), Dutch physician and physiologist

calculated the velocity c of a pressure wave in experiments with a water-filled rubber tube. Hence, the so-called Moens-Korteweg equation is given as

$$c = \sqrt{\frac{Eh}{2r\rho}}, \quad (2.47)$$

where E represents the Young's elastic modulus of the vessel wall, h the wall thickness, r the vessel radius, and ρ the density (of blood). Bramwell and Hill mentioned in 1922 that velocity calculation with the Moens-Korteweg equation is cumbersome, since all variables in equation (2.47) - except ρ - vary from artery to artery [26]. By means of Newton's equation for the velocity (c_0) of sound in air ($c_0 = \frac{B}{\rho}$), where B represents the bulk modulus, they obtained from the Moens-Korteweg equation the following expression

$$c_0 = \sqrt{\frac{VdP}{\rho dV}}, \quad (2.48)$$

where the term $(dV/dP)/V$ describes a relative increase in the volume of artery per pressure increase. Both equations are approximately equal, if small changes in vessel area and wall thickness are assumed.

The Moens-Korteweg equation as well as the Bramwell-Hill equation are still in use for the calculation of PWV as a marker of arterial stiffness [73, 176]. Moreover, a low velocity is related to efficient heart work. This can be observed directly in the Bramwell-Hill equation (2.48), as the output (volume) should be as large as possible for a given pressure [26].

Transfer function technique

As mentioned beforehand, the analysis of the central aortic pulse wave is of great interest since arterial stiffness and wave reflections, contributions to pulsatile hemodynamics, can be assessed. By means of transfer functions, a peripheral recording can be transformed to the aortic root. Technically, a transfer function is the linear mapping of the input to the output in the frequency domain. Assume, the pressure wave at site A is considered as input and represented as $p_A(t)$ in the time domain and as $P_A(\omega)$ in the frequency domain. Furthermore, $P_B(\omega)$ denotes the Fourier transformed pressure wave at site B considered as output. Hence, the transfer function between sites A and B is defined as

$$H_{AB} := \frac{P_B(\omega)}{P_A(\omega)}. \quad (2.49)$$

Each pressure wave in the frequency wave can be written with modulus M and phase ϕ as

$$P(\omega) = M \cdot e^{i\phi}. \quad (2.50)$$

Thus, the transfer function has the representation

$$H_{AB} = \frac{M_B \cdot e^{i\phi_B}}{M_A \cdot e^{i\phi_A}} = \frac{M_B}{M_A} \cdot e^{i(\phi_B - \phi_A)} =: M_{AB} \cdot e^{i\phi_{AB}}. \quad (2.51)$$

As a result, the transfer function itself can be expressed as amplitude and phase.

In 1970, O'Rourke recorded simultaneously pressure waves in the brachial artery and aortic arch during diagnostic catheterization and calculated the amplification in the frequency domain [137]. Karamanoglu et al. determined pooled brachial-aortal and radial-aortal transfer functions of corresponding harmonic components [82]. This enables the possibility to obtain central pressures accurately from peripheral pressure measurement with the same single generalized transfer function [82]. The characteristic modulus amplifications and phase shifts of pressure wave harmonics are visualized in figure 2.11. By means of applanation tonometry, the noninvasively measured pressure wave resembles the recorded signal from a high-fidelity transducer within the artery [35]. Several studies validated the transfer function technique calculated from carotid or radial applanation tonometry [35, 56, 142].

The ARCSolver (AIT Austrian Institute of Technology GmbH, Vienna, Austria) transfer function has similar parameters as published by Karamanoglu et al. (see figure 2.11)[189]. Hence, the Mobil-O-Graph device with inbuilt ARCSolver algorithms obtains an aortic pressure waveform from a single brachial cuff reading. Furthermore, the agreement with common accepted tonometric measurement methods was shown [189].

Augmentation index

At the beginning of ventricular ejection, aortic pressure is increasing with blood flow. However, the aortic pressure wave continues to increase while flow is already decreasing. This pressure increase can be attributed to the return of the reflected wave. One forward and one backward wave should represent the cumulation of all forward and backward waves, respectively. The augmentation index (AIx) is defined as ratio of augmented pressure to pulse pressure. While the pulse pressure is well-defined, the assessment of the augmented pressure depends on the determination of an inflection point (or "shoulder").

The calculation of an augmentation index is dated back to 1980, when Murgu et al. grouped patients based on the ratio $\Delta P/PP$, because this was an obvious differentiating

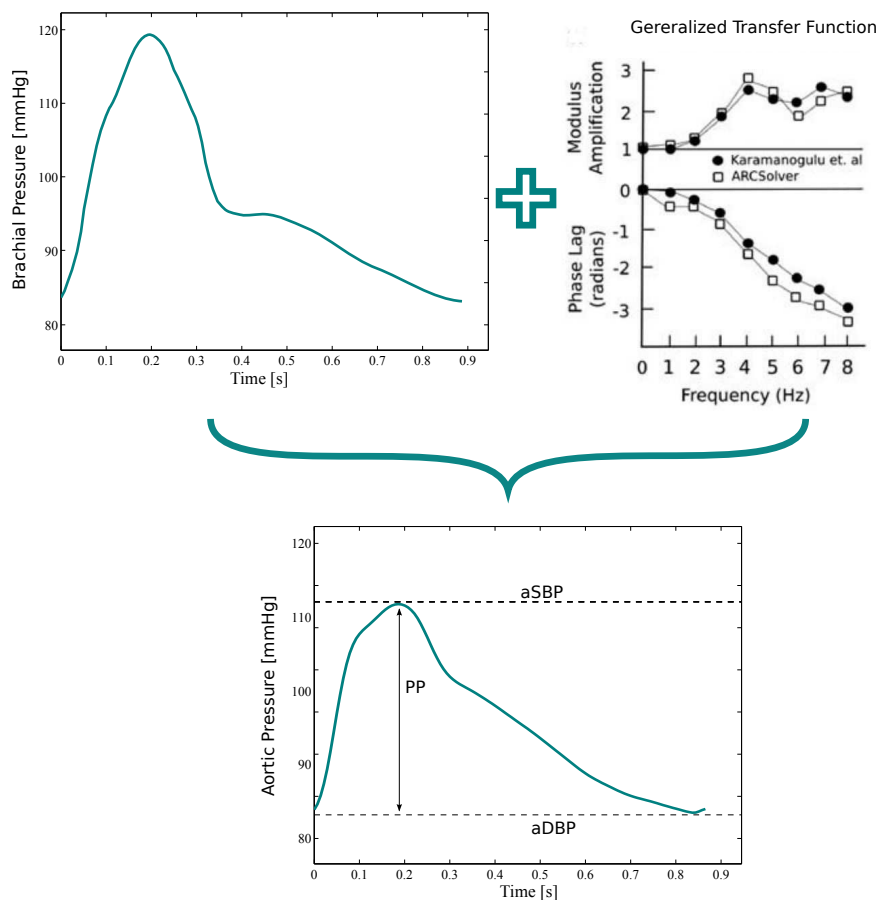


Figure 2.11: By means of a generalized transfer function, the brachial artery waveform is transformed to the aortic root. Adapted from [189].

parameter for their aortic pressure waveforms [132]. PP denotes the pulse pressure and ΔP represents the difference between an inflection point and the peak of the pressure wave. In previous studies, the inflection point was visually determined which led to subjective quantification [85]. Kelly et al. introduced an automatic assessment of the shoulder by the first zero crossing of the fourth pressure wave derivative [85]. Pressure can be augmented in late systole, extending into diastole or the entire reflected wave occurs in diastole. This usually depends on the age of the subjects (see figure 2.12).

As a result, the augmentation index (AIx) is defined as

$$AIx = \frac{P_2 - P_1}{PP} = \frac{AP}{PP}, \tag{2.52}$$

where the augmented pressure (AP) is obtained from the inflection point (P_i) and aortic

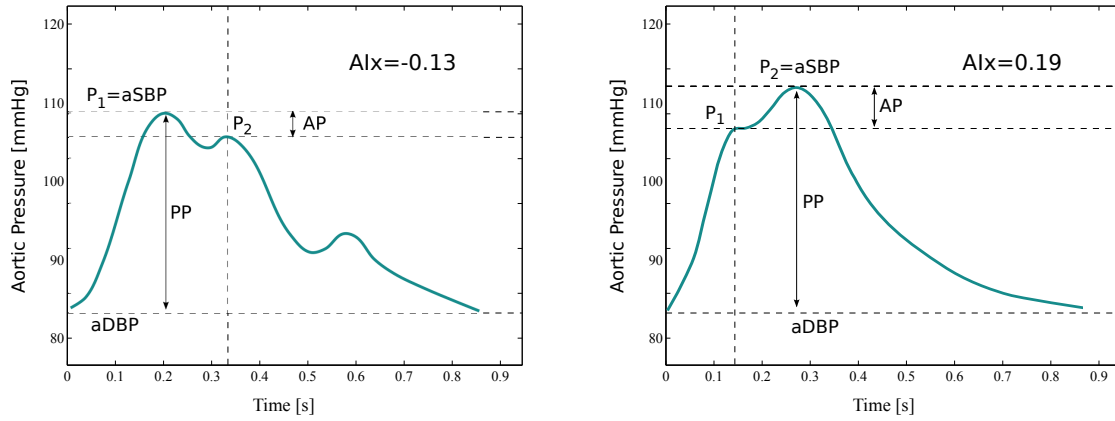


Figure 2.12: Calculation of augmentation index (AIx) from different aortic pressure waves. Usually, in young subjects the reflected wave occurs in diastole (left) leading to a negative value. With age, the reflected wave occurs in systole causing a higher amplitude (right).

systolic blood pressure (*aSBP*)

$$\left. \begin{array}{l} P_1 = P_i, \\ P_2 = aSBP \end{array} \right\} \text{ for } t(P_i) \leq t(aSBP). \text{ Otherwise } \begin{cases} P_1 = aSBP, \\ P_2 = P_i. \end{cases} \quad (2.53)$$

Thus, if the inflection point occurs later than the pressure maximum, the augmented pressure is negative. As a result, in the second case *AIx* is a negative number.

Pulse wave velocity

The pulse wave velocity (*PWV*) can be defined straight forward as

$$PWV = \frac{\Delta x}{\Delta t}, \quad (2.54)$$

where Δt denotes the time required to travel the distance Δx .

The travel distance Δx is obtained directly from the patient. Several possibilities how to measure (or estimate) this distance properly have been proposed. Common estimates depend on the body height [49, 190]. Huybrechts et al. compared real traveled path lengths using magnetic resonance imaging (MRI) [78]. An expert consensus document recommends to measure the distance as 80% of the direct carotid-femoral distance [182]. Traveled time (or transit time) can be assessed by the difference of the arrived pulse wave between the two measurement sites. Mostly, this is done by the foot-to-foot method, as the “foot” of the wave (minimum) can easily be determined and this region is only little affected by reflections [134]. Figure 2.13 illustrates this method with measurements at the carotid and femoral artery. The noninvasive carotid-femoral *PWV* is considered as

the gold-standard measurement of arterial stiffness [95, 182, 197]. The cut-off value for the increased risk of cardiovascular events is defined by 10 m/s [182, 197].

Assessment of the travel time is more accurate than determination of the travel distance [181, 190]. If the two pressure waves are not recorded simultaneously, synchronization can be accomplished by means of an ECG. Nevertheless, an extreme value (such as pressure wave minimum) can be affected by noise or choice of electronic filters [134]. Algorithms for the calculation of the pulse transit time and their stability and reliability are compared in [9].

Primary, aortic PWV was measured invasively during catheterization. In this scenario the traveled length is defined as the catheter length and can be measured precisely. As a matter of course, invasive methods are impractical in daily routine. Moreover, they can cause complications such as thrombosis, infections, and bleeding.

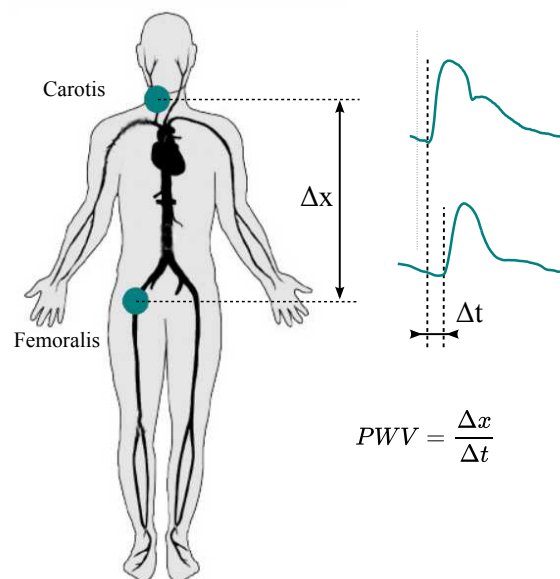


Figure 2.13: Carotid-femoral pulse wave velocity (PWV) obtained with travel distance Δx and travel time Δt obtained with foot-to-foot method.

With the Mobil-O-Graph and its inbuilt ARCSolver algorithms, the aortic PWV is estimated from a single oscillometric cuff pressure reading [70]. For this purpose, after the conventional blood pressure measurement the cuff is inflated to diastolic pressure level and pulse waves are recorded for 10s. By means of transfer functions (see section 2.4.2), a central pressure wave is generated. A model, with most relevant parameter include age, central pressure, and aortic characteristic impedance (see section 2.4.2) calculates an estimate of the aortic PWV [70]. This method has been compared with

invasively measured aortic PWV [70] and with the noninvasive gold-standard method, i. e., carotid-femoral PWV [192]. Good agreement of brachial-cuff derived aortic PWV was shown [70, 192].

2.4.3 Ambulatory hemodynamic monitoring

Recorded observations of 24 h patterns in organisms date already back to the 18th century [183]. Recently, the society has become increasingly interested in the circadian rhythm, as the 2017 Nobel Prize in Physiology or Medicine was awarded for discoveries of the molecular circadian clock. The cardiovascular system is sensitive to circadian variation, manifested with diurnal changes in blood pressure and heart rate [48, 183]. Figure 2.14 shows the 24 h rhythm which is influenced by cycles of light and dark. Other factors, such as temperature, stress and exercise can affect the circadian features as well. Especially for dialysis patients, shifts and fluctuations in volume status have great impact.

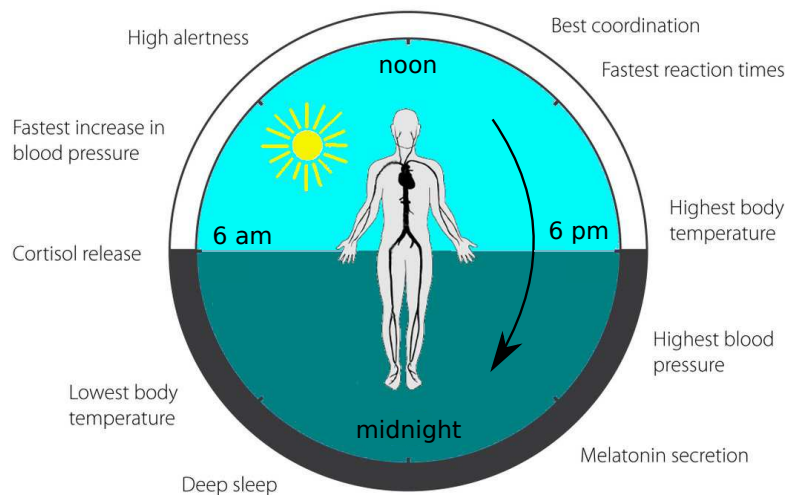


Figure 2.14: Features of the human circadian clock. Adapted from [83].

A Holter ECG is continuously recording the heart activity over 24 hours. Monitored subjects should not be restricted in their normal activities, only the electrical device should be kept dry. After the ECG recording is finished the signal analysis can be performed. For such long signals there is no way around automatic methods (see chapter 3).

With the use of a time triggered measurement process, the Mobil-O-Graph (I.E.M., Stolberg, Germany) allows ambulatory hemodynamic monitoring. To be more precise, the

Mobil-O-Graph 24 h PWA monitor is validated for 24 h ABPM [51, 193] and with inbuilt ARCSolver (AIT Austrian Institute of Technology GmbH, Vienna, Austria) algorithms PWA is subsequently performed. In this study, BP measurements and PWA parameters were automatically determined four times an hour at daytime and two times an hour per night (see section 2.1).

The use of ABPM has enabled a more comprehensive estimate of a patient's true BP [179]. In clinical practice, ABPM is widely used for the diagnosis of white coat hypertension. It is more robust and allows night-time readings. The 2018 ESC/ESH Guidelines for the management of arterial hypertension suggest ABPM for the diagnosis of hypertension [197].

Studies in CKD populations have shown that BP obtained by ambulatory monitoring is a stronger predictor of ESRD than office BP [1, 141]. Recently, the association between PWV (24 h and office) and mortality in hemodialysis patients was demonstrated but only 24 h PWV remained significant after adjustment for common risk factors [118]. Moreover, nocturnal systolic BP was showed as a predictor of cardiovascular mortality in hemodialysis patients [8].

Multi-Lead RR-Interval Computation

In this chapter, an algorithm to obtain an RR-interval series in a fully automated manner is presented. The agreement between the automated RR-series and a manual reviewed reference series is evaluated. Finally, HRV parameters of both RR-series are presented and compared.

Most results presented in this chapter were previously published in the article “Implementation and Verification of an Enhanced Algorithm for the Automatic Computation of RR-Interval Series Derived from 24h 12-Lead ECGs” published in “Physiological Measurements” (Hagmair et al. 2017 [69]).

3.1 State of the art

In the beginning of the 20th century, Einthoven¹ developed a system of electrographic standardization for medical diagnosis and was therefore awarded the Nobel Prize in 1924 [11]. Moreover, he recognized the potential of the ECG as a diagnostic and investigative tool. Frank Wilson² improved the electrocardiography by adding chest and limb leads to the Einthoven’s three standard leads (see section 2.2) [80].

Already in the late 1950s, the first automatized ECG analysis was carried out by a digital computer [175]. Nowadays millions of ECGs to detect cardiac problems are recorded annually. Most of them are automatically analyzed and interpreted [167]. Probably, the most prominent algorithm was proposed by Pan and Tompkins, where QRS detection is

¹Willem Einthoven (1860–1927), Dutch doctor and physiologist

²Frank Norman Wilson (1890–1952), American cardiologist

based on quadratic energy [139]. Other routines use adaptive filters [171] or are based on wavelets [46, 116]. Several of the traditional algorithms are only subsequently evaluated and not optimized for real-time analysis [155]. For the annotation of the single leads in this work, a real-time algorithm combining some of these methods was adapted [10]. This routine continuously calculates a so-called feature signal for the detection of R-peaks. Moreover, one after the other R-peaks are instantly classified (more details in section 3.3.2).

Beat-by-beat manual measurements for standard 12-lead ECGs (see section 2.2) are impractical in clinical practice. The technical progress, including advances in accuracy and powerful computer hardware, led to an increasing reliance on automated measurement of ECG intervals [89]. Laguna et al. examined automatic wave onset and offset points in multi-lead ECGs [93, 94]. In this setting, the information of all leads can be combined and there is the possibility to overcome the effect of disturbance in a single lead. The proposed algorithm of Laguna et al. compares the detected QRS positions between all leads. At the end, QRS complexes are only considered if they do not differ more than a predefined threshold from one lead to the other. Evaluation was done with the CSE multi-lead measurement database [196]. However, validation was done on short-term recordings and the number of measured beats in the database is rather small (around 120) [94].

The “Recommendations for the Standardization and Interpretation of the ECG” suggest to use global measurements of ECG intervals in multiple leads [88]. In particular for the determination of the QT-interval, the earliest onset and the latest offset of all leads yield a more accurate QT-interval in contrast to determination from single-leads [88]. Nevertheless, there is the possibility of overestimation with global measurements due to accepted information by routines which a human overreader would visually decline [88].

García-González et al. investigated the effect of the lead choice on HRV. For healthy subjects, they reported a standard deviation of the lead-to-lead difference RR-time series from 0.5 ms to more than 20 ms [58]. The leading cause of differences could be attributed to the various levels of noise between the leads, which strongly influenced the fiducial point assignment.

3.2 Aim of the study

Although several studies concerning the automatic ECG feature determination in a multi-lead ECG exist, to our knowledge there is no work dealing with corrected multi-lead RR-intervals. Consequently, the aim of this study is threefold: (1) to obtain a

corrected RR-interval series in a fully automated manner, (2) to evaluate the agreement between this automated RR-series and a manual reviewed reference time series, and finally (3) to calculate HRV parameters on 12-lead ECG data of ESRD patients.

3.3 Methods

The multi-lead RR-interval determination algorithm is a sequence of three procedures. At the beginning, all single leads are annotated and the procedure is followed by the multi-lead correction algorithm. At the end RR-intervals are computed. The whole procedure is illustrated in a flow chart (see figure 3.1).

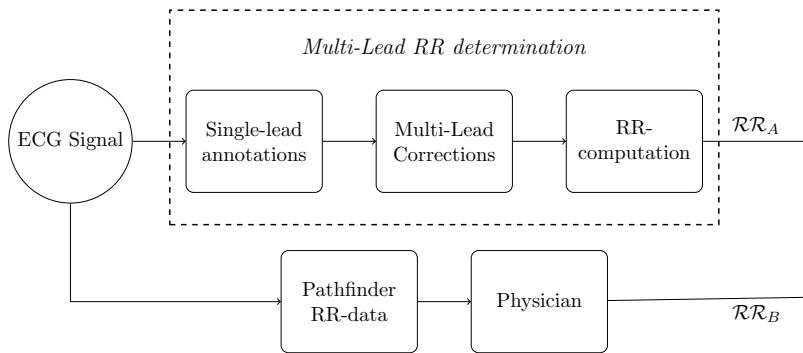


Figure 3.1: Steps from an ECG signal to RR-interval data. The top line shows the multi-lead RR determination (\mathcal{RR}_A). In the strand on the bottom, the two steps to end up with reference RR-data (\mathcal{RR}_B) are illustrated.

To assess the differences in comparison with a reference time series, quantification setup based on García-González et al. [57] was adapted. An overview of the quantification procedure is sketched in figure 3.5. All computations were performed in MATLAB (The MathWorks, Inc., Natick, Massachusetts, United States; R2013b).

3.3.1 Study population

Patients from the ISAR study, which is described in section 2.1, are included in this study only if raw ECG data and matching reference RR-data were available.

ECGs were analyzed with the Pathfinder [130] algorithm to detect AF, due to the apparent irregularity of ventricular rhythm in AF. They were classified into individuals with paroxysmal (60% or less AF of the 24 h ECG) or permanent AF (more than 60%). In addition, every ECG recording was manually reviewed by one rater for the presence of permanent AF. Patients were excluded, if they had an implanted cardiac pacemaker or a cardioverter defibrillator pacing the heart during the ECG recording.

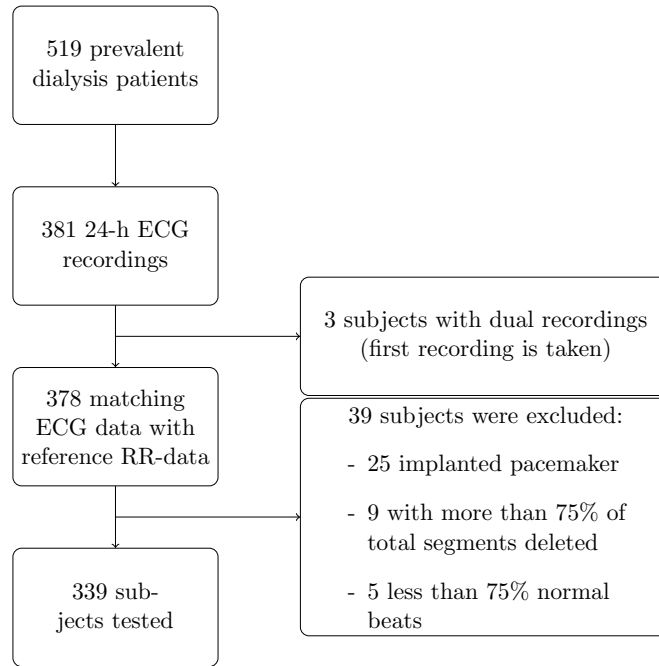


Figure 3.2: Flow chart of the study population.

In total, 378 approximately 24 h ECG recordings with a match of Pathfinder RR-data were available. The sample frequency of the raw ECGs was 128 Hz. Twenty-five patients were excluded due to a cardiac pacemaker. Nine subjects were excluded due to deletion of segments in the RR-time series (more than 75% of the total segments see section 3.3.5). Furthermore, five subjects were excluded since their Pathfinder beat code classification showed less than 75% normal beats. Figure 3.2 summarizes the flow chart of the study population and the final tested data ($n = 339$ subjects).

3.3.2 Single-lead annotation

All single leads are annotated with the algorithm of Bachler et al. [10]. Since R-peaks are the most prominent pattern of an ECG, they are detected foremost. This is done by a so-called feature signal (FS). It is a combination of the amplitude and the first derivative and calculated over a 100 ms moving window. Regions, where the feature signal exceeds the mean value of the last two seconds, define possible QRS complexes. To reduce false positive detections the following statistical plausibility checks are concerned

$$FS > \mu + 6\sigma^3, \quad \text{and} \quad (3.1)$$

$$\beta > 4. \quad (3.2)$$

μ denotes the average value of the last two seconds. σ is defined as the standard deviation within the last 400 ms and β denotes the kurtosis of the last 2.5 seconds of the

feature signal.

The R-peak is selected as the local maximum of the QRS region with the greatest difference to its surrounding minima. Afterwards, a correlation coefficient between the novel detected R-peak and a template of averaged R-peaks is computed. The new R-peak is accepted if the correlation exceeds a threshold of 0.7. The algorithm pays attention to reduce false negatives. Hence, the interval between the last and the novel R-peak is computed. In the case of the interval being 1.8 times longer than the previous RR-interval, another R-peak determination with lower limits is executed.

Furthermore, the R-peaks are classified by means of correlation coefficients. A new R-peak is compared to a predefined number of classes and assigned to the class with the highest correlation. These classes can also evolve dynamically over time. E. g., if the correlation between two classes is higher than with the last detected R-peak, the classes are joined. The last detected R-peak defines a new class. As a result for the j -th lead N_j R-peaks and corresponding classes are detected

$$\mathcal{R}_j := R_j(1), \dots, R_j(N_j), \quad (3.3)$$

$$\mathcal{C}_j := C_j(1), \dots, C_j(N_j). \quad (3.4)$$

The determination of subsequent features such as P-wave, and T-wave, with their on- and offset points and more details about the single lead annotations algorithm are described in [10].

3.3.3 Multi-lead correction

After all single lead annotations are accomplished, their combination can be used to make corrections. This is done with the multi-lead correction algorithm, which is based on an algorithm of Laguna et al. [94].

Every detected heartbeat of the single lead annotations is represented by its R-peak. E. g., $R_j(i)$ denotes the i -th R-peak in the j -lead and J the number of leads. In general, the number of detected R-peaks differs from lead to lead. Either R-peaks in a particular lead are missing or falsely detected. After the multi-lead correction the number of R-peaks matches between all J leads.

Two series S_1 and S_2 for ideally the same beat in all leads are assigned. S_1 contains the lead numbers with the earlier indices and the S_2 the lead numbers of the later indices.

By specifying a threshold of samples τ both sets for the fixed k -th beat are defined as

$$S_1 := \text{find} \left(R_j(k) \leq \min_{j=1, \dots, J} (R_j(k)) + \tau \right), \quad (3.5)$$

$$S_2 := \text{find} \left(R_j(k) \geq \max_{j=1, \dots, J} (R_j(k)) - \tau \right). \quad (3.6)$$

If both series are equal, it is assumed that the R-peaks have been detected correctly in all leads and the algorithm proceeds to the next beat, i. e., $k + 1$. If $S_1 \neq S_2$ is true, one of the extreme values has to be modified. Laguna et al. used the simple “argumentum ad populum” approach by comparing the length of both series and rejected the extreme value of the smaller series [94].

Either S_1 is shorter, so a false positive (FP) detection is assumed, or S_2 is shorter, which can be considered as false negative (FN) detection. For the first case, $\#S_1 < \#S_2$, let l denote the lead with the smallest index of the k -th beat. Potentially, the consecutive R-peak is the true detection. Consequently, the subsequent beats in lead l are shifted by one position to the left.

$$R_l(i + 1) \mapsto R_l(i) \quad \forall i \geq k. \quad (3.7)$$

Thus, the number of R-peaks in lead l is reduced by one element, i. e., $\#\mathcal{R}_l = N_l - 1$. For the second case, assume that $\#S_2 \leq \#S_1$ and moreover that the highest index for the k -th beat is detected in lead l . Hence, the detected beat in lead l and all subsequent beats are shifted one position to the right. For the FN detection a not a number (NaN) is inserted.

$$R_l(i - 1) \mapsto R_l(i) \quad \forall i \geq k + 1, \quad (3.8)$$

$$R_l(k) := NaN. \quad (3.9)$$

The vector \mathcal{R}_l is apparently one element longer, i. e., $\#\mathcal{R}_l = N_l + 1$.

The enhanced multi-lead correction algorithm pays attention to all beats detected in more than $1/3$ of the total number of leads. This is implemented by observing the intersection between S_1 and S_2 . If the intersection $S_1 \cap S_2$ is empty and S_1 contains more than $J/3$ beats, the maximum position of S_2 is delayed to the next beat (see equation (3.8)). The FN case has a “first-rate” position compared to the FP case. Figure 3.3 exemplary shows the enhanced multi-lead correction algorithm for seven leads. Although S_1 contains less R-peaks compared to S_2 , these detections are not discarded since they occur in more than a third of all leads, i. e., $3 \geq 7/3$.

The algorithm proceeds iterative from beat to beat. By repeated shifts with equa-

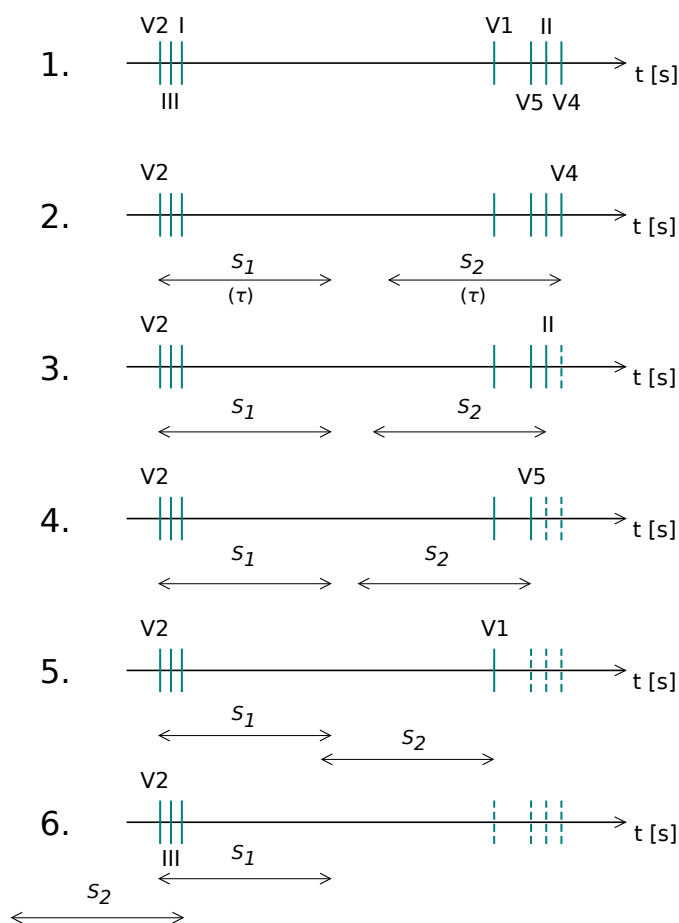


Figure 3.3: Six steps of the multi-lead correction algorithm. R-peaks of the various leads (I , II , III , $V1$, $V2$, $V4$, and $V5$) are represented as solid lines. S_1 is the first series, starting with the first index and includes all beats within the threshold τ . In contrast, S_2 includes the later indices (see step 2.). Lines are dotted if the R-peak is delayed to the next beat and new series S_1 and S_2 are determined.

tion (3.7) or equation (3.8) the series S_1 and S_2 are finally identical. As a result only synchronized R-peaks, detected in more than a third of all leads are remaining. Their maximum offset is predefined by the synchronization threshold τ . Laguna et al. [93, 94] used a threshold of 90 ms, which corresponds to 12 samples at a sampling frequency of 128 Hz.

The R-peaks \mathcal{R} and corresponding beat classes \mathcal{C} can be represented in matrices after

the multi-lead correction as follows

$$\mathcal{R} := \begin{pmatrix} R_1(1) & R_1(2) & \cdots & R_1(N) \\ R_2(1) & R_2(2) & \cdots & R_2(N) \\ \vdots & \vdots & \ddots & \vdots \\ R_J(1) & R_J(2) & \cdots & R_J(N) \end{pmatrix}, \quad \mathcal{C} := \begin{pmatrix} C_1(1) & C_1(2) & \cdots & C_1(N) \\ C_2(1) & C_2(2) & \cdots & C_2(N) \\ \vdots & \vdots & \ddots & \vdots \\ C_J(1) & C_J(2) & \cdots & C_J(N) \end{pmatrix}. \quad (3.10)$$

The total number of accepted R-peaks, i. e., the number of columns N , is not predetermined, since each row evolves according to the shifts. Two examples of the multi-lead correction algorithm are shown in figure 3.4.

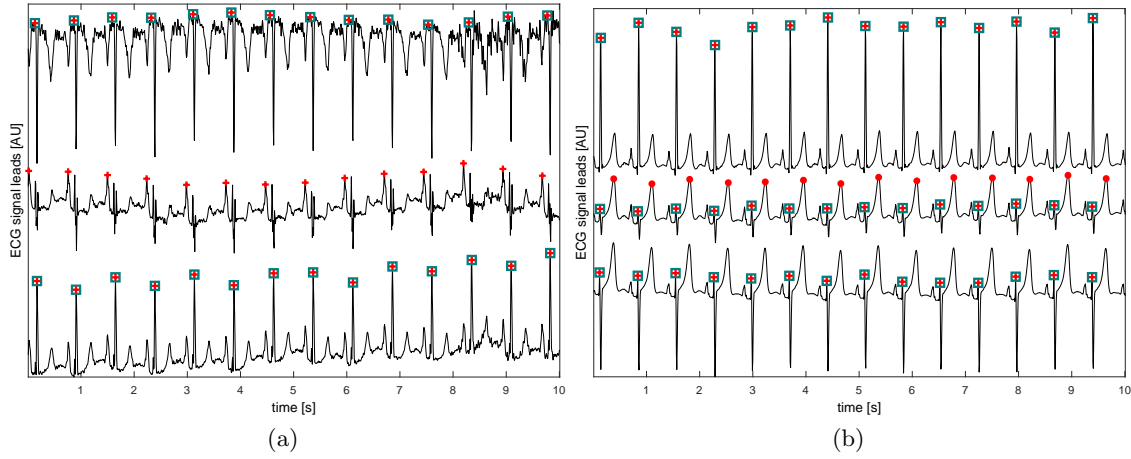


Figure 3.4: Three-lead ECG recordings with R-peak annotations. The single lead annotations are marked as red dots and red pluses, respectively. The accepted R-peaks after the multi-lead correction algorithm are marked as teal squares. On the left side (a), the R-peaks of the lead in the middle have been detected too late (P-peaks are falsely detected as R-peaks). The right figure (b) shows R-peaks and T-peaks detected in the second lead. Since the R-peaks (red pluses) are in the synchronization interval with the other leads, they have been accepted. False detected T-waves (red dots) have been discarded.

3.3.4 RR-interval computation

The computation of the multi-lead RR-intervals is a combination of the synchronized single-lead RR-intervals. The interbeat series is defined as

$$\mathcal{RR} := \{RR(1), \dots, RR(N-1)\}, \quad (3.11)$$

where the i -th interval is the median of the corrected lead RR-intervals on the i -th position

$$RR(i) := \text{median}_{j=1, \dots, J} \{R_j(i+1) - R_j(i)\}. \quad (3.12)$$

If the matrix of R-peaks \mathcal{R} is given in samples, dividing by the sampling frequency leads to RR-intervals in seconds. For averaging, the median was used instead of the mean since its robustness for skewed data. Due to the multi-lead correction algorithm, there is the unusual possibility that none of all leads contains two consecutive R-peaks as requested in equation (3.12). In this case, the RR-interval is calculated between R-peaks of different leads as

$$RR(i) := \text{median}_{j=1,\dots,J} \{R_j(i+1)\} - \text{median}_{j=1,\dots,J} \{R_j(i)\}. \quad (3.13)$$

Exemplary, four beats for a 6-lead ECG with a sampling frequency of 128 Hz are illustrated in table 3.1. In this example, the first beat was only detected in the first three leads and the second beat only in the last three leads. Hence, the first RR-interval has to be calculated with equation (3.13) as

$$RR(1) = \frac{1}{128} (\text{median}\{112, 114, 112\} - \text{median}\{12, 12, 13\}) = \frac{112 - 12}{128} \approx 781 \text{ ms.}$$

The second and third RR-interval can be calculated with equation (3.12) as

$$\begin{aligned} RR(2) &= \frac{1}{128} \text{median}\{210 - 112, 211 - 114, 210 - 112\} \\ &= \frac{1}{128} \text{median}\{98, 97, 98\} = \frac{98}{128} \approx 766 \text{ ms,} \quad \text{and} \\ RR(3) &= \frac{1}{128} \text{median}\{309 - 210, 309 - 210, 308 - 210, 310 - 211\} \\ &= \frac{1}{128} \text{median}\{99, 99, 98, 99\} = \frac{99}{128} \approx 773 \text{ ms.} \end{aligned}$$

	1	2	3	4
<i>I</i>	12	NaN	210	309
<i>II</i>	12	NaN	210	309
<i>III</i>	13	NaN	211	NaN
aVR	NaN	112	210	308
aVL	NaN	114	211	310
aVF	NaN	112	210	NaN

Table 3.1: The first four beats and their detections (in samples) in a 6-lead ECG sampled at 128 Hz. RR-intervals are calculated as $RR_1 = 100/128$ s, $RR_2 = 98/128$ s, and $RR_3 = 99/128$ s.

For the classification of the i -th interval, the most frequent classes of the current and the next beat are used. To ensure, that only intervals between two R-peaks of class 1

are assigned as class 1 RR-intervals, their maximum is used (usually class 1 represents normal R-peaks³). Precisely, the classification of the i -th RR-interval is defined as

$$C(i) := \lceil \max \{ \text{median}_{j=1, \dots, J} \{ C_j(i) \}, \text{median}_{j=1, \dots, J} \{ C_j(i+1) \} \} \rceil. \quad (3.14)$$

Finally, the series of RR-interval classes \mathcal{IC} is given as

$$\mathcal{IC} := \{ C(1), \dots, C(N-1) \} \quad (3.15)$$

3.3.5 Difference between two RR-series

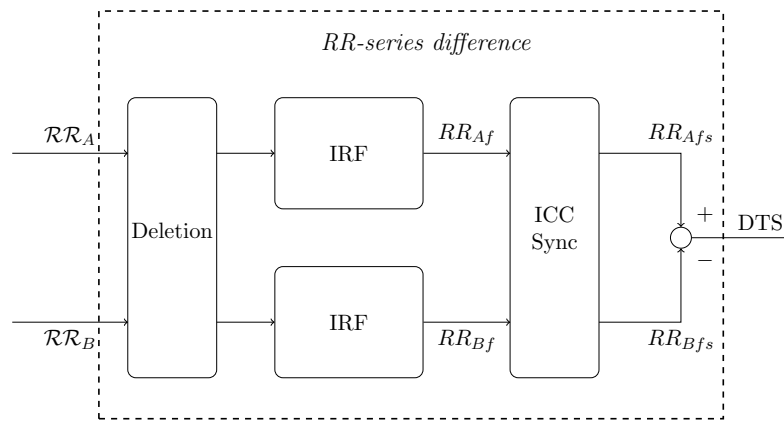


Figure 3.5: Starting with two different RR-series (\mathcal{RR}_A and \mathcal{RR}_B), the steps to obtain a difference time series (DTS) are shown. Filtering of both series is done by the impulse rejection filter (IRF). Synchronization is obtained by maximizing the intraclass correlation coefficient (ICC).

Assume, there are two different RR-series, namely \mathcal{RR}_A and \mathcal{RR}_B . Let \mathcal{RR}_B denote the reference series, which is manually reviewed (see figure 3.5). Before applying indicators for the comparison of \mathcal{RR}_A and \mathcal{RR}_B , some filtering procedures and a step for synchronization is necessary. This is due to the fact that a long-term recording of 24 hour includes around 10^5 RR-intervals.

At the beginning both series are cropped at the beginning and the end at approximately the same time. RR-intervals shorter than 0.3s or longer than 2s are deleted in both series. This procedure is a recommended step for pre-processing, when HRV parameters are calculated [174]. The next step is the segmentation of \mathcal{RR}_A into parts of 5 minutes each, a standardized length for short-term recordings [135]. If a segment (corresponds to approximately 300 beats) contains a heaped number of artifacts the segment is deleted and corresponding beats in \mathcal{RR}_B are removed as well. Therefore, a threshold of 12

³Strictly, class 1 represents the most frequent class. Almost always this is the normal sinus rhythm. See section 3.5

artifacts per segment was predefined.

Outliers in both series are detected with a median filter. McNames et al. employed the following test statistic for 5-min recordings [124] and called it impulse rejection filter (IRF)

$$D(i) := \frac{RR(i) - \widetilde{RR}}{1.483 \cdot \text{median} \left\{ \left| RR(i) - \widetilde{RR} \right| \right\}}, \quad (3.16)$$

where \widetilde{RR} denotes the median value of the entire RR-series. If the test statistic exceeds a threshold ($D(j) \geq 4$), the j -th RR-interval is replaced by the j -centered median of 5 RR-intervals.

Figure 3.6 shows the detection and correction via the impulse rejection filter. RR_{Af} and RR_{Bf} denote both filtered time series.

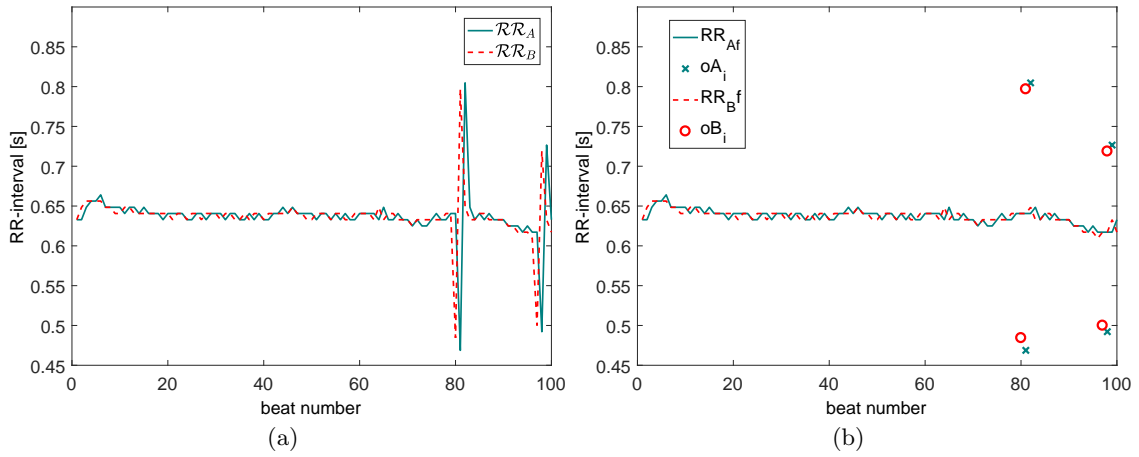


Figure 3.6: The left panel (a) shows exemplary 100 RR-intervals of the initial time series (RR_A and RR_B). In (b), the outliers oA and oB have been detected and corrected by the impulse rejection filter. RR_{Af} and RR_{Bf} denote the filtered RR-interval series.

For the synchronization of both time series, Fisher's intraclass correlation coefficient (ICC) is used. The ICC is computed on segments with $I = 300$ samples as follows

$$ICC = \frac{1}{I \cdot s^2} \sum_{i=1}^I (RR_{Af}(i) - \overline{RR}) (RR_{Bf}(i) - \overline{RR}), \quad (3.17)$$

where

$$\overline{RR} := \frac{1}{2I} \sum_{i=1}^I (RR_{Af}(i) + RR_{Bf}(i)), \quad (3.18)$$

$$s^2 := \frac{1}{2I} \left\{ \sum_{i=1}^I (RR_{Af}(i) - \overline{RR})^2 (RR_{Bf}(i) - \overline{RR})^2 \right\}. \quad (3.19)$$

By delaying or advancing one time series with respect to the other by no more than ten beats, a maximal ICC value is found. Synchronization between both series is assumed for the ICC maximum and succeeded RR-intervals are also shifted by this optimal lag. Only if the highest ICC is obtained at the boundary value, i. e., a lag of ten beats between both time series, the shifting and maximization procedure is repeated by a new maximum lag of 20 beats. In the case of a maximal ICC value still at the boundary, the shifting procedure is repeated for the last time allowing a maximum lag of 40 beats. Both series are kept without a lag and the maximum of the ICC is set to the corresponding ICC value, if the highest ICC value is computed at a lag of 40 beats.

Finally, the largest of both series is cropped to obtain the same number of samples

$$J := \min \{N_{Afs}, N_{Bfs}\}, \quad (3.20)$$

where N_{Afs} refers to the length of the filtered and synchronized series RR_{Afs} and N_{Bfs} denotes the length of RR_{Bfs} .

The difference time series (DTS) (see figure 3.7) is calculated as difference from both filtered and synchronized RR-series

$$DTS(i) := RR_{Afs}(i) - RR_{Bfs}(i), \quad i = 1, \dots, \dots J. \quad (3.21)$$

3.3.6 Agreement indicators

To assess the agreement between the RR-interval series \mathcal{RR}_A and \mathcal{RR}_B , twelve indicators were chosen. They can be divided in three parts: The first three indices represent the initial annotation and classification quality, followed by four indicators assessing the differences between both RR-series according to [57]. In the end, five HRV parameters were calculated on both series to see effects on these.

The Kolmogorov-Smirnov⁴ test was used to test if results were normally distributed. Data are presented as median and 95% central range, as consistently not normally dis-

⁴Andrey Kolmogorov (1903–1987) and Nikolai Smirnov (1900–1966), Soviet mathematicians

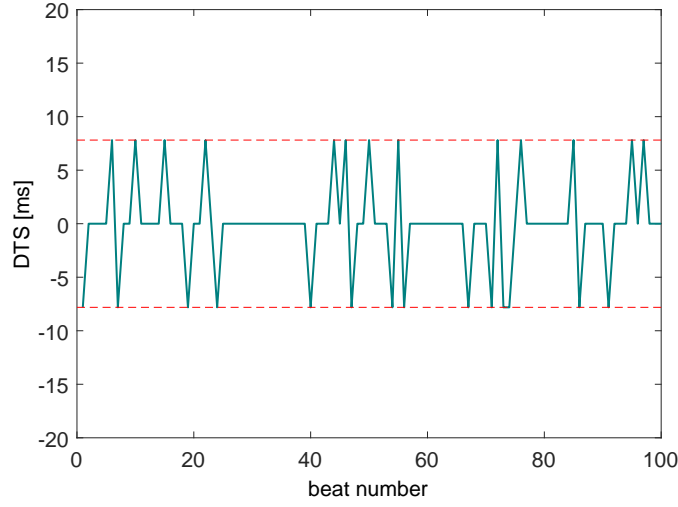


Figure 3.7: One-hundred data points of the difference time series (DTS). The dotted lines mark the precision (1/128 s), since the sampling frequency of the ECG is 128 Hz.

tributed. Furthermore, Bland-Altman⁵ plots are used to visualize limits of agreement and residual distribution.

As two different annotation algorithms were used, the initial ratios of normal beats in series \mathcal{RR}_A and the reference series \mathcal{RR}_B were specified as the first two indicators. $normA$ is defined by the corresponding interval classes $\mathcal{IC}_A = \{C_A(i)\}_{i=1}^{N_A-1}$ (see equations (3.14), (3.15)) as the ratio of normal beats (class 1) to the total number of beats in \mathcal{RR}_A , precisely

$$normA := \frac{\#\{C_A(i) = 1\}_{i=1}^{N_A-1}}{N_A - 1}. \quad (3.22)$$

The reference annotations of the Pathfinder software consists of seven classes (e. g., normal beats, aberrant beats, paced beats). Classes 2 (normal beats) and 4 (HRV excluded normal beats) represent normal beats. Hence, $normB$ is defined as

$$normB := \frac{\#\{C_B(i) = 2 \vee C_B(i) = 4\}_{i=1}^{N_B-1}}{N_B - 1}. \quad (3.23)$$

As segments were deleted if more than 12 not normal beats occurred over disjoint 300 intervals of \mathcal{RR}_A , the percentage of deleted segments ($\%delSeg$) was defined as an index for heaped artifacts or ectopic beats.

To allow a generalization of results and not just being valid for selected HRV parameters, four indicators of the RR-series difference computation were selected. They were chosen in accordance with García-González et al. [57]. After applying the IRF on both RR-

⁵Martin Bland (1947–) and Doug Altman (1948–2018), British statisticians

series, the percentage of outliers ($\%oA$ and $\%oB$) were assigned as a quality statistic. Exemplary for \mathcal{RR}_A , it is defined with equation (3.16) as

$$\%oA := \frac{\#\{D_A(i) \geq 4\}_{i=1}^{N_A-1}}{N_A - 1}. \quad (3.24)$$

The synchronization between both time series is assessed with the indicator $\%meanICC$. Although the ICC is maximized for each segment, an average value for each recording, denoted as $\%meanICC$ was computed. Further error calculation was done by calculating the root mean squared error (RMSE)

$$RMSE := \sqrt{\frac{1}{J} \sum_{i=1}^J DTS(i)^2}. \quad (3.25)$$

Additionally, five standard HRV parameters were calculated on both RR-series: Average NN-interval ($AVNN$), standard deviation of NN-intervals ($SDNN$), and root mean square of successive differences ($RMSSD$) from the time-domain methods (see section 2.3.2), the total power (totalP) and the low frequency to high frequency ratio (LF/HF) from the frequency-domain (see section 2.3.3).

3.4 Results

The multi-lead RR-interval computation algorithm was tested on 339 patients with matching reference RR-data (see figure 3.2).

	Total (n=339)	No AF (n=293)	AF (n=46)
$\%normA$	99.8 [94.9, 100.0]	99.8 [96.4, 100.0]	99.1 [93.4, 100.0]
$\%normB$	98.9 [87.1, 100.0]	99.0 [88.4, 100.0]	97.8 [85.9, 100.0]
$\%delSeg$	0.0 [0.0, 38.0]	0.0 [0.0, 26.9]	3.3 [0.0, 58.8]
$\%oA$	1.7 [0.3, 12.5]	1.8 [0.7, 11.0]	0.5 [0.0, 18.6]
$\%oB$	1.7 [0.2, 12.1]	1.8 [0.6, 11.3]	0.5 [0.0, 19.3]
$\%meanICC$	96.4 [76.6, 99.3]	96.7 [81.3, 99.3]	93.7 [15.2, 99.0]
$RMSE$ [ms]	7.5 [3.5, 87.3]	6.5 [3.4, 34.9]	45.9 [15.5, 176.0]

Table 3.2: Agreement indicators of both time series. Data presented as Median and 95% central range. The percentage of normal beats in \mathcal{RR}_A is represented by $\%normA$. In addition, the percentage of normal beats of the reference time series is given ($\%normB$). $\%oA$ and $\%oB$ specify the percentage of outliers in both time series. Deleted segments of 300 intervals each, are listed as $\%delSeg$. Although the intraclass correlation coefficient is maximized for each segment, an average value for each recording was computed $\%meanICC$. $RMSE$ denotes the root mean squared error.

Table 3.2 shows median values and the 95% central range for the first seven indicators. The study population was additionally split in two groups of patients, namely subjects with AF and without AF. The median values of the initial ratios of normal beats were close to 100% in both time series ($\%normA = 99.8$ and $\%normB = 98.9$). For the AF group, the reference annotations showed the smallest proportion of normal beats (97.8 [85.9, 100.0]). The median values of detected outliers were identical between both time series for the total population and throughout the groups. Moreover, the score of synchronization represented through $\%meanICC$ is 96.4 [76.6, 99.3]. The spread down to 15.2% for the 2.5th percentile of the AF group was remarkable. Excluding AF patients improves the $RMSE$ from 7.5 ms [3.5, 87.3] to 6.5 ms [3.4, 34.9].

The difference between outliers and ratio of initial normal beats for the total cohort are visualized in Bland-Altman plots in figure 3.8.

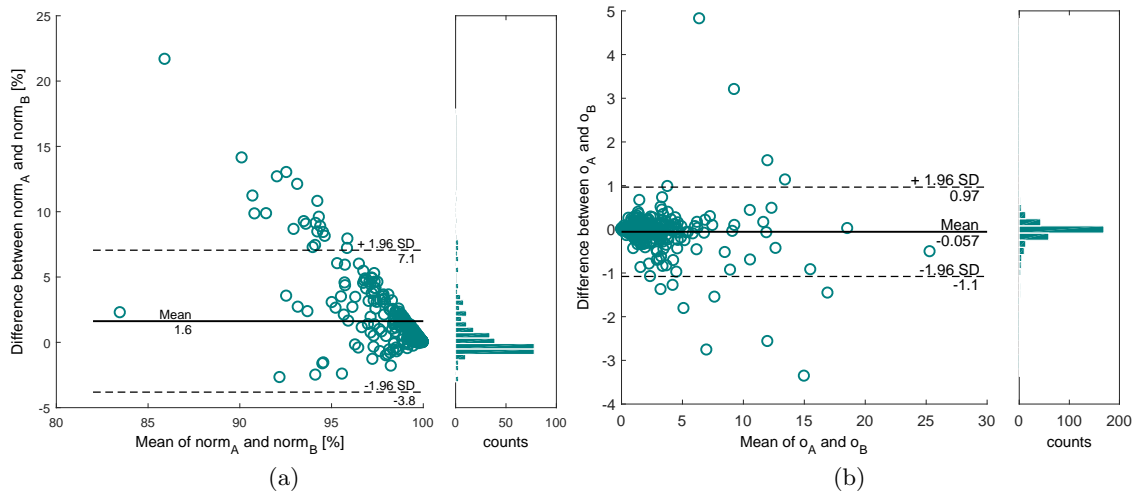


Figure 3.8: Bland-Altman plot of the (a) ratios of normal beats and (b) outliers. $normA$ represents the ratio of normal beats in RR_A and $normB$ the ratio of normal beats in RR_B , respectively. The ratios of outliers are specified as oA and oB .

HRV parameters calculated on the fully automated RR-series and the reference RR-interval series (RR_{Afs} and RR_{Bfs}) are listed in table 3.3. Five standard HRV parameters were calculated for subjects without AF ($n=293$). For RR_{Afs} the median of $RMSSD$ is 17.5 ms and for the reference time series 18 ms.

Furthermore, figure 3.9(a) shows a Bland-Altman plot of the parameter $RMSSD$. The limits of agreement range from -2.7 ms to 2.2 ms and their mean difference is -0.22 ms. The high similarity is underpinned by a quantile-quantile plot in figure 3.9(b). The linearity of datapoints suggests that data are equally distributed.

	Indices RR_{Afs}	Indices RR_{Bfs}
$AVNN$ [ms]	819 [606,1099]	819 [606,1099]
$SDNN$ [ms]	87.5 [45.4,170]	87.7 [45.6,171]
$RMSSD$ [ms]	17.5 [7.05,102]	18 [7.74,102]
$TotalP$ [ms^2]	8168 [2211,32828]	8130 [2184,32616]
LF/HF	1.92 [0.349,10.6]	1.84 [0.349,10]

Table 3.3: Median and central range values of selected HRV indices calculated on time series RR_{Afs} and RR_{Bfs} ($n = 293$, patients without atrial fibrillation), respectively. HRV indices are defined in section 2.3.

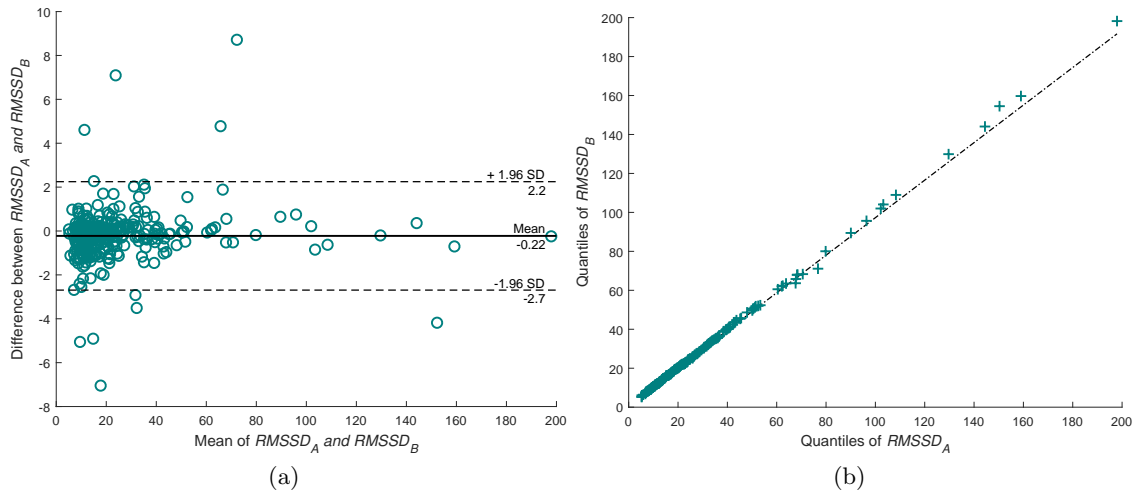


Figure 3.9: $RMSSD$ visualized as (a) Bland-Altman plot and (b) quantile-quantile plot. $RMSSD_A$ represents the $RMSSD$ of RR_A and $RMSSD_B$ the $RMSSD$ of RR_B , respectively.

3.5 Discussion

In this work, differences between an automatically obtained RR-interval series and a reference time series were examined. The results indicate a close match between both time series.

To be more precise, initially the ratio of normal beats shows a small difference between the reference annotations and the classification of the multi-lead correction algorithm. Although their mean difference is just 1.6%, a clear trend in the Bland-Altman plot (see figure 3.8(a)) is visible. Recordings with an average value of less than 92% of normal beats were less stringent classified in \mathcal{RR}_A . Furthermore, the gap is larger in patients with AF (see table 3.2).

Naturally, recordings with a high ratio of deleted segments ($\%delSeg$) contain a high number of accumulation points of artifacts. In the AF group, the 97.5th percentile ranges up to 58%. A benefit of segment deletion in contrast to the complete reject of a recording is the possible analysis of particular daytime periods. E.g., night hours, dialysis duration or other fragments can be analyzed if they are not affected. The use of clean data (normal RR-intervals) is especially of great interest for further HRV calculation [14]. Hence, outlier detection was performed using the IRF. This filter was already evaluated on 5-min records and is appropriate for biomedical signals, because it only modifies the signal in segments where an artifact is discovered [124].

Inspection of the Bland-Altman plot, figure 3.8(b), shows the perfect agreement of detected outliers between both time series. No trend and therefore, no systematic error is visible. On average, the ratio of initial normal beats was higher in \mathcal{RR}_A . As the percentage of outliers is the same in both RR-series, this means that more normal beats of \mathcal{RR}_A have been detected as outliers by the IRF. This high FP rate can be explained by the less stringent classification procedure of Bachler et al. [10], where class 1 represents the most frequent beats.

In comparison with [57], the outlier ratios in this study are higher. This discrepancy could be attributed to the different study participants (ESRD patients vs. young healthy subjects). Furthermore, the different recording lengths (24 h vs. maximum of 1 h). Even if the outlier detection is performed on segments of 300 beats, data from 24 h recordings can not be as smooth as in short-term recordings due to activities of daily living. Day/night changes and dialysis times are another influence. The lower number of outliers in AF patients is a result of the segment deletion procedure. As these recordings include a heaped number of not normal beats, the number of deleted segments is higher compared to the other group.

AF patients show considerably lower ICC values. Their 2.5th percentile spreads down to a value of 15.2%. Removal of subjects with AF increases the ICC to remarkable 96.4% [76.6,99.3]. García-González et al. observed a synchronization rate of 99% for 22 healthy subjects. However, remark the different measurement conditions (ambulatory vs. laboratory). Another major difference is the sampling frequency of 128 Hz in this study vs. 5 kHz.

The maximum feasible precision is determined by the sampling frequency. In detail, the error resolution is its reciprocal

$$\Delta t := \frac{1}{128 \text{ Hz}} \approx 8 \text{ ms.} \quad (3.26)$$

Figure 3.7 shows exemplarily the DTS and the feasible precision lines for one subject. The median of the RMSE is with 7.5 ms below Δt . The rather high value of the 97.5th percentile ($RMSE = 97.3$ ms) can again be attributed to the AF patients. Among them, their median value is 45.9 ms [15.5,176] compared to 6.5 ms [3.4,34.9] for subjects without AF.

García-González et al. investigated the dependency of an RR-interval series to the lead choice. Most prominent differences could be attributed to the different levels of noise among the leads [58]. In this work, the multi-lead correction algorithm overcomes this effect since only synchronized R-peaks in more than a third of all leads are remaining. Additionally, the computation of the multi-lead RR-series is more robust by using the median (see equation (3.12)).

For the calculation of HRV parameters, only sinus rhythm beats should be used. Ectopic beats are very common in AF [115]. Even a single ectopic beat can spoil the HRV assessment, particular the PSD estimation [117]. Hence, these beats must be removed [115], or edited by interpolation [158] or other filtering techniques [92]. According to Hogue et al., all portions of AF segments have to be removed [74]. Thus, the group of AF patients is excluded before performing HRV analysis.

HRV parameters calculated from the automated multi-lead RR-series showed a good agreement with the parameters calculated on the reference interval series (see table 3.3). Figure 3.9(a) shows no systematic difference and a negligible bias of -0.22 ms for the parameter $RMSSD$. Furthermore, the lines of agreement were below the feasible error resolution Δt . Other HRV parameters, as specified in table 3.3 are showing similar results with no systematic errors as well. Low $SDNN$ values (88 ms [46,170]) are in line with other studies in chronic kidney disease patients [28].

Covic et al. demonstrated the association between left ventricular hypertrophy (LVH) and cardiovascular mortality in dialysis patients [42]. Therefore, different ECG criteria were used. For the independent predictor “Novacode” QRS fiducial points from specified leads are needed [42, 71]. As a future perspective, missing detections in a specified lead can be obtained from the other leads, by extending the multi-lead correction algorithm. In particular, the inspection of QT-intervals and the corrected (heart rate independent) QTc-interval are of great interest for CKD patients [45].

Conclusion

In conclusion, this work showed great similarity between a fully automated multi-lead RR-series and a reference interval series, obtained by commercial equipment and manually reviewed. Moreover, no systemic differences between calculated HRV parameters of both series could be observed. In future investigations, the multi-lead correction algorithm could be used to make corrections in each single lead.

HRV Parameters for Risk Prediction

This chapter investigates nonlinear HRV parameters and their application in risk prediction. While the last chapter examined the automatic calculation of 24 h RR-interval data, this chapter exploits HRV data from a short and stable time period during the night.

Most results presented in this chapter were previously published in the article “Challenging Recently Published Parameter Sets for Entropy Measures in Risk Prediction for End-Stage Renal Disease Patients” (Hagmair et al. 2017 [68]).

4.1 State of the art

The variation of the heart rate can be used as a marker for the cardiovascular health status. This was already discovered more than 55 years ago, when changes in the beat-to-beat intervals were associated with fetal distress [76]. It can be defined as the initial point for the quantification of heart rate variability (HRV), which represents the variation of the heart rate and is based on normal-to-normal interbeat intervals.

A large number of HRV measures has been introduced in the second half of the 20th century. Exemplarily, the power spectral analysis in heart rate fluctuations was investigated by Akselrod et al. in 1981 [4]. Traditional HRV measures from the time and frequency domain have been most commonly used, but in the last two decades there was an increasing interest in nonlinear measures and methods from chaos theory. Sassi et al. discussed the contribution of fractal analysis, nonlinear dynamical systems, short-term complexity, and entropy to the understanding of HRV [165].

The usefulness of HRV for risk stratification has become more and more evident. Beginning in 1987, the association of low *SDNN* values and increased mortality in patients after MI was shown by Kleiger et al. [87]. Nine years later, the predictive value of the nonlinear parameter detrended fluctuation exponent was reported in patients with MI [16]. Furthermore, the prognostic information of HRV was demonstrated in other cohorts such as CHF patients [110], patients with CKD [32, 47], and patients undergoing hemodialysis [31, 36, 86, 174]. However, Sassi et al. highlighted in their review the gap between sophisticated signal processing algorithms by mathematicians and engineers on the one side and the limited success in clinical applications of the advanced HRV approaches [165].

Entropy measures are part of this new family quantifying the variability of the heart rate [75]. In 1991, Pincus introduced approximate entropy (*ApEn*) - a measure to quantify the amount of regularity in data [144]. In the same year, a clinical pilot study was conducted to test the performance of *ApEn* in clinical data [147]. *ApEn* showed significant differences between sick and healthy newborn. However, healthy ranges for the new parameter were not established at that time and values for given data can vary significantly with different parameters [147]. Boskovic et al. described in their work the flip-flop effect [23]. This effect specifies the reversed order of measures for some different parameters. E. g., assume the entropy of signal A is higher compared to the entropy of signal B for a fixed threshold parameter r . If the entropy of signal B is higher compared to signal A for a different input parameter r , it is termed flip-flop effect. Because of this inconsistency, Richman and Moorman made a further development: the sample entropy (*SampEn*), which does not count self-matches as *ApEn* does and is less dependent on dataset length [152]. Another enhancement was reported by Porta et al. and named as corrected approximate entropy (*CAPEn*) [148]. In contrast to *ApEn*, where self-matches lead to a bias to regularity, *CAPEn* penalizes self-matches in the opposite direction by adding information [148].

Further improvement of the entropy was done by Chen et al. in 2007, by replacement of the binary boundary decision with a modified exponential function, named fuzzy function [37]. Hence, the improved entropy named fuzzy entropy (*FuzzyEn*) still assesses the regularity of time series, but more independent from the selection of parameters, in particular the boundary radius r [37]. *FuzzyEn* was firstly applied to characterize an electromyogram (EMG), though Chen et al. mentioned the broad spectrum of applications in other noisy and relatively short physiological signals, due to its robustness to noise [37]. Finally, the fuzzy measure entropy (*FuzzyME*) was proposed particular for HRV analysis in 2013 [102]. This novel parameter makes use of both local and global

characteristics in heart-rate data and aims to reflect the entire complexity [102]. Liu et al. reported, that *FuzzyMEn* was the only entropy showing significant differences between 60 heart failure (HF) patients and a healthy control group of 60 subjects [102].

All entropies have the difficulty of parameter selection in common. Their choice is not trivial and controversially discussed. Especially, the threshold parameter r has to be determined with caution due to the flip-flop effect [23]. Over the last years, a great deal of research has focused on the selection of parameter sets for various applications [6, 30, 101, 108, 120, 121, 206]. The vast majority of the studies are mainly based on cross-sectional data. Together these studies provide important insights and agreements on some parameters. However, longitudinal evidence is still scarce [121].

4.2 Aim of the study

The aim of the study is to assess the predictive value of nonlinear HRV measures in patients undergoing hemodialysis. In particular, published parameter sets for different entropy measures are used for risk prediction in ESRD patients.

4.3 Methods

In this section, first the included patients and methods for baseline clinical assessments are described. The main focus of this section is the definition of the used entropy measures. At the end of this section, methods for the statistical and survival analyses are presented.

4.3.1 Study Population

Patients are a subgroup of the ISAR cohort, which is described in section 2.1. The flow chart of the study population is illustrated in figure 4.1. In total, 381 patients had usable RR-data in the determined time interval (2:00-2:30 am). Patients were excluded if they had an implanted cardiac pacemaker or a cardioverter-defibrillator pacing the heart ($n=27$), or atrial fibrillation ($n=54$). Only recordings with more than 75% sinus rhythm beats were eligible (20 recordings removed).

Baseline clinical data consists of age, height, weight and blood samples. At the time of enrollment, cardiovascular risk factors (diabetes, hypertension, and smoking) were obtained. A calculation of the adapted CCI alleviated the comparison of risk factors and comorbidities in statistical analyses. Based on the original CCI [34], Liu et al. improved the index for the mortality analysis in dialysis patients [103]. Due to incomplete clinical data, 15 patients were excluded for the final analysis ($n=265$).

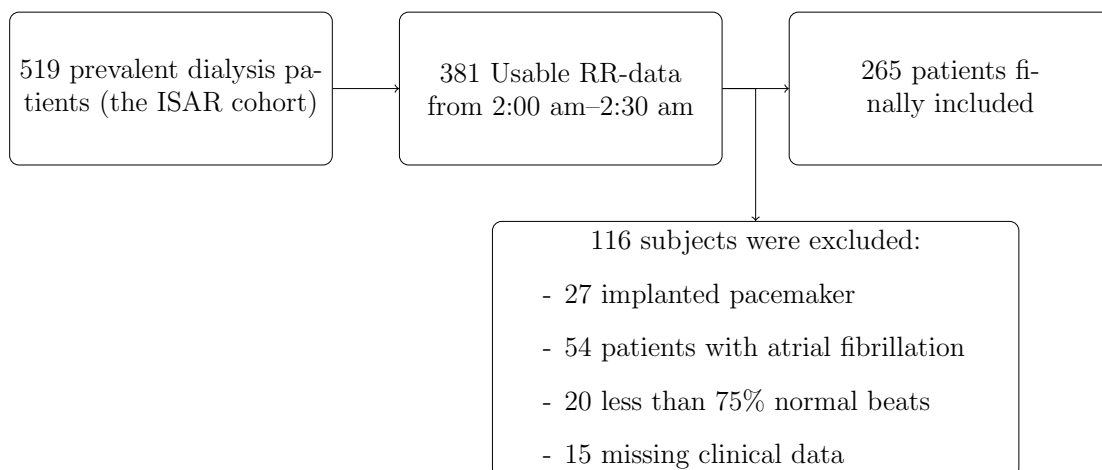


Figure 4.1: Flow chart of the study population.

4.3.2 HRV indices and entropy measures

At first, RR-interval data were filtered. According to Bauer et al., RR-intervals had to be between 300 ms and 2000 ms and consecutive differences less than 200 ms [12]. Moreover, RR-intervals with more than 20% difference to the mean of the last five preceding sinus RR-intervals were filtered [12]. To emphasize the usage of sinus beat intervals only, the filtered RR-interval series is named NN-interval series (i. e., normal-to-normal beat intervals).

For the calculation of HRV parameters, especially entropy measures, RR-interval data between 2.00 a.m. and 2.30 a.m. were used. This time interval was chosen, to ensure standardized conditions. Standard HRV parameters as in chapter 3 were also calculated on these NN-intervals. Additionally, a geometric measure the *HRVTI* (see section 2.3.2) was computed. Frequency domain parameters were obtained by means of the Lomb-Scargle periodogram (see section 2.3.3). All measures were computed on standard 5-min segments and averaged.

Entropy

In contrast to standard HRV parameters, nonlinear indices seem to be able to describe complex processes generated by biological systems in a more efficient way [150]. Entropies are one of these nonlinear methods, quantifying the regularity of RR-interval series.

Approximate entropy

The first measure of the complexity of a system is the approximate entropy ($ApEn$) introduced by Pincus [144]. Analytically, $ApEn$ is defined as

$$ApEn(m, r) := \lim_{N \rightarrow \infty} \phi^m(r) - \phi^{m+1}(r), \text{ where} \quad (4.1)$$

$$\phi^m(r) := \frac{1}{N - m + 1} \sum_{i=1}^{N-m+1} \log C_i^m(r). \quad (4.2)$$

Given the N data points of filtered RR-intervals, i. e., $NN(1), \dots, NN(N)$, the first step is a phase space reconstruction of vectors Y_1, \dots, Y_{N-m+1} with

$$Y_i := \{NN(i), NN(i+1), \dots, NN(i+m-1)\} \in \mathbb{R}^m. \quad (4.3)$$

The correlation between vectors is based on Grassberger and Procaccia [63, 64] defined with the Chebyshev¹ norm as

$$C_i^m(r) := \frac{1}{N - m + 1} \sum_{j=1}^{N-m+1} \Theta(r - \|Y_i - Y_j\|_\infty), \quad (4.4)$$

where r is the radius and Θ denotes the Heaviside² function.

Finally, the $ApEn$ for N data points is calculated as

$$ApEn(m, r, N) := \phi^m(r) - \phi^{m+1}(r). \quad (4.5)$$

Corrected approximate entropy

The occurrence of $\log(0)$ in equation (4.2) is avoided, since self-matches are counted in equation (4.4). Unfortunately, this leads to a bias and suggests more similarity than is present [152]. Hence, Porta et al. formulated the corrected approximate entropy ($CAPEn$) [148]. Considering only $N - m + 1$ patterns (for $\phi^{m+1}(r)$) in equation (4.5), $ApEn$ can be written as

$$\widetilde{ApEn} := -\frac{1}{N - m + 1} \sum_{i=1}^{N-m+1} \log \frac{N_i(m, r)}{N_i(m-1, r)}, \text{ where} \quad (4.6)$$

$$N_i(m, r) := \sum_{j=1}^{N-m+1} \Theta(r - \|Y_i - Y_j\|_\infty). \quad (4.7)$$

¹Pafnuty Chebyshev (1821–1894), Russian mathematician

²Oliver Heaviside (1850–1925), British mathematician and physicist

A self-match is defined by $N_i = 1$, since $N_i \in \mathbb{N}$ and for $i = j$ follows $\|Y_i - Y_j\|_\infty = 0$. Hence, $\Theta(r) = 1, \forall r > 0$.

If $N_i(m-1, r) = 1$ then $N_i(m, r) = 1$ follows, since

$$1 \leq N_i(m, r) \leq N_i(m-1, r) = 1. \quad (4.8)$$

The bias towards regularity ($\log(1) = 0$; insert equation (4.8) in equation (4.6)) is corrected by the final definition of the *CApEn*

$$CApEn(m, r, N) := \begin{cases} \log\left(\frac{1}{N-L+1}\right), & \text{if } N_i(m, r) = 1 \text{ or } N_i(m-1, r) = 1, \\ \widetilde{ApEn}, & \text{otherwise.} \end{cases} \quad (4.9)$$

Sample entropy

Richman and Moorman introduced the *SampEn*. It has a similar definition as the *ApEn*, but has reduced bias, because self-matches are excluded [152]. By analogy with equation (4.3), phase space vectors

$$x_m(i) := \{NN(i+k)\}_{k=0}^{m-1} = Y_i \in \mathbb{R}^m \text{ and} \quad (4.10)$$

$$x_{m+1}(i) := \{NN(i+k)\}_{k=0}^m \in \mathbb{R}^{m+1}, i = 1, \dots, N-m+1 \quad (4.11)$$

are computed. With the adapted correlations

$$B_i^m(r) := \frac{1}{N-m+1} \sum_{j=1, j \neq i}^{N-m} \Theta(r - \|x_m(i) - x_m(j)\|_\infty) \text{ and} \quad (4.12)$$

$$A_i^m(r) := \frac{1}{N-m+1} \sum_{j=1, j \neq i}^{N-m} \Theta(r - \|x_{m+1}(i) - x_{m+1}(j)\|_\infty), \quad (4.13)$$

the probability $B^m(r)$ that two sequences match for m points (or $A^m(r)$ for $m+1$ points) are calculated by averaging

$$B^m(r) := \frac{1}{N-m} \sum_{i=1}^{N-m} B_i^m(r) \text{ and } A^m(r) := \frac{1}{N-m} \sum_{i=1}^{N-m} A_i^m(r). \quad (4.14)$$

Finally, *SampEn* is defined as

$$SampEn(m, r, N) := -\log \frac{A^m(r)}{B^m(r)}. \quad (4.15)$$

Fuzzy entropy

$ApEn$, $CApEn$ and $SampEn$ are defined with the Heaviside function Θ , a binary discontinuous function $\Theta \in \{0, 1\}$. To avoid the high sensitivity to slight changes of r , Chen et al. made use of the fuzzy membership function $\mu(x)$, introduced by Zadeh [205] which associates each point x with a real number in the range $[0, 1]$ [37].

Chen et al. employed the function $x \mapsto \exp(-(x/r)^n)$ as membership function with its properties being continuous and convex [38]. Precisely,

$$\mu(d_{ij}, n, r) := \exp(-(d_{ij}^n/r)), \text{ where} \quad (4.16)$$

d_{ij} is the Chebyshev distance between vectors x_i^m and x_j^m , i. e., $d_{ij} = \left\| x_i^m - x_j^m \right\|_{\infty}$. These vectors are defined similar to equation (4.10), but the baseline is removed

$$x_i^m := \{NN(i+k)\}_{k=0}^{m-1} - \frac{1}{m} \sum_{j=0}^{m-1} NN(i+j). \quad (4.17)$$

The additional parameter n acts as weight of vector's similarity. Consequently, ϕ_i^m and ϕ_i^{m+1} are calculated without self-matches as

$$\phi_i^m(r) := \frac{1}{N-m-1} \sum_{j=1, j \neq i}^{N-m} \mu(d_{ij}, n, r). \quad (4.18)$$

By averaging

$$\phi^m(r) := \frac{1}{N-m} \sum_{i=1}^{N-m} \phi_i^m(r) \text{ and } \phi^{m+1}(r) := \frac{1}{N-m} \sum_{i=1}^{N-m} \phi_i^{m+1}(r) \quad (4.19)$$

$FuzzyEn$ is defined as

$$FuzzyEn(m, r, n, N) := \log \phi^m(r) - \log \phi^{m+1}(r) = -\log \frac{\phi^{m+1}(r)}{\phi^m(r)}. \quad (4.20)$$

Fuzzy measure entropy

In 2013, Liu et al. extended the $FuzzyEn$ to the fuzzy measure entropy ($FuzzyME_n$) by discriminating between local and global similarity. Local segment vectors are defined as in equation (4.17) $XL_m(i) := x_i^m$. For the global sequence segment, the mean value of the entire series is subtracted

$$XF_m(i) := \{NN(i+k)\}_{k=0}^{m-1} - \frac{1}{N} \sum_{j=1}^N NN(j). \quad (4.21)$$

Local and global distances can be calculated as

$$dL_m(i, j) = \|XL_m(i) - XL_m(j)\|_\infty \text{ and} \quad (4.22)$$

$$dF_m(i, j) = \|XF_m(i) - XF_m(j)\|_\infty. \quad (4.23)$$

$$(4.24)$$

Consequently, a local $\mu_L(dL_m(i, j), n_L, r_L)$ and global $\mu_F(dF_m(i, j), n_F, r_F)$ fuzzy function is obtained with equation (4.16).

Steps (4.18)-(4.19) are calculated with local and global fuzzy functions. Finally, *FuzzyME* is defined as

$$FuzzyME(m, n_L, r_L, n_F, r_F, N) := -\log \frac{\phi L^{m+1}(r)}{\phi L^m(r)} - \log \frac{\phi F^{m+1}(r)}{\phi F^m(r)}. \quad (4.25)$$

Entropy parameter selection

Most of the entropies should be calculated on a time series of length $N > 200$ [5, 152, 206] due to the sensitivity. For particular distance thresholds the recording length should fulfill $N > 1000$ [120]. To ensure this condition, NN-intervals of 30 min of each recording were taken. A typical resting heart rate of 60 beats per minute results a time series length of 1800 data points.

For the template length, i. e., embedding dimension, $m = 2$ was chosen. This is in accordance with most of other studies [6, 38, 39, 102, 120, 144, 145, 203, 206].

Another parameter needed for the calculation of all entropies is the distance threshold (or radius) r . There are different suggestions for the choice of r , depending on the data. One approach is to fix a value $r \in [0.1 \cdot \sigma, 0.25 \cdot \sigma]$, where σ denotes the standard deviation (SD) of the time series [144, 146, 203]. Chon et al. used Monte Carlo simulations to maximize the entropy *ApEn* and hence obtained an optimal threshold r_{Chon} for a fixed m [39]. In this work, each entropy is calculated with two different threshold parameters:

- $r_{\text{Chon}} := \hat{r}_{\text{max}}(m = 2)$ as defined in equation (2) in [39], and
- $r_\sigma := 0.2 \cdot \sigma$.

The fuzzy entropies need a further parameter, the gradient n as weight for the fuzzy function. According to Chen et al., a larger n weights more the closer vectors [38]. Though, a large n leads to missing detailed information [38]. Mayer et al. tried different weighting factors in the interval [1, 6] according to a fixed radius. For $r = r_{\text{Chon}}$ best results with $n_L = 2, n_F = 1$ were achieved, when discriminating between nonpathological and pathological data. For $r = r_\sigma$, optimal weighting factors resulted in $n_L = 1, n_F = 3$

(see Tables 1-2 [120]). This setup was also used in this work.

Table 4.1 summarizes the parameters for the entropy calculation. Each entropy H is calculated twice: once with the parameters based on r_{Chon} ; on the other hand with parameters for r_{σ} .

	$r = r_L = r_F$	m	$n = n_L$	n_F
$H(r_{\text{Chon}})$	r_{Chon}	2	2	1
$H(r_{\sigma})$	$0.2 \cdot \sigma$	2	1	3

Table 4.1: Parameter sets used for each entropy H calculation. Template length m , the weighting factor(s) n , n_L and n_F , and the threshold parameter(s) r , r_L and r_F .

4.3.3 Statistics

Baseline continuous data are presented as mean and SD for normally distributed data. Otherwise the median and inter-quartile range (IQR) are shown. Categorical baseline data are summarized as number and percentage. Group differences were assessed by the t-test for normally distributed data. Otherwise, the Wilcoxon³ rank-sum test was used. Normality was tested using the Kolmogorov-Smirnov test. All-cause mortality was defined as the endpoint.

Cox⁴ proportional hazard models were used to determine hazard ratios and their 95% confidence interval (CI) [43]. Variables for the Cox models were visually inspected and skewed data was transformed by a standard logarithmic transformation. Only *CApEn* was transformed with a Box-Cox transformation, i. e., power transformation [25]. Univariate Cox regression analyses were performed to identify associations between variables and all-cause mortality, which defined the end point in this work. Univariate significant predictors were adjusted according to parameters from literature (Model A) and for covariates significant in univariate analysis (Model B). In detail, Suzuki et al. extracted age, serum albumin, hsCRP, and calcium \times phosphate as independent risk factors in ESRD patients [174]. These parameters define model A in this work.

Furthermore, interactions between risk predictors and heart disease (HD) status (defined as the presence of heart failure, valvular HD or other heart/vascular diseases) were identified by interaction terms. Detailed subgroup analysis, based on heart disease (HD) status was carried out for (borderline) significant interaction terms. All computations

³Frank Wilcoxon (1892–1965), Irish American chemist and statistician.

⁴Sir David Roxbee Cox (1924–), British statistician

were performed using MATLAB (The MathWorks, Inc., Natick, MA, USA; R2016b). Statistical significance was declared, if the p-value was smaller than 0.05.

4.4 Results

The median follow-up time of the included 265 patients was 43 months. During follow-up, 70 subjects died (26%). Mean age of the study population was 62 years and two thirds were men. Of the included subjects, 94% showed a presence of hypertension. Furthermore, the use of antihypertensive drugs was very common (89%). The median duration per dialysis session was 4.23 h. Baseline characteristics of the included 265 subjects are summarized in table 4.2.

Traditional HRV parameters as well as entropy measures calculated at baseline, are presented in table 4.3.

In table 4.4, hazard ratios (HRs) of all significant risk predictors (defined as model B) of the univariate Cox models are presented. Adapted CCI and high-sensitivity C-reactive protein (hsCRP) showed the highest HRs with values of 1.24 (1.16, 1.33) and 1.26 (1.02, 1.56), respectively. Consequently, an increase of one increased the risk of death about 25% for one of either variable. The hazard ratio of the dialysis duration per session 0.52 (0.30, 0.89) showed a smaller mortality risk for longer dialysis duration. I. e., the chance of survival is almost doubled if the dialysis session is extended by one hour.

The unadjusted hazard ratios of HRV and entropy measures are shown in table 4.5. Significant predictor variables were adjusted with both models. $SDNN$, $HRVTI$, LF , LF/HF , and $totalP$ of the traditional HRV measures predicted mortality significantly in univariate analysis. LF (HR 0.82; 95% CI 0.69 to 0.96; $p=0.01$ in univariate analysis) was significantly associated with mortality after adjustment with each of the two models ($p=0.05$ and $p=0.04$). LF/HF remained a significant predictor after adjustment with model B and borderline significant power after adjustment with model A. The $HR < 1$ showed that a higher ratio of LF/HF is associated with an increased chance of survival.

Only two of the entropy measures, namely $FuzzyEn$ and $CApEn$ significantly predicted mortality in univariate analysis. But only if the radius is set to the entropy maximizing parameter r_{Chon} . Both entropies retained significant risk predictors after adjusting with parameters from literature (Model A). After adjustment with Model B, none of the entropies was a significant predictor of mortality.

Variable	All Data, $n = 265$
Age (years)	62 (15.1 SD)
Sex—male, n (%)	175 (66%)
Body weight (kg)	77.1 (19 SD)
Height (m)	1.71 (0.08 SD)
Body mass index (kg/m ²)	25 [22.5, 28.7]
Presence of diabetes, n (%)	92 (35%)
Presence of hypertension, n (%)	250 (94%)
Current smokers, n (%)	72 (27 %)
Adapted CCI (-)	2 [1,5]
Dialysis vintage (mo)	47.3 [23.8, 79.4]
Dialysis duration per session (h)	4.23 [4.02, 4.55]
UFV (mL)	2196 (1157 SD)
Kt/V (-)	1.47 (0.40 SD)
Serum albumin (g/dl)	4.03 (0.40 SD)
hsCRP (mg/dL)	0.37 [0.16, 0.89]
Total cholesterol (mg/dl)	181 (44.8 SD)
HDL cholesterol (mg/dl)	42 [36, 52]
LDL cholesterol (mg/dl)	112 (36 SD)
Calcium \times phosphate (mmol ² /L ²)	3.94 (1.13 SD)
Antihypertensive drugs, n (%)	237 (89%)
Statins, n (%)	97 (37%)
Anticoagulant, n (%)	29 (11%)

Table 4.2: Baseline data of included patients. Data given as number (%) for categorical. Continuous data is presented as mean (SD) or median [IQR].

CCI = Charlson comorbidity index; mo = months; UFV = ultrafiltration volume; hsCRP = high-sensitivity C-reactive protein; Kt/V = dialyzer clearance of urea \cdot dialysis time/volume of distribution of urea; HDL = high-density lipoprotein; LDL = low-density lipoprotein.

HRV Parameters	All Data, $n = 265$
$AVNN$ (ms)	887 (131 SD)
$SDNN$ (ms)	33.9 (17.5 SD)
$RMSSD$ (ms)	13.4 [9.42, 20.2]
$pNN50$ (%)	0.54 [0.08, 2.48]
$HRVTI$ (-)	30.3 (9.84 SD)
$TotalP$ (ms^2)	1090 [495, 2198]
LF (ms^2)	189 [72, 461]
HF (ms^2)	59.9 [25.6, 158]
LF/HF (-)	3.21 [1.37, 6.41]
Entropies	
$ApEn(r_{Chon})$ (-)	0.34 [0.18, 0.53]
$ApEn(r_\sigma)$ (-)	1.05 (0.294 SD)
$SampEn(r_{Chon})$ (-)	3.36 (0.597 SD)
$SampEn(r_\sigma)$ (-)	0.97 (0.35 SD)
$FuzzyEn(r_{Chon})$ (-)	3.58 (0.58 SD)
$FuzzyEn(r_\sigma)$ (-)	0.69 (0.24 SD)
$FuzzyMEn(r_{Chon})$ (-)	6.95 [6.29, 7.74]
$FuzzyMEn(r_\sigma)$ (-)	1.61 (0.55 SD)
$CApEn(r_{Chon})$ (-)	7.4 [7.23, 7.53]
$CApEn(r_\sigma)$ (-)	1.36 (0.49 SD)

Table 4.3: Heart rate variability (HRV) parameters of the time and frequency domain and entropy measures at baseline. Data given as mean (SD) or median [IQR]. HRV Parameters defined in section 2.3. Entropies defined in section 4.3.2.

Interaction analysis revealed borderline significant interactions between the entropy measures and the HD status ($p \in [0.06, 0.08]$, if $r = r_\sigma$ was chosen). Hence, the cohort was divided into two groups and a subgroup analysis was performed. The group without HD consists of 99 patients with 32 events. In the second group (with HD), 166 subjects with 38 events are included. Table 4.6 shows HRV parameters for each group at baseline as well as significant differences between these groups.

As a result, the entropy measures were separately tested for their predictive power in the two subgroups (see table 4.7). For patients without HD, none of the entropies was a significant predictor of mortality. On the other hand, considering the subgroup of HD patients all entropies except $CApEn$ predicted mortality significantly, if the radius was defined with the SD: $r = r_\sigma = 0.2 \cdot \sigma$. The entropies remained independent risk factors in the HD subgroup, no matter which adjustment model was chosen (see table 4.8).

Additionally, figure 4.2 illustrates the HRs of all entropy measures for the total cohort

Predictors — Model B	Unit	HR (95% CI)	<i>p</i>
Age*	1 year	1.05 (1.03, 1.07)	< 0.001
Height	1 cm	0.97 (0.94, 1.00)	0.04
Adapted CCI	1	1.24 (1.16, 1.33)	< 0.001
Dialysis duration per session	1 h	0.52 (0.30, 0.89)	0.02
Serum albumin*	1 g/dL	0.24 (0.13, 0.45)	< 0.001
hsCRP*	log(1 mg/dL)	1.26 (1.02, 1.56)	0.04
Anticoagulant	No/Yes	0.31 (0.17, 0.55)	< 0.001

Table 4.4: Significant univariate predictors of mortality: conventional risk factors ($n = 265$). HR = hazard ratio; CI = confidence interval; CCI = Charlson comorbidity index; hsCRP = high-sensitivity C-reactive protein. * indicates the significant predictors found in a similar study [174].

and the subgroups with and without HD. Adjusted HRs with both models are illustrated, if univariate analysis was significant.

4.5 Discussion

Several studies have shown the importance of parameter selection for different entropy measures [38, 102, 203, 206]. In this work, recently published parameter sets [120, 121] were challenged in their prediction value in a very special cohort. I.e., without optimization for the present data, entropy measures were used for risk prediction in high-risk patients, namely hemodialysis patients, with a five year survival of around 40% [162].

Baseline clinical and traditional HRV data were in agreement with a similar HRV study, except the measure *SDNN* which was around 2.5 times lower in this work [174]. The discrepancy is a result of the different data length and time of the day, which was 24 h in the study of Suzuki et al. opposed to 30 min in 5 min segments in the present study. This is underpinned by the fact that the 24 h *SDNN* measure is in agreement with the Japanese ESRD cohort (see table 3.3). Furthermore, the lower *SDNN* values at night are in line with the work of Rubinger et al. [154].

Univariate Cox regression analysis revealed known clinical- and dialysis-related risk factors in ESRD patients [41]. Age, albumin, and C-reactive protein (CRP) independently predicted mortality (compare table 4.4) and were used in adjustment models. All HRV measures with predictive power had a hazard ratio below one. As a higher HRV reflects the faster and more flexible adaption to internal and external influences, it is associated with an increased chance of survival. *SDNN*, *HRVTI*, *LF*, and *LF/HF* were identified as significant risk predictors for all-cause mortality. After adjustment with both

Variable	Unit	Unadjusted		Model A		Model B	
		HR (95% CI)	<i>p</i>	HR (95% CI)	<i>p</i>	HR (95% CI)	<i>p</i>
<i>AVNN</i>	10 ms	1.01 (0.99, 1.03)	0.3	-	-	-	-
<i>SDNN</i>	log(ms)	0.66 (0.43, 1.01)	0.05	0.76 (0.47, 1.21)	0.25	0.67 (0.41, 1.10)	0.12
<i>RMSSD</i>	log(ms)	0.94 (0.63, 1.40)	0.75	-	-	-	-
<i>pNN50</i>	log(%)	1.02 (0.97, 1.07)	0.51	-	-	-	-
<i>HRVTI</i>	1	0.97 (0.94, 0.99)	0.01	0.98 (0.95, 1.00)	0.07	0.98 (0.95, 1.01)	0.12
<i>TotalP</i>	log(ms ²)	0.81 (0.65, 0.99)	0.04	0.87 (0.69, 1.10)	0.25	0.83 (0.65, 1.05)	0.12
<i>LF</i>	log(ms ²)	0.82 (0.69, 0.96)	0.01	0.84 (0.70, 1.00)	0.05	0.82 (0.68, 0.99)	0.04
<i>HF</i>	log(ms ²)	1.02 (0.85, 1.22)	0.84	-	-	-	-
<i>LF/HF</i>	1	0.74 (0.60, 0.90)	0.003	0.82 (0.66, 1.01)	0.06	0.74 (0.59, 0.92)	0.007
<i>ApEn(r_{Chon})</i>	log(1)	1.30 (0.95, 1.77)	0.1	-	-	-	-
<i>ApEn(r_σ)</i>	1	0.55 (0.25, 1.23)	0.15	-	-	-	-
<i>SampEn(r_{Chon})</i>	1	0.68 (0.45, 1.03)	0.07	-	-	-	-
<i>SampEn(r_σ)</i>	1	0.55 (0.27, 1.10)	0.09	-	-	-	-
<i>FuzzyEn(r_{Chon})</i>	1	0.59 (0.39, 0.90)	0.01	0.58 (0.37, 0.92)	0.02	0.65 (0.41, 1.04)	0.07
<i>FuzzyEn(r_σ)</i>	log(1)	0.65 (0.33, 1.27)	0.21	-	-	-	-
<i>FuzzyMEn(r_{Chon})</i>	log(1)	0.32 (0.09, 1.13)	0.08	-	-	-	-
<i>FuzzyMEn(r_σ)</i>	1	0.74 (0.48, 1.15)	0.18	-	-	-	-
<i>CApEn(r_{Chon})</i>	◇	0.91 (0.84, 0.98)	0.01	0.92 (0.84, 1.00)	0.04	0.92 (0.84, 1.01)	0.08
<i>CApEn(r_σ)</i>	1	0.90 (0.55, 1.47)	0.67	-	-	-	-

Table 4.5: Unadjusted and adjusted hazard ratios of heart rate variability (HRV) parameters ($n = 265$). ◇ Data was Box-Cox transformed with $\lambda = 13.81$ and divided by 1×10^{10} .

models only *LF* and *LF/HF* remained (borderline) significant. These results are in agreement with those obtained by Suzuki et al. [174], except for *LF*. Results from both studies differ from findings in post-myocardial infarction patients that traditional HRV measures have independent predictive power presented in [15, 87, 153, 207]. According to Suzuki et al., this contradiction may be attributed to the fact that post myocardial infarction studies did not adjust for albumin and CRP. The association of those clinical risk factors and cardiac vagal dysfunction could have annihilated the predictive power of traditional HRV measures [174].

For the nonlinear HRV measures, Suzuki et al. identified a decreased scaling exponent α_1 , a chaos descriptor of detrended fluctuation analysis, as an independent risk predictor in hemodialysis patients [174]. In this work, the measures to quantify chaotic properties in HRV are represented by the entropies. As a measure of unpredictability, a reduced entropy reflects an impairment of the heart rate regulation. Throughout, entropies with significant predictive power showed a HR below one (see tables 4.5, 4.7, and 4.8).

Reduced HRV for the HD group in comparison to the group without HD is shown in table 4.6. *SDNN*, *ApEn(r_σ)*, *SampEn(r_σ)*, and *FuzzyEn(r_{Chon})* showed (borderline)

	No HD ($n = 166$)	HD ($n = 99$)	p
<i>AVNN</i> (ms)	886 (130 SD)	889 (132 SD)	0.85
<i>SDNN</i> (ms)	35.4 (19 SD)	31.5 (14.5 SD)	0.06
<i>RMSSD</i> (ms)	13.7 [9.12,22.3]	12.3 [9.59,18.6]	0.24
<i>pNN50</i> (%)	0.55 [0.06,2.91]	0.48 [0.1,1.78]	0.85
<i>HRVTI</i> (-)	31.1 (10.3 SD)	29 (8.93 SD)	0.09
<i>TotalP</i> (ms ²)	1177 [495,2311]	924 [483,1800]	0.22
<i>LF</i> (ms ²)	212 [57,500]	160 [95,353]	0.46
<i>HF</i> (ms ²)	63.3 [25.3,172]	54 [27.7,134]	0.33
<i>LF/HF</i> (-)	2.87 [1.32,6.76]	3.35 [1.52,5.85]	0.59
<i>ApEn</i> (r_{Chon}) (-)	0.33 [0.17,0.53]	0.34 [0.21,0.52]	0.11
<i>ApEn</i> (r_{σ}) (-)	1.08 (0.28 SD)	1.01 (0.31 SD)	0.06
<i>SampEn</i> (r_{Chon}) (-)	3.38 (0.58 SD)	3.32 (0.63 SD)	0.44
<i>SampEn</i> (r_{σ}) (-)	1 (0.33 SD)	0.913 (0.36 SD)	0.05
<i>FuzzyEn</i> (r_{Chon}) (-)	3.64 (0.6 SD)	3.49 (0.55 SD)	0.05
<i>FuzzyEn</i> (r_{σ}) (-)	0.71 (0.24 SD)	0.66 (0.24 SD)	0.14
<i>FuzzyMEn</i> (r_{Chon}) (-)	7.06 [6.3,7.96]	6.74 [6.14,7.62]	0.08
<i>FuzzyMEn</i> (r_{σ}) (-)	1.65 (0.54 SD)	1.53 (0.57 SD)	0.08
<i>CApEn</i> (r_{Chon}) (-)	7.4 [7.22,7.54]	7.39 [7.25,7.48]	0.32
<i>CApEn</i> (r_{σ}) (-)	1.38 (0.47 SD)	1.32 (0.52 SD)	0.31

Table 4.6: Heart rate variability (HRV) parameters of the time and frequency domain and entropy measures at baseline for patients without heart disease (HD) and patients with HD. Data are given as mean (SD) or median [IQR].

significant differences. Another interesting observation is the choice of the radius for the entropy calculation. For the total study population, only entropy measures calculated using r_{Chon} showed significant predictive power. The opposite is true for the HD subgroup, where only entropies with r_{σ} achieved these results. It was found that using r_{Chon} captured effects in the entire cohort, but only resulted in a small change of particular entropy values. As a result, statistical significance was only reached in the complete cohort due to the larger sample size. One unanticipated finding was the vice versa situation in the HD group as only entropy values with r_{σ} achieved significant predictive power. Further investigations are needed to determine these effects. A limitation of this work is the number of covariates (7 in Model B) used for adjustment in relation to the number of fatal events in the subgroup analysis. Hence, these subgroup results should be interpreted with caution.

With regards to the illustrated HRs, their interpretation for transformed variables is not

Variable	Unit	no HD (n=166)		HD (n=99)	
		HR (95% CI)	<i>p</i>	HR (95% CI)	<i>p</i>
$ApEn(r_{Chon})$	log(1)	1.28 (0.85, 1.90)	0.23	1.27 (0.76, 2.11)	0.37
$ApEn(r_\sigma)$	1	1.21 (0.39, 3.77)	0.74	0.29 (0.09, 0.91)	0.03
$SampEn(r_{Chon})$	1	0.78 (0.44, 1.40)	0.41	0.64 (0.36, 1.12)	0.11
$SampEn(r_\sigma)$	1	1.04 (0.40, 2.73)	0.93	0.31 (0.11, 0.90)	0.03
$FuzzyEn(r_{Chon})$	1	0.66 (0.38, 1.14)	0.14	0.56 (0.30, 1.06)	0.08
$FuzzyEn(r_\sigma)$	log(1)	1.23 (0.46, 3.26)	0.67	0.39 (0.15, 1.00)	0.05
$FuzzyMEn(r_{Chon})$	log(1)	0.63 (0.12, 3.45)	0.60	0.19 (0.03, 1.18)	0.08
$FuzzyMEn(r_\sigma)$	1	1.12 (0.62, 2.03)	0.71	0.50 (0.25, 0.99)	0.05
$CApEn(r_{Chon})$	◇	0.99 (0.98, 1.00)	0.10	0.99 (0.98, 1.00)	0.06
$CApEn(r_\sigma)$	1	1.43 (0.74, 2.77)	0.29	0.57 (0.27, 1.20)	0.14

Table 4.7: Unadjusted hazard ratios of entropies for the subgroup patients without heart disease (no HD) and with heart disease. ◇ Data was Box-Cox transformed with $\lambda = 13.81$ and divided by 1×10^{10} .

Variable	Unadjusted		Model A		Model B	
	HR (95% CI)	<i>p</i>	HR (95% CI)	<i>p</i>	HR (95% CI)	<i>p</i>
$ApEn$	0.29 (0.09, 0.91)	0.03	0.13 (0.04, 0.44)	0.001	0.20 (0.05, 0.82)	0.02
$SampEn$	0.31 (0.11, 0.90)	0.03	0.15 (0.05, 0.46)	< 0.001	0.22 (0.06, 0.81)	0.02
$FuzzyEn^\dagger$	0.39 (0.15, 1.00)	0.05	0.21 (0.07, 0.58)	0.003	0.32 (0.10, 0.99)	0.05
$FuzzyMEn$	0.50 (0.25, 0.99)	0.05	0.32 (0.16, 0.67)	0.002	0.43 (0.19, 0.96)	0.04
$CApEn$	0.57 (0.27, 1.20)	0.14	-	-	-	-

Table 4.8: Unadjusted and adjusted HRs of entropies ($r = r_\sigma$) for the subgroup patients with heart disease (n=99). † indicates logarithmic transformation.

straightforward. For an untransformed predictor, one unit increase (holding all other variables constant) is associated with the hazard being multiplied by the respective HR value. HRs quantify the risk of additive changes of the predictor in contrast to multiplicative changes of the predictor for log-transformations. For a (natural) logarithmic-transformed predictor, an exponential-fold relative increase is associated with the hazard being multiplied by the respective HR value. However, there is no such demonstrative interpretation after a Box-Cox transformation [25]. The corrected approximate entropy calculated with the entropy maximizing parameter ($CApEn(r_{Chon})$) was Box-Cox transformed because of its right skewed distribution. According to Altman, the extreme values of variables with skewed distribution have a disproportionate effect on the Cox model [7]. Hence, $CApEn(r_{Chon})$ was transformed and a relation of absolute values and mortality needs to be interpreted carefully.

The generalizability of these results is subject to certain limitations. For instance, all participants were from dialysis centers in Munich and the suburban area and mainly Caucasians. Hence, deductions to other populations are limited. Second, as all-cause mortality was defined as study endpoint, the association of decreased HRV entropy with the specific pathologic causes of death is blurry. Furthermore, the association of low entropy values with simple poor clinical conditions seems more than unlikely, since the prognostic association of significant risk predictors was independent of clinical risk factors (Model A). Moreover, the number of fatal events was very low in subgroups divided based on the HD status. Hence, results depending on full adjustment models have to be interpreted with caution. Finally, this study suggests that entropies may be useful for risk prediction in ESRD patients, but it is unclear whether reduced entropy is treatable and modifiable by treatment to reduce risk. This fact needs further investigation.

Conclusion

In conclusion, the results of the study show that nonlinear HRV parameters are risk predictors for mortality in ESRD patients. In particular, entropy measures calculated with two parameter sets, significantly predict mortality. However, different entropy measures and the different parameter sets detect diverse effects in the RR-data. These results provide additional insights into the choice of parameters for these indicators and showed their value for risk prediction. This work shows the potential of entropy measures for risk stratification for future clinical application. Further research in this field would be of great help for patients on hemodialysis.

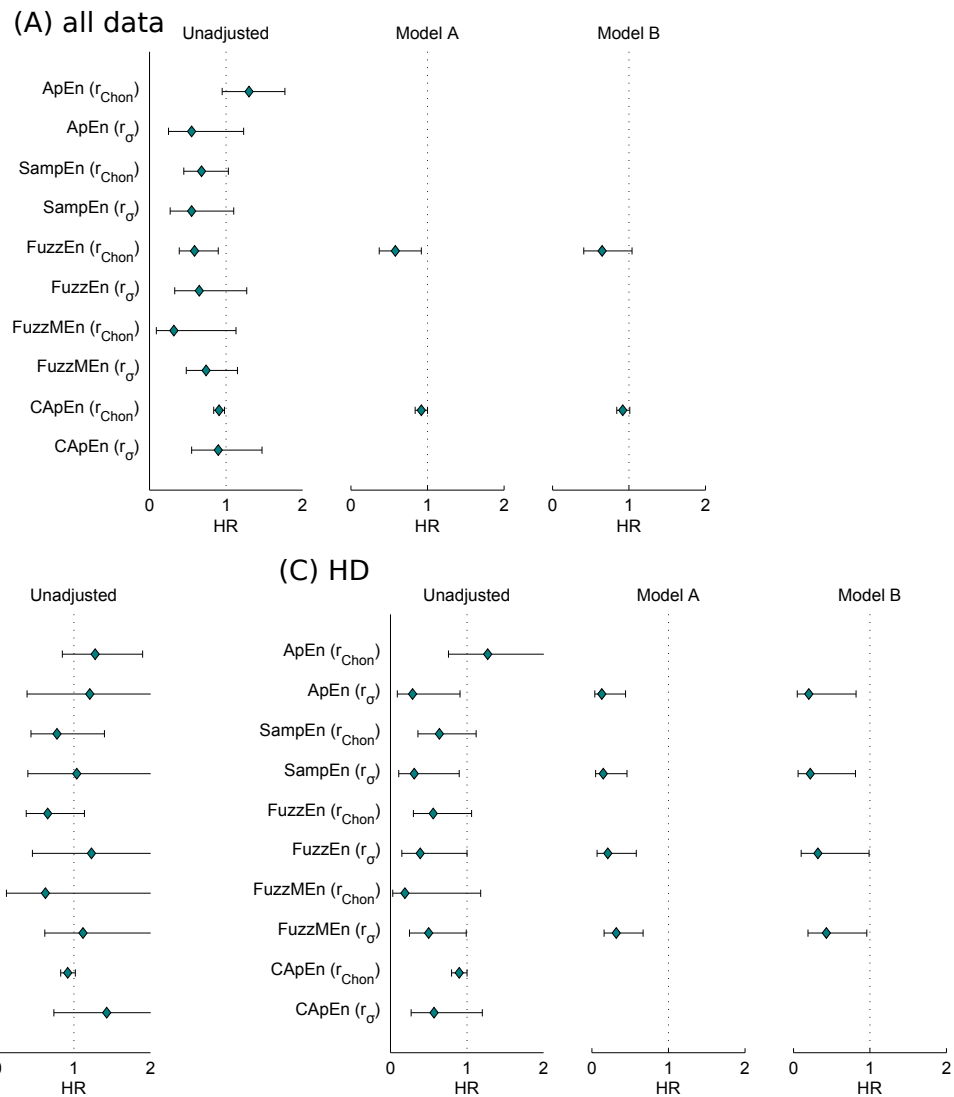


Figure 4.2: Hazard ratios (HRs) for (A) all 265 subjects; (B) subgroup of patients without heart disease (no HD; $n = 166$); and (C) patients with HD ($n = 99$). The HR for each entropy measure is visualized as diamond with corresponding 95% confidence interval.

Combined Pulse Wave and ECG Analysis

In the last chapter, different HRV parameters - mainly entropies - were used for risk stratification. This chapter begins by modeling survival outcome solely by PWA parameters. It will then go on to the main issue addressed in this work: the combined risk prediction and survival analysis of parameters obtained by PWA and HRV parameters (derived from the ECG).

5.1 State of the art

Dialysis patients have a 10 to 30 times higher mortality risk due to CVD than the general population [50, 164]. Hypertension is a formidable worldwide public-health problem due to high prevalence and concomitant risks of cardiovascular and kidney disease [84]. Especially in hemodialysis patients, hypertension is highly prevalent [2]. Hence, BP control is of great interest [3] and guidelines for the management of hypertension suggest ABPM as gold standard for the diagnosis of hypertension [112, 161].

Additional indices may be derived from ABPM, such as pulse wave velocity (PWV) or augmentation index (AIx). Carotid-femoral PWV has become an established parameter for the evaluation of arterial stiffness [112, 182]. Several studies showed that increased aortic stiffness, assessed by elevated PWV, is a predictor for mortality in ESRD patients [19, 20, 66, 140, 170]. In addition, systematic reviews summarize the association between aortic PWV and clinical endpoints [13, 185].

The AIx quantifies the wave reflections from arterial peripheral site [112]. The relationship between mortality and AIx in hemodialysis patients was as well demonstrated

[106]. *PP* amplification, a manifestation of arterial stiffness and arterial wave reflections predicted overall mortality in ESRD subjects [156].

In contrast to previous studies, the prevalent age group of hemodialysis patients is nowadays significantly older [126, 138, 162]. Recently, Sarafidis et al. investigated 170 hemodialysis patients with ambulatory 48 h recordings [160]. Furthermore, Koutroumbas et al. conducted a study where ABPM was performed for a 72 h period including the dialysis session and the subsequent interdialytic interval [91]. In both studies, the parameters were derived by the Mobil-O-Graph monitor and the mean age of the cohorts was approximately 64 ± 14 years [91, 160]. Increased risk during the third interdialytic day attended by significantly elevated AIx and PWV levels was reported [91].

The usefulness of HRV for risk stratification is already discussed in section 4.1. Exemplarily, the following studies investigated the prognostic value of HRV in hemodialysis patients [31, 36, 55, 72, 86, 174].

To the best of our knowledge, no previous study investigated risk prediction of the combined HRV and pulse wave parameters in ESRD patients. The only relevant study regarding risk stratification of combined ECG parameters and PWV was conducted in a CKD cohort [33]. Chandra et al. investigated the inverse relationship between HRV and PWV in 240 CKD patients and considered compositional outcomes consisting of CVD events, deaths and progression to ESRD [33]. They found that the risk of CVD or death was highest for patients with both: low HRV and high PWV. However, the number of deaths was low in this cohort ($n = 9$) leading to the definition of composite outcome of CVD or death in this study.

Besides the prediction variables, most of the studies with time-to-event data have in common that analysis was conducted with Cox proportional hazard models. These linear models allow simple interpretation of risks. However, they force a specific link between covariates and the response and in reality there is often no linear relation. Moreover, interactions between covariates can be incorporated, though must be specified by the analyst. Tree structured survival models can automatically detect interactions without the need to specify them in advance [24]. In addition, tree based methods group subjects with relatively homogeneous survival probabilities based on their covariates [97]. A further advantage is redundancy of logarithmic or more general monotonic transformations due to invariance.

Around the middle 1980s, researchers began to extend existing recursive partition schemes to survival data [40, 62]. Further developments, such as pruning algorithms to select

the tree complexity, were proposed in the following decade [96]. LeBlanc and Crowley carried out a review of survival trees in 1995 [97]. In recent years, there has been a focus on the development of multivariate survival trees [29]. Furthermore, in constructing conditional inference trees with stopping rules [77].

5.2 Aim of the study

The aim of this study is to combine the information from two noninvasive signals, namely the pulse wave and ECG, and to use their parameters for survival analysis. Thus, this study investigates biomarkers for hypertension, arterial stiffness and cardiac function aiming for an improved prognostic risk stratification in ESRD patients.

5.3 Methods

This section is concerned with the methodology used for this study. First, the included patients are described. The main focus of this section is the definition of classification trees and their further development: Survival trees. Finally, statistical methods for evaluation are presented and the implementation of this work is described.

5.3.1 Study population

Out of the total ISAR cohort ($n = 519$), 414 patients with a 24 h ABPM recording and 381 subjects with a 24 h ECG recording were available. Due to short recording time, incomplete laboratory values, or insufficient data quality the pulse wave (PW) study population was decreased to $n = 344$ [118, 122]. Patients with a cardiac pacemaker, less than 75% normal sinus rhythm beats, and atrial fibrillation decreased the HRV study population to $n = 290$. As a result, 234 patients with both measurements and complete laboratory values remained for the final analysis (see figure 5.1).

5.3.2 Classification and survival trees

Tree-based methods are an increasingly important area for regression and classification. They were introduced in 1963 by Morgan and Sonquist [131], but really gained interest with the classification and regression trees (CART) algorithm developed by Breiman about 20 years later [27].

Classification trees

Classification tree methods partition the predictor variables into rectangles. Finally, each rectangle is represented by a class label. For simplification only binary partitions

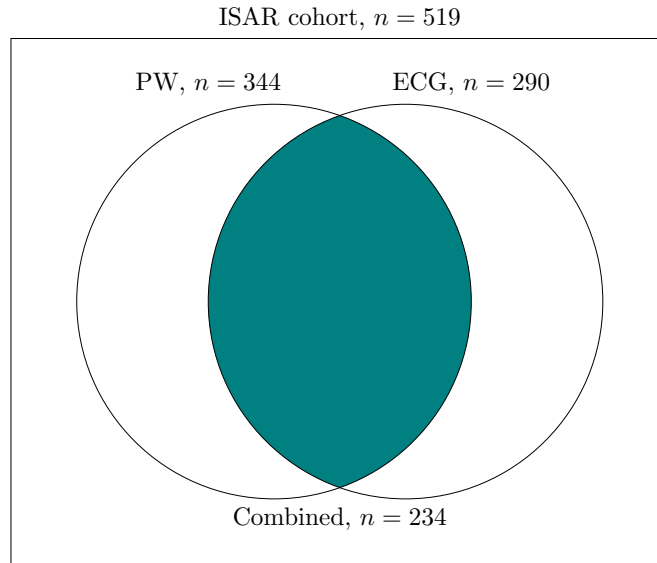


Figure 5.1: Available subjects with pulse wave (PW) recording ($n = 344$), electrocardiogram (ECG) recording ($n = 290$), and their intersection $n = 234$.

are considered.

Exemplarily, a classification tree is visualized in figure 5.2. At each node a split into two descendant subsets is performed until terminal nodes, which contain class labels, are reached. The first node where the entire data is split into two partitions is named root node. Same class labels can be attached to terminal nodes. However, terminal nodes form a partition of the entire data. The terminal nodes are often named leaf nodes.

In figure 5.2, a 2-class tree with three splits and four terminal nodes is visualized. The terminal nodes 3, 5, and 6 are classified as class 1. Class 2 is assigned to the leaf node 7. Each node in figure 5.2 (a) shows the leaf number on top [in brackets], the class label and the number of observations of the most frequently class in relation to the total observations. The separation of the predictor variables into disjunctive rectangles is shown in figure 5.2 (b).

The notation throughout this chapter is the following

- $I = (1, \dots, n)$ denotes the indices of patients,
- $(x_{i1}, \dots, x_{ip}) = X_i$ are the input (predictor) variables for the i -th subject,
- $y = (y_i), i \in I$ defines the binary output (class) vector, and
- $IK = (iK_1, \dots, iK_{n_K})$ represents the $n_K \leq n$ subjects included in node K.

The algorithm has to make decision about

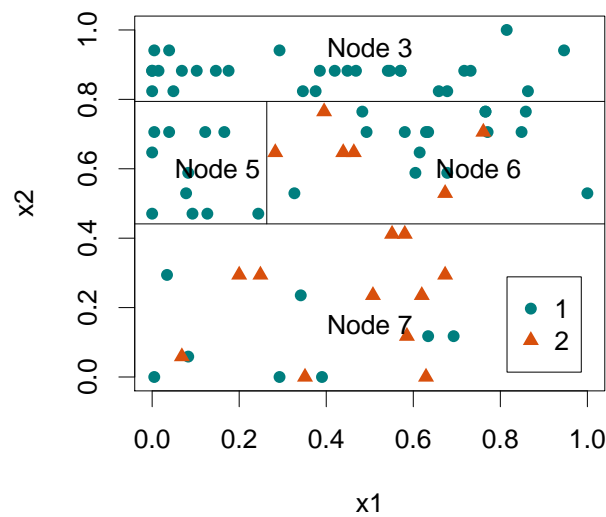
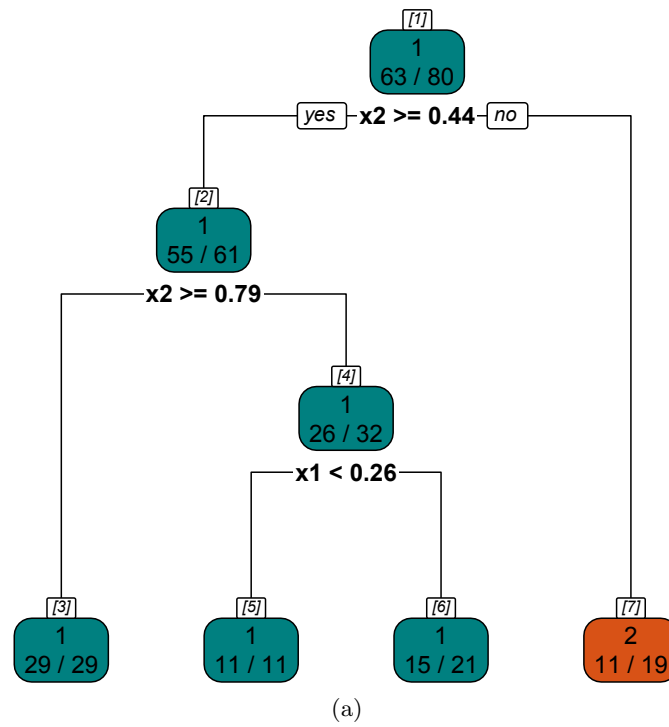


Figure 5.2: Illustration of a classification tree with 3 splits and 4 terminal nodes. The upper panel (a) shows for each terminal node $[K]$ the classification by its majority. Furthermore, the number of observations of the most frequent class / total observations is listed. In the bottom figure (b), the 2-dimensional predictor space with its partitions into rectangles is showed.

- which predictor variable is used for the split,
- the split point, and
- the form of the tree, i. e., declare terminal nodes or continue splitting.

For each splitting variable x_k the split point s defines two partitions

$$P_1(k, s) = \{(X_i)_{i \in I} | x_{ik} < s\} \text{ and } P_2(k, s) = \{(X_i)_{i \in I} | x_{ik} \geq s\}. \quad (5.1)$$

A split s of node K with node impurity $R(K)$ has two branches and the improved impurity can be defined according to Breiman [27] as

$$\Delta R(s, K) = R(K) - [p_L \cdot R(K_{\text{left son}}) + p_R \cdot R(K_{\text{right son}})], \quad (5.2)$$

where p_L is defined as proportion of cases going into the left son and p_R is defined as proportion of cases going into the right son, respectively. Typical impurity functions are the misclassification error or the Gini index [27]. For a two-class problem, where p denotes the proportion of observations in one class, they are defined as

$$R(K) = \begin{cases} 1 - \max(p, 1 - p) & \dots \text{ misclassification rate,} \\ 2p(1 - p) & \dots \text{ Gini index.} \end{cases} \quad (5.3)$$

Figure 5.3 illustrates both impurity functions. Both criteria are similar, but Gini index is differentiable, and thus numerically more stable. The default splitting criterion of the R function `rpart()` is the Gini index.

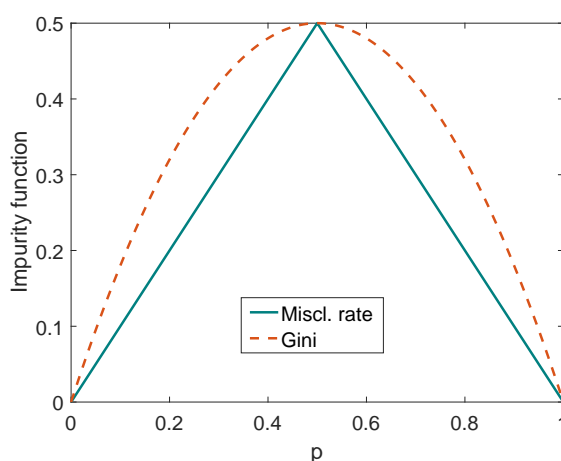


Figure 5.3: Comparison of impurity functions for two-class problem. p denotes the proportion of observations in one class.

The idea behind getting the right sized tree T is the following. Initially, a large tree

T_0 is built until terminal nodes are either small or pure. Afterwards, this large tree is pruned using cost complexity pruning as is done in CART [27].

Let \tilde{T} denote the set of terminal nodes and $|\tilde{T}|$ the number of terminal nodes. A subtree T' of the initial tree T_0 is denoted by $T' \preceq T_0$. It is obtained by reduction of inner nodes. Remark, both trees have the same root node.

Breiman defined the cost complexity of a tree T in [27] as

$$R_\alpha(T) = \sum_{K \in \tilde{T}} R(K) + \alpha |\tilde{T}|, \quad (5.4)$$

with a tuning parameter $\alpha \geq 0$. It is a tradeoff between goodness of fit ($\alpha = 0 \Rightarrow$ full tree T_0) and tree size (large α results in a small tree).

Ten-fold cross-validation was used to choose the best value for α . This means that all data is randomly divided into 10 parts and subsequently one part is chosen to be the test set and the other 9 parts are defined as training data for the model. The minimum estimated cross-validated error yields the complexity parameter α . To be more precise, α corresponding to the smallest tree size within one standard error of the minimum estimated cross-validated error is picked. Figure 5.4 exemplarily illustrates the selection of the tuning parameter α .

Survival trees

In contrast to ordinary classification methods, the output variable y is not a vector of length n . It is redefined as a $n \times 2$ matrix $y_i = (t_i, c_i)_{i=1}^n$, where t_i denotes the observation time and c_i the observed event for the i -th subject.

The basic classification tree concept, as described in the last section, can be used for the development of survival trees. LeBlanc and Crowley proposed an algorithm which is implemented with small improvements in the `rpart` package [96, 177]. This section presents the techniques based on [96].

Initially, an estimated event rate is calculated by the number of events and the total time

$$\hat{\lambda}_I = \frac{\sum_{i \in I} c_i}{\sum_{i \in I} t_i}. \quad (5.5)$$

This estimator of the cumulative hazard rate is referred as Nelson-Aalen estimator.

By exploiting an equivalence between proportional hazards full likelihood and the Pois-

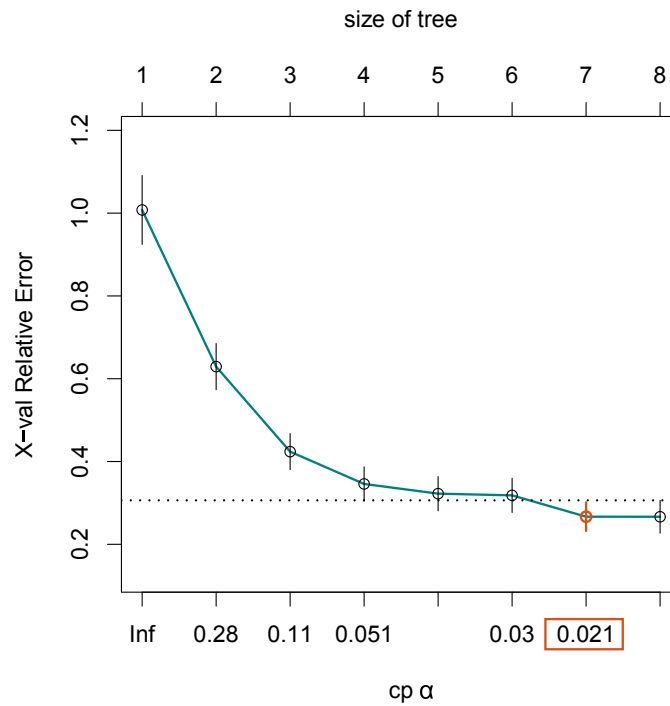


Figure 5.4: Selection of the complexity parameter (cp) α . The dashed line represents the minimum plus 1 standard error for the estimated cross-validated error. Hence, the smallest tree with an estimated error below the dashed line is of size 7 (6 splits). Corresponding $\alpha = 0.021$ is selected.

son¹ model likelihood, LeBlanc and Crowley suggested to use the null deviance from a Poisson model as impurity function. Since deviance measures how well the tree fits the data, the improvement in node K can be written as

$$\Delta R(s, K) = D(K) - (D_{\text{left son}} + D_{\text{right son}}). \tag{5.6}$$

The null deviance for a fitted Poisson regression is defined as

$$D = 2 \sum_{i=1}^n \left[y_i \log \left(\frac{y_i}{\hat{\mu}} \right) - (y_i - \hat{\mu}) \right]. \tag{5.7}$$

Correspondingly, the within node deviance of node K is defined with response c_i and estimated mean $\hat{\lambda}_K t_i$ as

$$D_K = 2 \sum_{\substack{i \in IK \\ c_i > 0}} \left[c_i \log \left(\frac{c_i}{\hat{\lambda}_K t_i} \right) - (c_i - \hat{\lambda}_K t_i) \right] + 2 \sum_{\substack{i \in IK \\ c_i = 0}} \hat{\lambda}_K t_i. \tag{5.8}$$

However, there is a problem with this simple estimate if the estimated node event rates $\hat{\lambda}_K$ are defined as Nelson-Aalen estimators as in equation (5.5). Suppose that a terminal

¹Siméon Denis Poisson (1781–1840), French mathematician, engineer and physicist

node contains just one event $c_j = 1$. Hence, there exists a cross validated estimate $\hat{\lambda}_K = 0$ when c_j is chosen to be in the test set. As a result, the calculation of the deviance includes the term

$$\dots + c_j \log(c_j/0) + \dots, \quad (5.9)$$

which is not defined for $c_j \neq 0$.

To overcome this problem, a shrinkage estimate was proposed by Therneau et al. in [177] as follows. The initial observed overall event rate is defined as in equation (5.5)

$$\mu := \frac{\sum_{i \in I} c_i}{\sum_{i \in I} t_i}. \quad (5.10)$$

If the true rates for the nodes are assumed to be gamma-distributed, i. e., $\lambda_K \sim \Gamma(\mu, \sigma)$, the Bayes estimate of the event rate for node K is defined as

$$\hat{\lambda}_K = \frac{\alpha + \sum_{i \in IK} c_i}{\beta + \sum_{i \in IK} t_i}, \quad (5.11)$$

where $\alpha = 1/k^2$, $\beta = \alpha/\mu$ and k denotes the coefficient of variation $k = \sigma/\mu$.

For the sake of simplicity, the baseline hazard is assumed to be linear between observed deaths. Hence, a parametric exponential model yields scaled observation times \tilde{t}_i such that a Kaplan-Meier plot of the data will be a straight line (plotted on log-scale), i. e., $\sum_{i \in I} \tilde{t}_i = \sum_{i \in I} c_i$. Equivalently, the overall relative death rate can be written as

$$\mu = \frac{\sum_{i \in I} c_i}{\sum_{i \in I} \tilde{t}_i} = 1. \quad (5.12)$$

Finally, all other proportional, relative risk estimates are calculated analogous to equation (5.11) with a default value of $k = 1$. Hence,

$$\hat{\lambda}_K = \frac{1 + \sum_{i \in IK} c_i}{1 + \sum_{i \in IK} \tilde{t}_i}. \quad (5.13)$$

5.3.3 Statistics

Baseline continuous data are summarized as mean (SD) for normally distributed data and as median [IQR] else-wise, depending on the Kolmogorov-Smirnov test for normality. Categorical baseline data are summarized as number (percentage). Associations between different pulse wave parameters were evaluated with Pearson's correlation coefficient. The investigated endpoints of this work were all-cause mortality.

Furthermore, the survival function is estimated by the Kaplan-Meier^{2,3} estimator. Patients were grouped according to the survival tree partitions, i. e., corresponding to the terminal nodes.

The nonparametric estimator, i. e., survival function $\hat{S}(t)$, is defined in [81] as

$$\hat{S}(t) = \prod_{i:t_i \leq t} \left(1 - \frac{d_i}{n_i}\right), \quad (5.14)$$

with event times t_i , corresponding number of events d_i that happened at t_i , and subjects at risk n_i up to time t_i .

The plot of the survival function is a series of declining horizontal steps, starting at $\hat{S}(t) = 1$. A major advantage of the Kaplan-Meier estimate is the ability to handle censored data. E. g., if a patient is lost to follow-up or is still alive (without event occurrence) at last follow-up.

5.3.4 Implementation

Computations were performed in R (R Foundation for Statistical Computing, Vienna, Austria; 3.4.2) [149]. The following packages available on CRAN were used

- `rpart`: recursive partitioning and regression trees [177],
- `rpart.plot`: plot an `rpart` model [127], and
- `survival`: survival analysis [178].

For the pulse wave analysis survival tree, ten parameters derived by the Mobil-O-Graph (see figure 5.6) were used as input, i. e., $X \in \mathbb{R}^{344 \times 11}$. The output matrix y with binary event variable and integer event time is of size $y \in \mathbb{N}^{344 \times 2}$.

For the computation of the HRV survival tree, the observation matrix X is of size $X \in \mathbb{R}^{290 \times 11}$ and the corresponding output matrix y is of size $y \in \mathbb{N}^{290 \times 2}$, respectively.

The input matrix (data frame) X for the combined analysis contains 21 baseline characteristics (see table 2.1), ten parameters from PWA, and eleven HRV parameters as defined in section 2.3. Hence, $X \in \mathbb{R}^{234 \times 42}$ and $y \in \mathbb{N}^{234 \times 2}$, respectively.

²Edward Lynn Kaplan (1920–2006), American mathematician.

³Paul Meier (1924–2011), American statistician.

5.4 Results

The findings are grouped into three parts. First, the results of the survival tree derived from solely PWA parameters are presented. Second, results obtained from HRV analysis are set out. Finally, the outcomes obtained from the combined tree are shown.

PWA survival tree

As mentioned in section 2.1, the latest follow-up took place in 2016. Out of the PWA group ($n = 344$), 115 subjects died (33%). With a minimum node size of 20 patients and default settings of the `rpart` package an initial tree with 17 nodes was built. According to cross-validation, the initial tree was pruned with a complexity parameter $\alpha = 0.05$. The resulting tree has only one split and is shown in appendix A, figure A.1 (a). Moreover, matching Kaplan-Meier curves are visualized in figure A.1 (b).

According to Mayer et al. the status of AF or HF has great impact on the association of ABPM and mortality [122]. Adding this parameter to the model, a more sophisticated tree is developed (11 nodes with an optimal complexity parameter $\alpha = 0.02$). The algorithm automatically elects the presence of AF or HF as root node.

Figure 5.5 shows the final PWA-survival tree with five splits and six terminal nodes. On top of each box, the leaf number is specified. The color of each box is related to the estimated relative risk, which is listed in each box together with the number of events/number of included subjects. The covariate and its split value are indicated in the left branch below each split.

Furthermore, correlations between the ten PWA parameters are visualized in figure 5.6. Central pressures were highly correlated with peripheral pressures (marked dark blue). PWV showed the lowest correlation among all indices ($r < 0.5$).

HRV survival tree

From the HRV dataset ($n=290$), 76 patients died (26%). The initial tree with a minimum node size of 20 patients, complexity parameter $\alpha = 0.01$, and 10-fold cross validation consists of 15 nodes. Figure 5.7 (a) shows the (optimal) pruned survival tree ($\alpha = 0.05$). Furthermore, a Kaplan-Meier plot is presented to the right, see figure 5.7 (b).

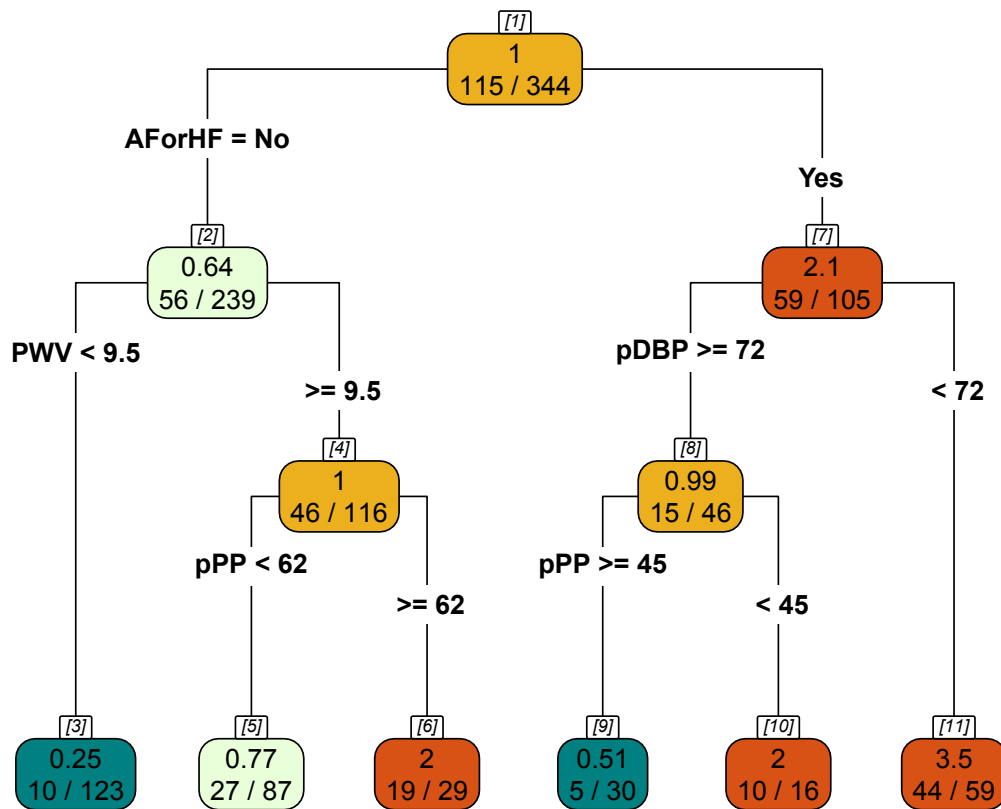


Figure 5.5: Pulse wave analysis (PWA) survival tree of $n = 344$ subjects. AForHF denotes patients with either one or both of the conditions: Atrial fibrillation (AF) or heart failure (HF). Further variables are: Pulse wave velocity (PWV), peripheral pulse pressure (pPP), and peripheral diastolic blood pressure (pDBP).

Combined survival tree

Out of the combined cohort ($n = 234$), 59 subjects died (25%). Table 5.1 summarizes the baseline characteristics of the 234 subjects (first column). Patients with AF are excluded (before HRV analysis) and 21 heart failure patients are included (11%).

The initial survival tree consists of 25 nodes. Figure 5.8 shows the final pruned tree ($\alpha = 0.04$ selected by cross-validation) with five terminal nodes. Again, the color of the box corresponds to the estimated risk in each node. On top of each box, the node number is listed whereas the covariate and its split value are indicated below. Patients matching the condition are included in the left branch (true statement). Each node lists the estimated relative risk and, and the number of events/number of included subjects.

Figure 5.9 shows Kaplan-Meier estimates of the survival functions grouped for the terminal nodes. Subjects with an adapted CCI greater or equal to 5 tend to have lower survival time. Leaf 8 shows the worst survival pattern with a median survival time of 1291 days. The largest node (node 3) is formed by subjects with adapted CCI < 5 and

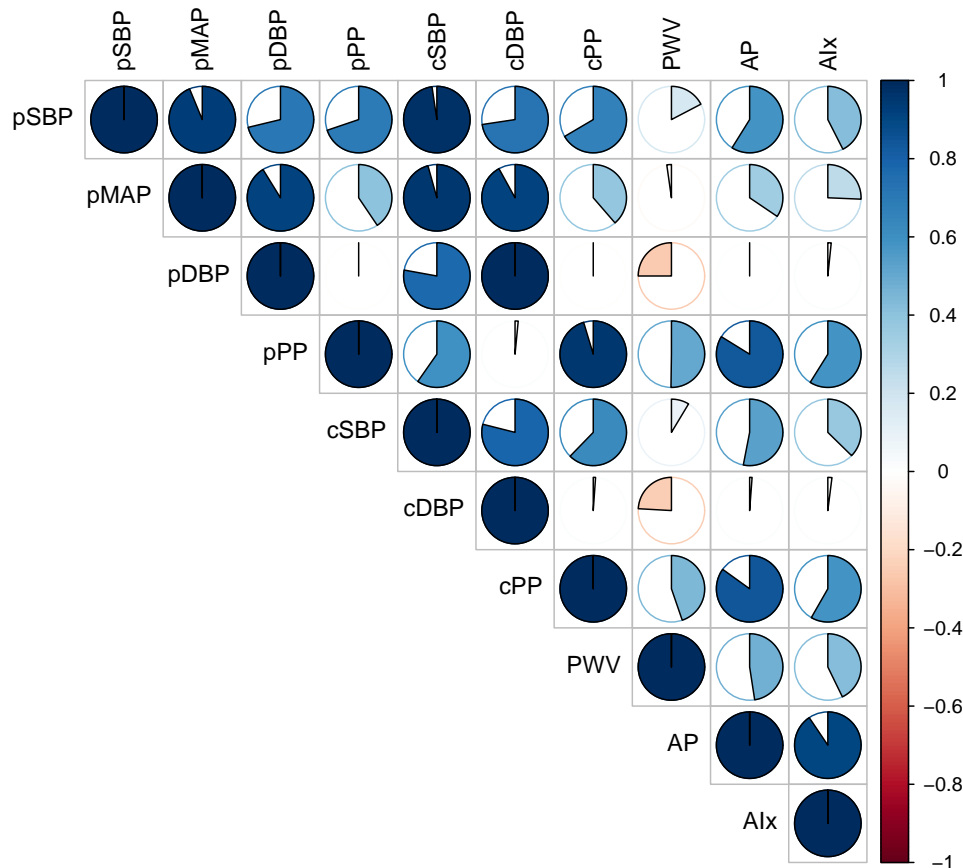


Figure 5.6: Correlations between pulse wave analysis parameters of $n = 344$ subjects. Peripheral (p) and central (c) pressures: Systolic blood pressure (SBP), diastolic blood pressure (DBP), pulse pressure (PP), mean arterial pressure (MAP). Further indices are: pulse wave velocity (PWV), augmented pressure (AP) and augmentation index (AIx).

serum albumin ≥ 4.1 . With only 4 events out of 96 subjects these subjects have a good survival probability. Apart from the obvious differences (node 3 or node 6 with all the other curves), there is a significant difference in survival curves between node 7 and 8 (log-rank test $p = 0.024$).

5.5 Discussion

Consistent with Mayer et al., the inverse association of pulse pressure (PP) with all-cause mortality between the subgroups according to absence or presence of AF and/or HF can be observed [122]. To be more precise, patients with AF or HF tend to have a lower survival time for small PP values ($pPP < 45$ mmHg). The opposite is true

Variable	all (n=234)	Node 3 (96)	Node 6 (25)	Node 7 (32)	Node 8 (19)	Node 9 (62)
Events, n (%)	59 (25 %)	4 (4 %)	0 (0 %)	9 (28 %)	13 (68 %)	33 (53 %)
Age (years)	62.4 (15.3 SD)	58.3 (15.5 SD)	54.3 (17.1 SD)	63.3 (16.2 SD)	69.5 (10.9 SD)	69.4 (10.7 SD)
Sex—male, n(%)	150 (64 %)	66 (69 %)	19 (76 %)	17 (53 %)	6 (33 %)	42 (68 %)
Body weight (kg)	76.1 (17.5 SD)	77.8 (18.1 SD)	69.5 (15.3 SD)	76.1 (18.5 SD)	70.9 (15.2 SD)	77.7 (17.1 SD)
Height (m)	1.7 [1.65,1.76]	1.71 [1.68,1.79]	1.7 [1.67,1.77]	1.7 [1.65,1.77]	1.64 [1.6,1.68]	1.72 [1.62,1.76]
Body mass index (kg/m ²)	26 (5.25 SD)	26 (5.23 SD)	23.7 (4.53 SD)	26.3 (5.55 SD)	26.1 (5.14 SD)	26.7 (5.34 SD)
Presence of diabetes, n(%)	79 (34 %)	24 (25 %)	6 (24 %)	7 (22 %)	8 (42 %)	34 (55 %)
Presence of hypertension, n (%)	220 (94 %)	92 (96 %)	19 (76 %)	31 (97 %)	18 (95 %)	60 (97 %)
Heart failure, n (%)	25 (11 %)	1 (1 %)	1 (4 %)	2 (6 %)	1 (5 %)	20 (32 %)
Adapted CCI	3.05 (2.73 SD)	1.54 (1.34 SD)	1.52 (1.39 SD)	1.84 (1.59 SD)	2.63 (1.42 SD)	6.74 (1.94 SD)
Dialysis vintage (mo)	60.3 (55.9 SD)	56.4 (41.6 SD)	93.2 (85.7 SD)	72.9 (81.9 SD)	38 (40.8 SD)	53.3 (41 SD)
UFV (l)	2.2 [1.5,3]	2.2 [1.4,2.8]	2.5 [2,3]	2.35 [1.55,2.95]	2.5 [1.57,2.95]	2.1 [1.4,3]
Kt/V	1.46 [1.25,1.64]	1.46 [1.29,1.7]	1.51 [1.35,1.67]	1.36 [1.1,1.63]	1.32 [1.21,1.83]	1.5 [1.2,1.63]
Dialysis duration per session (h)	4.45 (0.7 SD)	4.51 (0.78 SD)	4.88 (0.97 SD)	4.39 (0.65 SD)	4.13 (0.24 SD)	4.31 (0.44 SD)
Serum albumin (g/dl)	4.02 (0.4 SD)	4.33 (0.25 SD)	3.78 (0.24 SD)	3.73 (0.25 SD)	3.59 (0.34 SD)	3.94 (0.38 SD)
hsCRP	0.72 (1.28 SD)	0.49 (0.72 SD)	0.86 (0.71 SD)	0.66 (0.77 SD)	0.56 (0.53 SD)	1.08 (2.15 SD)
Total cholesterol (mg/dl)	177 [153,210]	183 [163,212]	156 [133,200]	183 [164,205]	172 [160,204]	164 [146,213]
Calcium × phosphate (mmol ² /l ²)	3.77 [3.13,4.59]	3.92 [3.24,4.74]	3.62 [2.74,4.57]	3.69 [3.1,4.29]	3.52 [2.85,4.11]	3.78 [3.15,4.58]
Antihypertensive drugs, n(%)	209 (89 %)	87 (91 %)	17 (68 %)	29 (91 %)	16 (84 %)	60 (97 %)
Statins, n (%)	88 (38 %)	36 (38 %)	3 (12 %)	7 (22 %)	8 (42 %)	34 (55 %)
Anticoagulant, n(%)	25 (11 %)	8 (8 %)	2 (8 %)	2 (6 %)	3 (16 %)	10 (16 %)

Table 5.1: Baseline data of combined survival tree subjects ($n = 234$). Data given as number (%) for categorical. Continuous data is presented as mean (SD) or median [IQR].

CCI = Charlson comorbidity index; mo = months; UFV = ultrafiltration volume; hsCRP = high-sensitivity C-reactive protein; Kt/V = dialyzer clearance of urea · dialysis time/volume of distribution of urea.

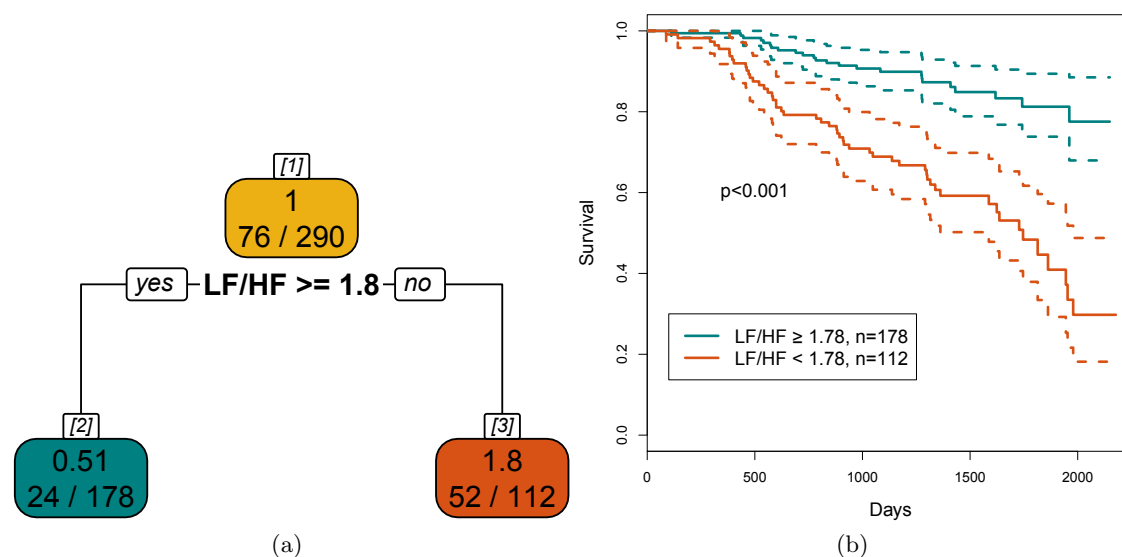


Figure 5.7: On the left side (a), the HRV survival tree of $n=290$ subjects with its splitting variable low frequency to high frequency ratio (LF/HF) is plotted. The right figure (b) shows corresponding Kaplan-Meier estimates.

for subjects without these conditions, higher PP ($pPP \geq 62$ mmHg, see figure 5.5) is associated with an increased risk.

Peripheral indices ($pPP, pSBP$) appear in the survival tree, beside PWV - a measure of arterial stiffness. However, there is a strong relation between peripheral and central values (e. g., $r = 0.95$ between pPP and cPP ; see figure 5.6). Central DBP almost resembles $pDBP$ ($r > 0.99$, $cDBP - pDBP = 1.37$ mmHg ± 0.49). This little change can also be seen in figure 2.8). The PWV cutoff values of 9.5 m/s (see figure 5.5) and 9.1 m/s (see figure A.1), respectively are inline with previous studies [19, 118]. Furthermore, it is inline with the consensus advice of 10 m/s (exact calculated 9.6 m/s) for carotid-femoral PWV [182]. The results also accords with recent observations which showed that ambulatory PWV was associated with mortality in hemodialysis subjects [118, 160].

Despite this finding provides support for established threshold values, it must be interpreted with caution. Especially, since important influencing factors such as age or comorbidities are not taken into consideration in this model. The predictive power of the 24h frequency domain HRV measure LF/HF is inline with the results of Suzuki et al.[174], who investigated hemodialysis patients. Figure 5.7 provides a Kaplan-Meier curves stratified by $LF/HF < 1.78$ and ≥ 1.78 . To develop a full picture, a combined survival tree including 21 baseline clinical data covariates, 10 PWA parameters (see figure 5.6), and 11 traditional HRV indices (see section 2.3) was built.

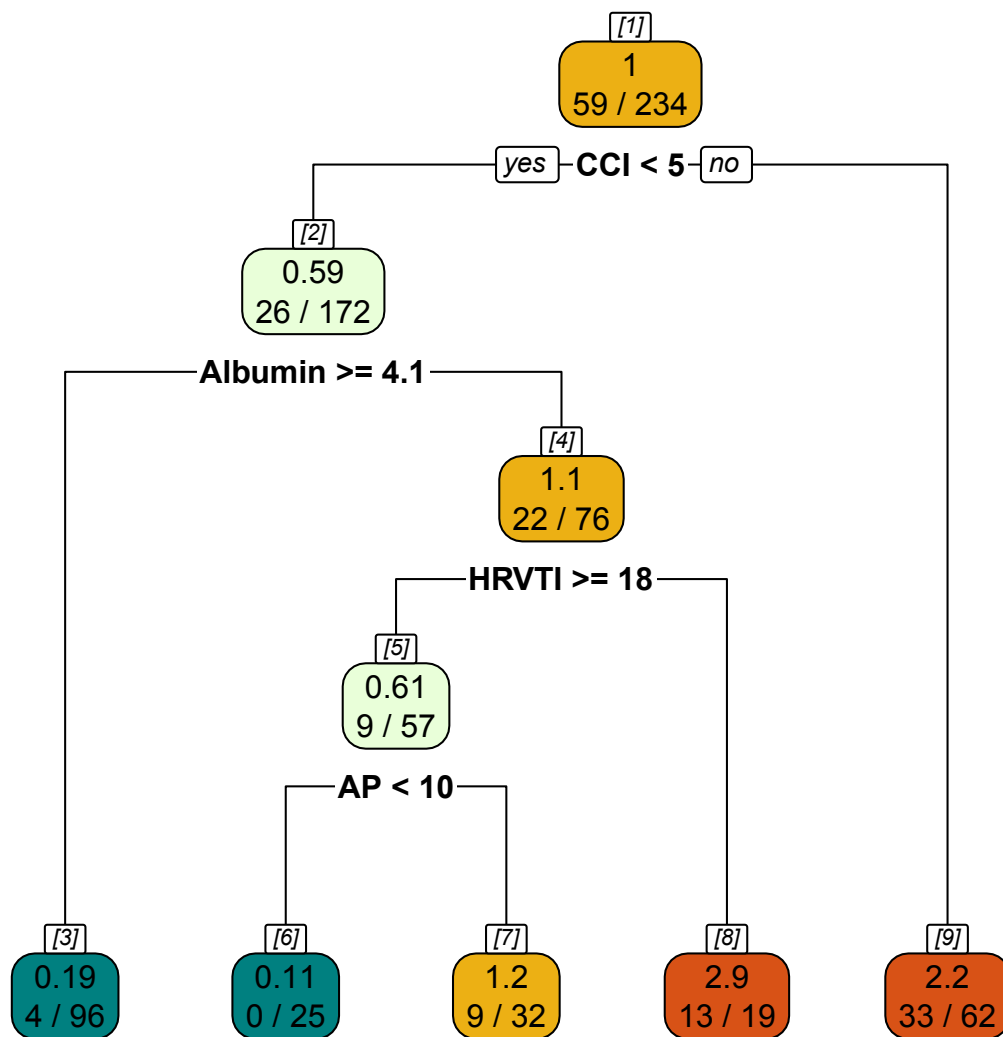


Figure 5.8: Combined survival tree of $n = 234$ subjects. Splitting variables are: Charlson comorbidity index (CCI), serum albumin, augmented pressure (AP), and HRV triangular index (HRVTI).

The results of the combined survival tree (see figure 5.8) show that comorbidities are the first split variable. More than half of the dead had a CCI index greater than or equal to five. The left branch includes patients with less comorbid conditions and a high serum albumin. Hence, the survival probability for the subjects in node 3 is approximately five times higher than in the initial cohort. While the margins show obvious results, most interesting findings appear in the middle of the combined survival tree (terminal nodes 6-8). Patients with a low CCI (< 5) and/or a low serum albumin level show very different risk estimates, varying from 2.9 times higher to a ninth of the initial risk. The first separation is done with *HRVTI*, a measure obtained from the ECG. Low heart rate variability, i. e., a small *HRVTI* is associated with a high risk [135]. This finding is in accordance with previous studies in ESRD patients [55, 72, 174]. Moreover, Hayano

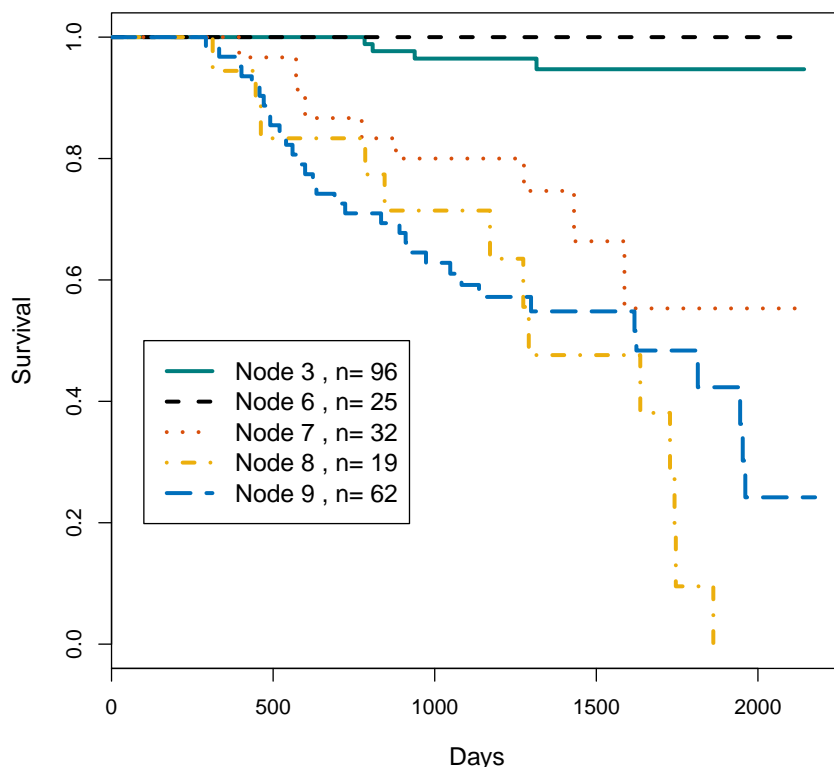


Figure 5.9: Kaplan-Meier estimates for the terminal nodes of the combined survival tree. The node numbers correspond to the nodes of the survival tree as visualized in figure 5.8.

et al. reported a similar separation value for the association of $HRVTI$ with all-cause mortality ($HRVTI < 22$) [72]. A possible explanation for $HRVTI$ being the one HRV parameter appearing in the tree might be the larger predictive power of measures reflecting long-term fluctuations [55].

By means of the AP , a parameter obtained from PWA, the remaining 57 subjects could be classified into patients with high risk and patients with good probability of survival. Relating to the initial cohort, the 32 subjects in node 7 with $AP \geq 10$, have an 20% increased mortality risk. On the other hand, the 25 patients with $AP < 10$ show the best survival probability ($\hat{\lambda}_6 = 0.11$) and even undercut the estimated risk of the leftmost terminal node ($\hat{\lambda}_3 = 0.19$). Referring to their parent node, the right branch resulted in a doubled risk and the left son in less than a fifth.

The study population showed an unbalanced gender distribution (approximately two-thirds men, see table 5.1). One unanticipated finding was that mainly women belong to

node 8 (13 out of 19), which revealed the worst survival pattern and highest risk estimate.

The most important clinically relevant finding was that patients with a low comorbidity score and/or low serum albumin showed extremely different risk estimates. Combined HRV and pulse wave analysis revealed separate survival prognosis. Although low serum albumin is usually a strong risk predictor in hemodialysis patients [36, 174], the group of patients with high HRV and low augmented pressure levels had no events. The association between increased arterial wave reflections and mortality in ESRD patients was reported [106]. In this study, wave reflections were assessed by *AP*. However, there is a strong relation between *AP* and *AIx* ($r = 0.9$) and a surrogate split of $AIx < 27\%$ in node 5 would show a similar picture.

Overall, the main strength of this study is that a variety of measurements was available including clinical, ECG and pulse wave parameters from a substantial sample of patients. Moreover, with survival tree methods multivariable survival models could be developed. However, several limitations have to be considered. The major limitation of survival trees is the fact that only covariates which are selected as best split at one of the nodes are shown in the tree. With traditional Cox hazard models all statistically significant covariates are considered. However, these limitations can be avoided/minimized by additionally considering the correlations of the covariates. Another limitation is the limited recording time of 24 hours. Hence, the dialysis-off day could not be incorporated in the analysis.

Conclusion

In conclusion, with the proposed tree-structured models comprehensive survival analysis could be obtained. The association of increased PWV with mortality in hemodialysis patients is clearly supported by the current findings. This study examines the opposed association between *PP* and survival based on the patients' cardiac disease.

Comorbid conditions emerge as initial risk predictor in the combined survival tree. Moreover, tree-based analysis clearly supported that decreased HRV assessed by *HRVTI* comprises an increased mortality risk in ESRD patients. In addition, a widespread noninvasive assessment of wave reflections in hemodialysis patients could serve as an important tool in event prediction. Threshold values, obtained from the survival tree analysis, are tested on the entire population for verification (see appendix A). To improve risk stratification, 24 h ABPM and 24 h HRV should be measured in regular intervals.

Further research should be undertaken to investigate the effect of the individual comorbid condition.

Summary and Conclusions

End-stage renal disease (ESRD) is associated with a very high cardiovascular morbidity. The expected remaining lifetime for dialysis patients is disconcerting. Compared to age-matched counterparts in the general population, patients between 55-64 years are expected to live 20 years less. Better understanding of the complex cardiovascular processes would be an important step for prevention and treatment.

Consequently, the aim of this thesis was to investigate models for cardiovascular risk stratification in ESRD patients. Specifically, parameters derived by PWA and ECG recordings together with clinical data and endpoints (all-cause mortality) were used.

The first aim of this thesis was to develop an algorithm to obtain RR-intervals from 24 h multi-lead ECGs to quantify heart rate variability (HRV). Compared to manual reviewed reference series the automatically obtained interbeat interval series matched with respect to their synchronization and absolute deviation. A negligible error of 7.5 ms at a sampling frequency of 128 Hz and a high synchronization rate of 96.4% were achieved. Excluding AF patients further improved the agreement. Consequently, HRV parameters were obtained on the subgroup of patients without AF (n=293). HRV analysis showed similar results with no systematic differences compared to the parameters gained from the reference series.

Accordingly, standard HRV parameters together with nonlinear entropy measures were used for risk prediction. Fuzzy entropy and corrected approximate entropy provided significant hazard ratios, which remained significant after adjustment for common risk factors. The obtained results and interaction analysis indicated to group patients in

two groups according to heart disease (HD) status. In the subgroup of patients with HD, almost all entropies predicted mortality significantly and remained significant after adjustment.

The combination of parameters derived from 24 h recordings of the pulse wave and the ECG were used for comprehensive survival analysis. A multivariable survival tree model incorporates common risk predictors and indices from both biosignals in 234 hemodialysis patients. This study has shown that the assessment of pressure wave reflections and HRV might serve as important tools in event prediction.

Although 500 patients were included in the ISAR study, synchronous recordings were available only for about half of the subjects. As a result, the number of fatal events (n=59) limits the number of covariates in multivariable survival analysis. Moreover, it was not possible to incorporate the dialysis-off day in the analysis due to the limited recording time of 24 hours.

In conclusion, two noninvasive measured signals with their parameters provide a valuable contribution to improved risk stratification in hemodialysis patients. Prognostic groups with dichotomous thresholds can easily be determined from survival trees. A further study should be carried out to validate the findings using a different ESRD cohort. Considerably more emphasis should be placed on the recognition of potentially modifiable risk factors and clinical benefit.

Supplementary material

Figure A.1 (a) shows the pruned survival tree of exclusively PWA parameters. Cross-validation yields $\alpha = 0.05$, resulting in a tree with only one split. Hence, the corresponding Kaplan-Meier estimate for PWV is visualized in figure A.1 (b). Log-rank test was used to test for differences.

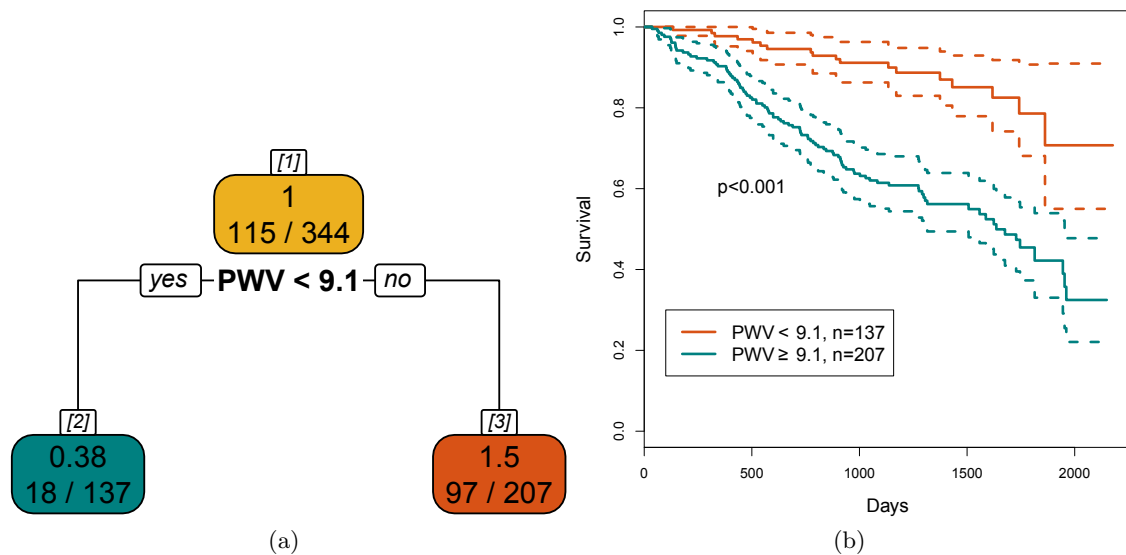


Figure A.1: On the left side (a), the PWA survival tree of $n=344$ subjects with its splitting variable pulse wave velocity (PWV) is plotted. The right figure (b) shows corresponding Kaplan-Meier estimates.

Figure A.2 shows Kaplan-Meier estimates separated by HRV triangular index ($HRVTI$) and augmented pressure (AP), respectively for all subjects of the combined cohort ($n=234$). Threshold values are obtained from combined survival tree (see figure 5.8).

Log-rank test was used to test for differences.

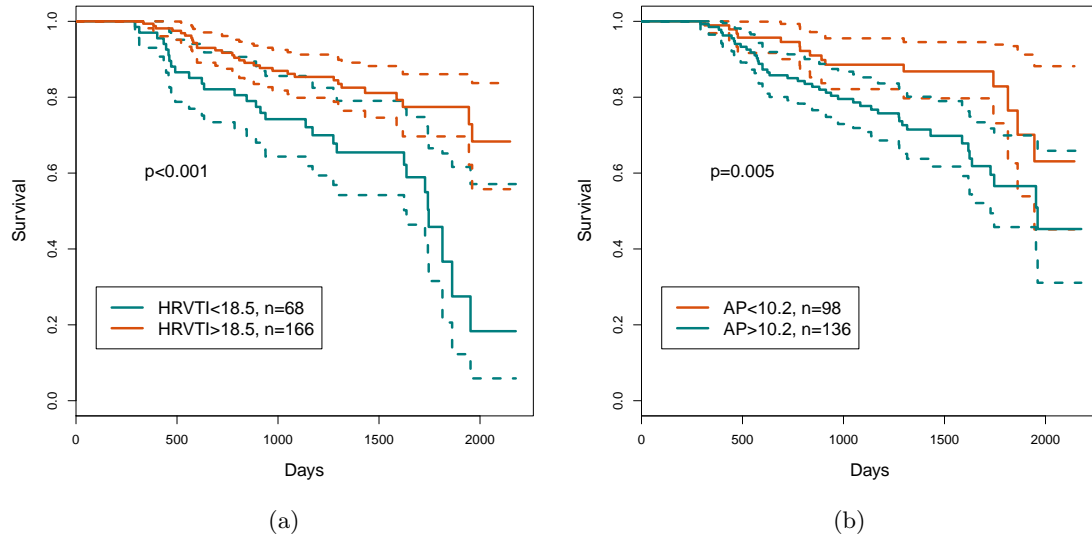


Figure A.2: Kaplan-Meier estimates of the (a) HRV triangular index ($HRVTI$) and (b) augmented pressure (AP).

List of Figures

1.1	Expected remaining lifetime for ESRD patients	2
1.2	Prognosis of CKD by <i>GFR</i> and albuminuria categories	4
1.3	Incident cases in the US and Austria	5
1.4	Prevalent cases in the US and Austria.	6
1.5	Prevalent dialysis patients in the US, Austria, and Germany	7
2.1	Schematic representation of hemodialysis circuit	12
2.2	ECG electrode placement	14
2.3	ECG of two normal heartbeats	15
2.4	Calculation of the TINN	18
2.5	Power spectral density estimate with frequency bands	19
2.6	Marey’s sphygmograph	22
2.7	Noninvasive oscillometric brachial blood pressure measurement	24
2.8	Comparison of arterial pressure waveforms	25
2.9	Harmonics of pressure wave	29
2.10	Estimation of characteristic Impedance Z_c	30
2.11	Brachial and aortic pressure waveform from generalized transfer function	33
2.12	Calculation of AIx from different aortic pressure waves	34
2.13	Carotid-femoral PWV	35
2.14	Features of the human circadian clock	36
3.1	Flow chart multi-lead RR determination	40
3.2	Flow chart of data	41
3.3	Stepwise illustration of multi-lead correction algorithm	44
3.4	Accepted multi-lead R-peak annotations	45
3.5	Flow chart differences of RR-series	47

3.6	Outliers detected and corrected by the impulse rejected filter	48
3.7	Difference time series between filtered and synchronized RR-series	50
3.8	Bland-Altman plots of normal beats and outliers	52
3.9	Bland-Altman plot and QQ-plot of RMSSD	53
4.1	Flow chart of data	60
4.2	Entropy hazard ratios	74
5.1	Set diagram of patient population	78
5.2	Classification tree example	79
5.3	Comparison of impurity functions	80
5.4	Selection of complexity parameter	82
5.5	PWA survival tree	86
5.6	Correlations between PWA parameters	87
5.7	HRV survival tree	89
5.8	Combined survival tree	90
5.9	Kaplan-Meier estimates of the combined survival tree	91
A.1	PWA survival tree	95
A.2	Kaplan-Meier estimates of HRVTI and AP	96

List of Tables

1.1	CKD stages according to glomerular filtration rate	4
2.1	Baseline data of the ISAR cohort	10
2.2	Definition of HRV frequency domain measures	19
3.1	Exemplary four beats and their detections in a 6-lead ECG	46
3.2	Agreement indicators of time series for all subjects and grouped by AF . .	51
3.3	HRV indices calculated on RR_{Afs} and RR_{Bfs} , respectively	53
4.1	Parameter sets used for each entropy calculation	65
4.2	Baseline data of included patients	67
4.3	HRV parameters and entropy measures at baseline	68
4.4	Significant univariate conventional risk predictors of mortality	69
4.5	Unadjusted and adjusted hazard ratios of HRV parameters	70
4.6	HRV parameters and entropy measures grouped by heart disease status .	71
4.7	Unadjusted hazard ratios of entropies grouped by heart disease status . .	72
4.8	Hazard ratios of entropies for patients with heart disease	72
5.1	Baseline data of combined survival tree subjects	88

Acronyms

- ABPM** ambulatory blood pressure monitoring
- AF** atrial fibrillation
- AIx** augmentation index
- ANS** autonomic nervous system
- AV** atrioventricular
- BP** blood pressure
- BUN** blood urea nitrogen
- CART** classification and regression trees
- CCI** Charlson comorbidity index
- CHF** congestive heart failure
- CI** confidence interval
- CKD** chronic kidney disease
- CRP** C-reactive protein
- CVD** cardiovascular disease
- DBP** diastolic blood pressure
- DTS** difference time series
- ECG** electrocardiogram
- EDTA** European Dialysis and Transplant Association

EMG electromyogram

ERA European Renal Association

ESC European Society of Cardiology

ESH European Society of Hypertension

ESRD end-stage renal disease

FFT fast Fourier transformation

FN false negative

FP false positive

GFR glomerular filtration rate

HD heart disease

HF heart failure

HR hazard ratio

HRV heart rate variability

hsCRP high-sensitivity C-reactive protein

ICC intraclass correlation coefficient

IQR inter-quartile range

IRF impulse rejection filter

ISAR rISk strAtification in end-stage Renal disease

KDIGO Kidney Disease: Improving Global Outcomes

LVH left ventricular hypertrophy

MAP mean arterial pressure

MI myocardial infarction

MRI magnetic resonance imaging

p.m.p. per million population

PSD power spectral density

PWA pulse wave analysis

PWV pulse wave velocity

RMSE root mean squared error

RRT renal replacement therapy

SBP systolic blood pressure

SD standard deviation

URR urea reduction ratio

USRDS United States Renal Data System

Nomenclature

<i>AP</i>	augmented pressure	[mmHg]	p. 33
<i>ApEn</i>	approximate entropy		p. 58
<i>AVNN</i>	average NN-interval	[ms]	p. 51
<i>CApEn</i>	corrected approximate entropy		p. 58
<i>FS</i>	feature signal	[s]	p. 41
<i>FuzzyEn</i>	fuzzy entropy		p. 58
<i>FuzzyMEn</i>	fuzzy measure entropy		p. 58
<i>GFR</i>	glomerular filtration rate	[ml/ml/1.73m ²]	p. 4
<i>HF</i>	high frequency	[ms ²]	p. 19
<i>HRVTI</i>	HRV triangular index	[ms]	p. 17
<i>Kt/V</i>	fractional urea clearance		p. 13
<i>LF</i>	low frequency	[ms ²]	p. 19
<i>LF/HF</i>	low frequency to high frequency ratio		p. 19
<i>NaN</i>	not a number		p. 43
<i>NN50</i>	number of interval differences of successive NN-intervals greater than 50 ms		p. 17
<i>P_i</i>	inflection point	[mmHg]	p. 33
<i>pNN50</i>	percentage of interval differences of succes- sive NN-intervals greater than 50 ms	[%]	p. 17
<i>PP</i>	pulse pressure	[mmHg]	p. 24
<i>PWV</i>	pulse wave velocity	[m/s]	p. 34
<i>Q</i>	volume flow	[ml/s]	p. 26

<i>RMSE</i>	root mean square error	[ms]	p. 51
<i>RMSSD</i>	root mean square of successive differences	[ms]	p. 17
<i>SampEn</i>	sample entropy		p. 58
<i>SDNN</i>	standard deviation of NN-intervals	[ms]	p. 16
<i>TINN</i>	triangular interpolation of NN-interval histogram	[ms]	p. 16
<i>totalP</i>	total power	[ms ²]	p. 19
<i>VLFF</i>	very low frequency	[ms ²]	p. 19
<i>Z_c</i>	characteristic impedance	[mmHg·s/l]	p. 30
<i>Z_{in}</i>	input impedance		p. 29

Bibliography

- [1] R. Agarwal and M. Andersen. Prognostic importance of ambulatory blood pressure recordings in patients with chronic kidney disease. *Kidney International*, 69(7): 1175 – 1180, 2006. ISSN 0085-2538.
- [2] R. Agarwal, A. R. Nissenson, D. Battle, D. W. Coyne, J. Trout, and D. G. Warnock. Prevalence, treatment, and control of hypertension in chronic hemodialysis patients in the United States. *The American Journal of Medicine*, 115(4):291–297, 2003. ISSN 0002-9343.
- [3] R. Agarwal, M. Andersen, K. Bishu, and C. Saha. Home blood pressure monitoring improves the diagnosis of hypertension in hemodialysis patients. *Kidney International*, 69(5):900–906, 2006. ISSN 0085-2538. doi: 10.1038/sj.ki.5000145.
- [4] S. Akselrod, D. Gordon, F. A. Ubel, D. C. Shannon, A. Berger, and R. J. Cohen. Power spectrum analysis of heart rate fluctuation: a quantitative probe of beat-to-beat cardiovascular control. *Science*, 213(4504):220–222, 1981.
- [5] M. Aktaruzzaman and R. Sassi. Parametric estimation of sample entropy in heart rate variability analysis. *Biomedical Signal Processing and Control*, 14:141–147, 2014.
- [6] R. Alcaraz, D. Abásolo, R. Hornero, and J. J. Rieta. Optimal parameters study for sample entropy-based atrial fibrillation organization analysis. *Computer Methods and Programs in Biomedicine*, 99(1):124–132, 2010. ISSN 0169-2607.
- [7] D. G. Altman. *Practical statistics for medical research*. Chapman and Hall, 1991. ISBN 0412276305.
- [8] J. Amar, I. Vernier, E. Rossignol, V. Bongard, C. Arnaud, J. J. Conte, M. Salvador, and B. Chamontin. Nocturnal blood pressure and 24-hour pulse pressure are potent

- indicators of mortality in hemodialysis patients. *Kidney International*, 57(6):2485 – 2491, 2000. ISSN 0085-2538.
- [9] M. Bachler, C. Mayer, B. Hametner, and S. Wassertheurer. Increasing Stability of Real-Time Pulse Wave Velocity Estimation by Combining Established and New Approaches. In K. Al-Begain, D. Al-Dabass, A. Orsoni, R. Cant, and R. Zobel, editors, *8th EUROSIM Congress on Modelling and Simulation, EUROSIM2013 (EUROSIM2013)*, pages 47 – 51, Cardiff, United Kingdom, Sept. 2013. The Institute of Electrical and Electronics Engineers. doi: 10.1109/EUROSIM.2013.18. ISBN 978-0-7695-5073-2.
- [10] M. Bachler, C. Mayer, B. Hametner, S. Wassertheurer, and A. Holzinger. Online and Offline Determination of QT and PR Interval and QRS Duration in Electrocardiography. In Q. Zu, B. Hu, and A. Elçi, editors, *Pervasive Computing and the Networked World*, volume 7719 of *Lecture Notes in Computer Science*, pages 1–15. Springer, Berlin Heidelberg, 2013. ISBN 978-3-642-37014-4. doi: 10.1007/978-3-642-37015-1_1.
- [11] S. S. Barold. Willem einthoven and the birth of clinical electrocardiography a hundred years ago. *Cardiac Electrophysiology Review*, 7(1):99–104, 2003.
- [12] A. Bauer, M. Malik, P. Barthel, R. Schneider, M. A. Watanabe, A. J. Camm, A. Schömig, and G. Schmidt. Turbulence dynamics: An independent predictor of late mortality after acute myocardial infarction. *International Journal of Cardiology*, 107(1):42–47, 2006. ISSN 0167-5273. doi: 10.1016/j.ijcard.2005.02.037.
- [13] Y. Ben-Shlomo, M. Spears, C. Boustred, M. May, S. G. Anderson, E. J. Benjamin, P. Boutouyrie, J. Cameron, C.-H. Chen, J. K. Cruickshank, S.-J. Hwang, E. G. Lakatta, S. Laurent, J. Maldonado, G. F. Mitchell, S. S. Najjar, A. B. Newman, M. Ohishi, B. Pannier, T. Pereira, R. S. Vasan, T. Shokawa, K. Sutton-Tyrell, F. Verbeke, K.-L. Wang, D. J. Webb, T. W. Hansen, S. Zoungas, C. M. McEniery, J. R. Cockcroft, and I. B. Wilkinson. Aortic pulse wave velocity improves cardiovascular event prediction: An individual participant meta-analysis of prospective observational data from 17,635 subjects. *Journal of the American College of Cardiology*, 63(7):636 – 646, 2014. ISSN 0735-1097. doi: <http://dx.doi.org/10.1016/j.jacc.2013.09.063>.
- [14] G. G. Berntson and J. R. Stowell. ECG artifacts and heart period variability: Don't miss a beat! *Psychophysiology*, 35(1):127–132, 1998.
- [15] J. T. Bigger, J. L. Fleiss, R. C. Steinman, L. M. Rolnitzky, R. E. Kleiger, and J. N. Rottman. Frequency domain measures of heart period variability and mortality

- after myocardial infarction. *Circulation*, 85(1):164–171, 1992. ISSN 0009-7322. doi: 10.1161/01.CIR.85.1.164.
- [16] J. T. Bigger, R. C. Steinman, L. M. Rolnitzky, J. L. Fleiss, P. Albrecht, and R. J. Cohen. Power law behavior of RR-interval variability in healthy middle-aged persons, patients with recent acute myocardial infarction, and patients with heart transplants. *Circulation*, 93(12):2142–2151, 1996.
- [17] G. E. Billman. Heart rate variability - a historical perspective. *Frontiers in Physiology*, 2:86–, Nov. 2011. ISSN 1664-042X.
- [18] G. E. Billman. The LF/HF ratio does not accurately measure cardiac sympatho-vagal balance. *Frontiers in physiology*, 4:26, 2013.
- [19] J. Blacher, A. P. Guerin, B. Pannier, S. J. Marchais, M. E. Safar, and G. M. London. Impact of aortic stiffness on survival in end-stage renal disease. *Circulation*, 99(18):2434–2439, 1999. doi: 10.1161/01.CIR.99.18.2434.
- [20] J. Blacher, M. E. Safar, A. P. Guerin, B. Pannier, S. J. Marchais, and G. M. London. Aortic pulse wave velocity index and mortality in end-stage renal disease. *Kidney International*, 63(5):1852–1860, 2003. ISSN 0085-2538. doi: 10.1046/j.1523-1755.2003.00932.x.
- [21] A. Boardman, F. S. Schindwein, A. P. Rocha, and A. Leite. A study on the optimum order of autoregressive models for heart rate variability. *Physiological Measurement*, 23(2):325, 2002.
- [22] J. Booth. A short history of blood pressure measurement. *Proceedings of the Royal Society of Medicine*, 70(11):793–799, 1977.
- [23] A. Boskovic, T. Loncar-Turukalo, N. Japundzic-Zigon, and D. Bajic. The flip-flop effect in entropy estimation. In *Intelligent Systems and Informatics (SISY), 2011 IEEE 9th International Symposium on*, pages 227–230, 2011. doi: 10.1109/SISY.2011.6034328.
- [24] I. Bou-Hamad, D. Larocque, and H. Ben-Ameur. A review of survival trees. *Statist. Surv.*, 5:44–71, 2011. doi: 10.1214/09-SS047.
- [25] G. E. P. Box and D. R. Cox. An analysis of transformations. *Journal of the Royal Statistical Society. Series B (Methodological)*, 26(2):211–252, 1964. ISSN 00359246.
- [26] J. C. Bramwell and A. V. Hill. The velocity of the pulse wave in man. *Proceedings of the Royal Society of London. Series B, Containing Papers of a Biological Character*, 93(652):298–306, 1922.

- [27] L. Breiman. *Classification and regression trees*. The Wadsworth statistics probability series. Chapman and Hall, CRC, Boca Raton, Florida [et al.], 1984. ISBN 0412048418.
- [28] A. Buonacera, M. Boukhris, S. D. Tomasello, A. Campagna, C. Cilia, G. Tripepi, S. D. Marca, V. Terranova, M. Pisano, G. Mastro Simone, A. R. Galassi, B. Stan-canelli, A. Cataliotti, and L. Malatino. Impact of left ventricular remodeling and renal function on 24 h-ECG recordings and cardiovascular outcome in elderly hypertensive patients. *European Journal of Internal Medicine*, pages –, 2016. ISSN 0953-6205. doi: <http://dx.doi.org/10.1016/j.ejim.2016.01.001>.
- [29] P. Calhoun, X. Su, M. Nunn, and J. Fan. Constructing multivariate survival trees: The MST package for R. *Journal of Statistical Software*, 83(12):1–21, 2018.
- [30] P. Castiglioni and M. Di Rienzo. How the threshold "r" influences approximate entropy analysis of heart-rate variability. In *Computers in Cardiology, 2008*, pages 561–564, 2008. doi: 10.1109/CIC.2008.4749103.
- [31] C. T. Chan. Heart rate variability in patients with end-stage renal disease: an emerging predictive tool for sudden cardiac death? *Nephrology Dialysis Transplantation*, 23(10):3061–3062, 2008.
- [32] P. Chandra, R. L. Sands, B. W. Gillespie, N. W. Levin, P. Kotanko, M. Kiser, F. Finkelstein, A. Hinderliter, R. Pop-Busui, S. Rajagopalan, and R. Saran. Predictors of heart rate variability and its prognostic significance in chronic kidney disease. *Nephrology Dialysis Transplantation*, 27(2):700–709, 2012.
- [33] P. Chandra, R. Sands, B. Gillespie, N. Levin, P. Kotanko, M. Kiser, F. Finkelstein, A. Hinderliter, S. Rajagopalan, D. Sengstock, et al. Relationship between heart rate variability and pulse wave velocity and their association with patient outcomes in chronic kidney disease. *Clinical nephrology*, 81(1):9–19, 2014.
- [34] M. E. Charlson, P. Pompei, K. L. Ales, and C. MacKenzie. A new method of classifying prognostic comorbidity in longitudinal studies: Development and validation. *Journal of Chronic Diseases*, 40(5):373 – 383, 1987. ISSN 0021-9681. doi: [http://dx.doi.org/10.1016/0021-9681\(87\)90171-8](http://dx.doi.org/10.1016/0021-9681(87)90171-8).
- [35] C.-H. Chen, C.-T. Ting, A. Nussbacher, E. Nevo, D. A. Kass, P. Pak, S.-P. Wang, M.-S. Chang, and F. C. Yin. Validation of carotid artery tonometry as a means of estimating augmentation index of ascending aortic pressure. *Hypertension*, 27(2):168–175, 1996. doi: 10.1161/01.HYP.27.2.168.
- [36] S.-C. Chen, J.-C. Huang, Y.-C. Tsai, R. N. Hsiu-Chin Mai, R. N. Jui-Hsin Chen, P.-L. Kuo, J.-M. Chang, S.-J. Hwang, and H.-C. Chen. Heart rate variability

- change before and after hemodialysis is associated with overall and cardiovascular mortality in hemodialysis. *Scientific Reports*, 6:20597–, Feb. 2016.
- [37] W. Chen, Z. Wang, H. Xie, and W. Yu. Characterization of surface EMG signal based on fuzzy entropy. *Neural Systems and Rehabilitation Engineering, IEEE Transactions on*, 15(2):266–272, 2007. ISSN 1534-4320. doi: 10.1109/TNSRE.2007.897025.
- [38] W. Chen, J. Zhuang, W. Yu, and Z. Wang. Measuring complexity using fuzzyen, apen, and sampen. *Medical Engineering & Physics*, 31(1):61–68, 2009. ISSN 1350-4533. doi: 10.1016/j.medengphy.2008.04.005.
- [39] K. Chon, C. Scully, and S. Lu. Approximate entropy for all signals. *IEEE Engineering in Medicine and Biology Magazine*, 28(6):18–23, 2009. ISSN 0739-5175. doi: 10.1109/MEMB.2009.934629.
- [40] A. Ciampi, J. Thiffault, J.-P. Nakache, and B. Asselain. Stratification by stepwise regression, correspondence analysis and recursive partition: a comparison of three methods of analysis for survival data with covariates. *Computational statistics & data analysis*, 4(3):185–204, 1986.
- [41] L. M. Cohen, R. Ruthazer, A. H. Moss, and M. J. Germain. Predicting six-month mortality for patients who are on maintenance hemodialysis. *Clinical Journal of the American Society of Nephrology*, 5(1):72–79, 2010. ISSN 1555-9041.
- [42] A. C. Covic, L.-D. Buimistriuc, D. Green, A. Stefan, S. Badarau, and P. A. Kalra. The prognostic value of electrocardiographic estimation of left ventricular hypertrophy in dialysis patients. *Annals of Noninvasive Electrocardiology*, 18(2):188–198, 2013. ISSN 1542-474X. doi: 10.1111/anec.12007.
- [43] D. R. Cox. Regression models and life-tables. *Journal of the Royal Statistical Society. Series B (Methodological)*, 34(2):187–220, 1972. ISSN 00359246.
- [44] J. T. Daugirdas. Second generation logarithmic estimates of single-pool variable volume kt/v: an analysis of error. *Journal of the American Society of Nephrology*, 4(5):1205–1213, 1993. ISSN 1046-6673.
- [45] B. Di Iorio and A. Bellasi. QT interval in CKD and haemodialysis patients. *Clinical Kidney Journal*, 2013. doi: 10.1093/ckj/sfs183.
- [46] A. Diery, D. Rowlands, T. Cutmore, and D. James. Automated ECG diagnostic P-wave analysis using wavelets. *Computer Methods and Programs in Biomedicine*, In Press, Corrected Proof:–, 2010. ISSN 0169-2607. doi: DOI:10.1016/j.cmpb.2010.04.012.

- [47] P. Drawz, D. Babineau, C. Brecklin, J. He, R. Kallem, E. Soliman, D. Xie, D. Appleby, A. Anderson, and M. Rahman. Heart rate variability is a predictor of mortality in chronic kidney disease: A report from the CRIC study. *Am J Nephrol*, 38(6):517–528, 2013. ISSN 0250-8095. doi: 10.1159/000357200.
- [48] W. J. Elliott. Circadian variation in blood pressure: Implications for the elderly patient. *American Journal of Hypertension*, 12(S2):43S–49S, 02 1999. ISSN 0895-7061. doi: 10.1016/S0895-7061(98)00279-9.
- [49] J. Filipovský, O. Mayer, M. Dolejšová, and J. Seidlerová. The assessment of carotid–femoral distance for aortic pulse wave velocity: Should it be estimated from body height? *Artery Research*, 4(1):19–23, 2010. ISSN 1872-9312. doi: 10.1016/j.artres.2010.01.002.
- [50] R. N. Foley, P. S. Parfrey, and M. J. Sarnak. Clinical epidemiology of cardiovascular disease in chronic renal disease. *American Journal of Kidney Diseases*, 32(5):S112–S119, 1998.
- [51] P. M. Franssen and B. P. Imholz. Evaluation of the Mobil-O-Graph new generation ABPM device using the ESH criteria. *Blood pressure monitoring*, 15(4):229–231, 2010.
- [52] U. Frei and QuaSi-Niere task group. Quality assurance in renal replacement therapy (RRT)—background of a developing German National Registry for RRT. *Nephrology Dialysis Transplantation*, 10(4):442–443, Apr. 1995. ISSN 0931-0509. doi: 10.1093/ndt/10.4.442.
- [53] U. Frei and H. Schober-Halstenberg. Annual report of the german renal registry 1998. quasi-niere task group for quality assurance in renal replacement therapy. *Nephrology, dialysis, transplantation: official publication of the European Dialysis and Transplant Association-European Renal Association*, 14(5):1085–1090, 1999.
- [54] U. Frei and H. Schober-Halstenberg. Jahresberichte der QuaSi-Niere gGmbH iL. <http://www.bundesverband-niere.de/bundesverband/quasi-niere/jahresberichte.html>, 2008. [Online; accessed 25-January-2019].
- [55] H. Fukuta, J. Hayano, S. Ishihara, S. Sakata, S. Mukai, N. Ohte, K. Ojika, K. Yagi, H. Matsumoto, S. Sohmiya, and G. Kimura. Prognostic value of heart rate variability in patients with end-stage renal disease on chronic haemodialysis. *Nephrology Dialysis Transplantation*, 18(2):318–325, 2003.
- [56] D. Gallagher, A. Adji, and M. F. O’Rourke. Validation of the transfer function technique for generating central from peripheral upper limb pressure waveform, 2004.

- [57] M. A. García-González, M. Fernández-Chimeno, F. Guede-Fernández, V. Ferrer-Mileo, A. Argelagós-Palau, L. Álvarez Gómez, E. Parrado, J. Moreno, L. Capdevila, and J. Ramos-Castro. A methodology to quantify the differences between alternative methods of heart rate variability measurement. *Physiological Measurement*, 37(1):128, 2016.
- [58] M. García-González, J. Ramos-Castro, and M. Fernández-Chimeno. The effect of electrocardiographic lead choice on RR time series. In *Engineering in Medicine and Biology Society, EMBC, 2011 Annual International Conference of the IEEE*, pages 1933–1936. IEEE, 2011.
- [59] L. Geddes, M. Voelz, C. Combs, D. Reiner, and C. F. Babbs. Characterization of the oscillometric method for measuring indirect blood pressure. *Annals of biomedical engineering*, 10(6):271–280, 1982.
- [60] A. S. Go, G. M. Chertow, D. Fan, C. E. McCulloch, and C.-y. Hsu. Chronic kidney disease and the risks of death, cardiovascular events, and hospitalization. *New England Journal of Medicine*, 351(13):1296–1305, 2004. doi: 10.1056/NEJMoa041031. PMID: 15385656.
- [61] E. Goldberger. A simple, indifferent, electrocardiographic electrode of zero potential and a technique of obtaining augmented, unipolar, extremity leads. *American Heart Journal*, 23(4):483–492, 1942. ISSN 0002-8703. doi: 10.1016/S0002-8703(42)90293-X.
- [62] L. Gordon and R. A. Olshen. Tree-structured survival analysis. *Cancer treatment reports*, 69(10):1065–1069, 1985.
- [63] P. Grassberger and I. Procaccia. Characterization of strange attractors. *Phys. Rev. Lett.*, 50:346–349, Jan. 1983.
- [64] P. Grassberger and I. Procaccia. Measuring the strangeness of strange attractors. *Physica D: Nonlinear Phenomena*, 9(1):189–208, 1983. ISSN 0167-2789. doi: 10.1016/0167-2789(83)90298-1.
- [65] A. Grassmann, S. Gioberge, S. Moeller, and G. Brown. Esrd patients in 2004: global overview of patient numbers, treatment modalities and associated trends. *Nephrology Dialysis Transplantation*, 20(12):2587–2593, 2005. doi: 10.1093/ndt/gfi159.
- [66] A. P. Guerin, J. Blacher, B. Pannier, S. J. Marchais, M. E. Safar, and G. M. London. Impact of aortic stiffness attenuation on survival of patients in end-stage renal failure. *Circulation*, 103(7):987–992, 2001. ISSN 0009-7322. doi: 10.1161/01.CIR.103.7.987.

- [67] A. Guyton and J. Hall. *Textbook of medical physiology*. WB Saunders Company, Philadelphia, Pennsylvania, 10th edition, 2000.
- [68] S. Hagmair, M. Bachler, M. C. Braunisch, G. Lorenz, C. Schmaderer, A.-L. Hasenau, L. v. Stülpnagel, A. Bauer, K. D. Rizas, S. Wassertheurer, and C. C. Mayer. Challenging recently published parameter sets for entropy measures in risk prediction for end-stage renal disease patients. *Entropy*, 19(11), 2017. ISSN 1099-4300. doi: 10.3390/e19110582.
- [69] S. Hagmair, M. C. Braunisch, M. Bachler, C. Schmaderer, A.-L. Hasenau, A. Bauer, K. D. Rizas, S. Wassertheurer, and C. C. Mayer. Implementation and verification of an enhanced algorithm for the automatic computation of RR-interval series derived from 24 h 12-lead ECGs. *Physiological Measurement*, 38(1): 1–14, 2017.
- [70] B. Hametner, S. Wassertheurer, J. Kropf, C. Mayer, B. Eber, and T. Weber. Oscillometric estimation of aortic pulse wave velocity: comparison with intra-aortic catheter measurements. *Blood pressure monitoring*, 18(3):173–176, 2013.
- [71] E. W. Hancock, B. J. Deal, D. M. Mirvis, P. Okin, P. Kligfield, and L. S. Gettes. AHA/ACCF/HRS recommendations for the standardization and interpretation of the electrocardiogram Part V: electrocardiogram changes associated with cardiac chamber hypertrophy – a scientific statement from the american heart association electrocardiography and arrhythmias committee, council on clinical cardiology; the american college of cardiology foundation; and the heart rhythm society endorsed by the international society for computerized electrocardiology. *Journal of the American College of Cardiology*, 53(11):992–1002, 2009. doi: 10.1016/j.jacc.2008.12.015.
- [72] J. Hayano, H. Takahashi, T. Toriyama, S. Mukai, A. Okada, S. Sakata, A. Yamada, N. Ohte, and H. Kawahara. Prognostic value of heart rate variability during long-term follow-up in chronic haemodialysis patients with end-stage renal disease. *Nephrology, dialysis, transplantation: official publication of the European Dialysis and Transplant Association-European Renal Association*, 14(6):1480–1488, 1999.
- [73] E. Hermeling, A. P. Hoeks, M. H. Winkens, J. L. Waltenberger, R. S. Reneman, A. A. Kroon, and K. D. Reesink. Noninvasive assessment of arterial stiffness should discriminate between systolic and diastolic pressure ranges. *Hypertension*, 55(1): 124–130, 2010. doi: 10.1161/HYPERTENSIONAHA.109.143867.
- [74] C. W. Hogue, P. P. Domitrovich, P. K. Stein, G. D. Despotis, L. Re, R. B. Schuessler, R. E. Kleiger, and J. N. Rottman. RR interval dynamics before atrial

- fibrillation in patients after coronary artery bypass graft surgery. *Circulation*, 98(5):429–434, 1998. doi: 10.1161/01.CIR.98.5.429.
- [75] A. Holzinger, M. Hörtenhuber, C. Mayer, M. Bachler, S. Wassertheurer, A. J. Pinho, and D. Koslicki. On entropy-based data mining. In A. Holzinger and I. Jurisica, editors, *Interactive Knowledge Discovery and Data Mining in Biomedical Informatics*, volume 8401 of *Lecture Notes in Computer Science*, pages 209–226. Springer Berlin Heidelberg, 2014. ISBN 978-3-662-43967-8. doi: 10.1007/978-3-662-43968-5_12.
- [76] E. Hon and S. Lee. The fetal Electrocardiogram. I. The Eelectrocardiogram of the dying fetus. *American journal of obstetrics and gynecology*, 87:804–813, 1963.
- [77] T. Hothorn, K. Hornik, and A. Zeileis. Unbiased recursive partitioning: A conditional inference framework. *Journal of Computational and Graphical statistics*, 15(3):651–674, 2006.
- [78] S. A. Huybrechts, D. G. Devos, S. J. Vermeersch, D. Mahieu, E. Achten, T. L. de Backer, P. Segers, and L. M. van Bortel. Carotid to femoral pulse wave velocity: a comparison of real travelled aortic path lengths determined by MRI and superficial measurements. *Journal of hypertension*, 29(8):1577–1582, 2011.
- [79] K. J. Jager, M. Pippias, M. Noordzij, V. S. Stel, A. Kramer, M. Bonthuis, F. J. Caskey, P. Castro de la Nuez, H. Cernevsikis, J.-M. des Grottes, et al. The European Renal Association – European Dialysis and Transplant Association (ERA-EDTA) Registry Annual Report 2015: a summary. *Clinical Kidney Journal*, 11(1):108–122, Jan. 2018. ISSN 2048-8505. doi: 10.1093/ckj/sfx149.
- [80] J. Kahn and J. Howell. Frank Norman Wilson. *Clinical cardiology*, 10(10):616–618, 1987.
- [81] E. L. Kaplan and P. Meier. Nonparametric estimation from incomplete observations. *Journal of the American Statistical Association*, 53(282):457–481, 1958. doi: 10.1080/01621459.1958.10501452.
- [82] M. Karamanoglu, M. O’rourke, A. Avolio, and R. Kelly. An analysis of the relationship between central aortic and peripheral upper limb pressure waves in man. *European heart journal*, 14(2):160–167, 1993.
- [83] M. Karlén. Circadian clock. <https://www.nobelprize.org/prizes/medicine/2017/press-release/>, January 2017. Accessed 2019-02-27.
- [84] P. M. Kearney, M. Whelton, K. Reynolds, P. Muntner, P. K. Whelton, and J. He. Global burden of hypertension: analysis of worldwide data. *The lancet*, 365(9455):217–223, 2005.

- [85] R. Kelly, C. Hayward, A. Avolio, and M. O’rourke. Noninvasive determination of age-related changes in the human arterial pulse. *Circulation*, 80(6):1652–1659, 1989.
- [86] N. Kida, Y. Tsubakihara, H. Kida, S. Ageta, M. Arai, Y. Hamada, and N. Matsuura. Usefulness of measurement of heart rate variability by holter ECG in hemodialysis patients. *BMC Nephrology*, 18(1):8, 2017. ISSN 1471-2369. doi: 10.1186/s12882-016-0423-3.
- [87] R. E. Kleiger, J. Miller, J. Bigger, and A. J. Moss. Decreased heart rate variability and its association with increased mortality after acute myocardial infarction. *The American Journal of Cardiology*, 59(4):256 – 262, 1987. ISSN 0002-9149. doi: [https://doi.org/10.1016/0002-9149\(87\)90795-8](https://doi.org/10.1016/0002-9149(87)90795-8).
- [88] P. Kligfield, L. S. Gettes, J. J. Bailey, R. Childers, B. J. Deal, E. W. Hancock, G. van Herpen, J. A. Kors, P. Macfarlane, D. M. Mirvis, et al. Recommendations for the standardization and interpretation of the electrocardiogram: Part i: The electrocardiogram and its technology a scientific statement from the American heart association electrocardiography and arrhythmias committee, council on clinical cardiology; the American college of cardiology foundation; and the heart rhythm society endorsed by the international society for computerized electrocardiology. *Journal of the American College of Cardiology*, 49(10):1109–1127, 2007. ISSN 0735-1097.
- [89] P. Kligfield, F. Badilini, I. Rowlandson, J. Xue, E. Clark, B. Devine, P. Macfarlane, J. de Bie, D. Mortara, S. Babaeizadeh, R. Gregg, E. D. Helfenbein, and C. L. Green. Comparison of automated measurements of electrocardiographic intervals and durations by computer-based algorithms of digital electrocardiographs. *American Heart Journal*, 167(2):150 – 159.e1, 2014. ISSN 0002-8703. doi: <http://doi.org/10.1016/j.ahj.2013.10.004>.
- [90] D. Korteweg. Über die Fortpflanzungsgeschwindigkeit des Schalles in elastischen Röhren. *Annalen der Physik*, 241(12):525–542, 1878.
- [91] G. Koutroumbas, P. I. Georgianos, P. A. Sarafidis, A. Protogerou, A. Karpetas, P. Vakianis, V. Raptis, V. Liakopoulos, S. Panagoutsos, C. Syrganis, and P. Pasadakis. Ambulatory aortic blood pressure, wave reflections and pulse wave velocity are elevated during the third in comparison to the second interdialytic day of the long interval in chronic haemodialysis patients. *Nephrology Dialysis Transplantation*, 30(12):2046–2053, 2015. doi: 10.1093/ndt/gfv090.
- [92] N. Kumaravel and C. Santhi. Nonlinear filters for preprocessing heart rate vari-

- ability signals. *International Journal of Computer Science and Network Security*, 10:250–254, 2010.
- [93] P. Laguna, D. Vigo, R. Jane, and P. Caminal. Automatic wave onset and offset determination in ECG signals: Validation with the CSE database. In *Computers in Cardiology 1992, Proceedings of*, pages 167–170, Oct. 1992. doi: 10.1109/CIC.1992.269420.
- [94] P. Laguna, R. Jané, and P. Caminal. Automatic detection of wave boundaries in multilead ECG signals: Validation with the CSE database. *Comput. Biomed. Res.*, 27(1):45–60, Feb. 1994. ISSN 0010-4809. doi: 10.1006/cbmr.1994.1006.
- [95] S. Laurent, J. Cockcroft, L. Van Bortel, P. Boutouyrie, C. Giannattasio, D. Hayoz, B. Pannier, C. Vlachopoulos, I. Wilkinson, and H. Struijker-Boudier. Expert consensus document on arterial stiffness: methodological issues and clinical applications. *European Heart Journal*, 27(21):2588–2605, 2006. doi: 10.1093/eurheartj/ehl254.
- [96] M. LeBlanc and J. Crowley. Relative risk trees for censored survival data. *Biometrics*, pages 411–425, 1992.
- [97] M. LeBlanc and J. Crowley. *A review of tree-based prognostic models*, pages 113–124. Springer US, Boston, MA, 1995. ISBN 978-1-4615-2009-2. doi: 10.1007/978-1-4615-2009-2_6.
- [98] A. S. Levey, P. E. De Jong, J. Coresh, M. E. Nahas, B. C. Astor, K. Matsushita, R. T. Gansevoort, B. L. Kasiske, and K.-U. Eckardt. The definition, classification, and prognosis of chronic kidney disease: a kdigo controversies conference report. *Kidney international*, 80(1):17–28, 2011.
- [99] A. Levin, P. E. Stevens, R. W. Bilous, J. Coresh, A. L. De Francisco, P. E. De Jong, K. E. Griffith, B. R. Hemmelgarn, K. Iseki, E. J. Lamb, et al. Kidney disease: Improving global outcomes (kdigo) ckd work group. kdigo 2012 clinical practice guideline for the evaluation and management of chronic kidney disease. *Kidney International Supplements*, 3(1):1–150, 2013.
- [100] R. G. Linford and N. W. Ryan. Pulsatile flow in rigid tubes. *Journal of Applied Physiology*, 20(5):1078–1082, 1965. doi: 10.1152/jappl.1965.20.5.1078.
- [101] C. Liu, C. Liu, P. Shao, L. Li, X. Sun, X. Wang, and F. Liu. Comparison of different threshold values r for approximate entropy: application to investigate the heart rate variability between heart failure and healthy control groups. *Physiological Measurement*, 32(2):167, 2011.

- [102] C. Liu, K. Li, L. Zhao, F. Liu, D. Zheng, C. Liu, and S. Liu. Analysis of heart rate variability using fuzzy measure entropy. *Computers in Biology and Medicine*, 43(2):100–108, 2013. ISSN 0010-4825. doi: 10.1016/j.compbimed.2012.11.005.
- [103] J. Liu, Z. Huang, D. T. Gilbertson, R. N. Foley, and A. J. Collins. An improved comorbidity index for outcome analyses among dialysis patients. *Kidney international*, 77(2):141–151, 2010.
- [104] T. Liyanage, T. Ninomiya, V. Jha, B. Neal, H. M. Patrice, I. Okpechi, M. hui Zhao, J. Lv, A. X. Garg, J. Knight, A. Rodgers, M. Gallagher, S. Kotwal, A. Cass, and V. Perkovic. Worldwide access to treatment for end-stage kidney disease: a systematic review. *The Lancet*, 385(9981):1975–1982, 2015. ISSN 0140-6736.
- [105] N. Lomb. Least-squares frequency analysis of unequally spaced data. *Astrophysics and space science*, 39(2):447–462, 1976.
- [106] G. M. London, J. Blacher, B. Pannier, A. P. Guérin, S. J. Marchais, and M. E. Safar. Arterial wave reflections and survival in end-stage renal failure. *Hypertension*, 38(3):434–438, 2001. doi: 10.1161/01.HYP.38.3.434.
- [107] E. Lowrie. The urea reduction ratio (URR): A simple method for evaluating hemodialysis treatment. *Contemp Dial Nephrol*, 12:11–20, 1991.
- [108] S. Lu, X. Chen, J. Kanters, I. Solomon, and K. Chon. Automatic selection of the threshold value r for approximate entropy. *Biomedical Engineering, IEEE Transactions on*, 55(8):1966–1972, 2008. ISSN 0018-9294. doi: 10.1109/TBME.2008.919870.
- [109] C. Lucas, B. Wilcox, B. Ha, and G. W. Henry. Comparison of time domain algorithms for estimating aortic characteristic impedance in humans. *IEEE transactions on biomedical engineering*, 35(1):62–68, 1988.
- [110] T. H. Mäkikallio, H. V. Huikuri, U. Hintze, J. Videbæk, R. D. Mitrani, A. Castellanos, R. J. Myerburg, and M. Møller. Fractal analysis and time- and frequency-domain measures of heart rate variability as predictors of mortality in patients with heart failure. *The American Journal of Cardiology*, 87(2):178–182, 2001. ISSN 0002-9149.
- [111] A. Malliani, M. Pagani, F. Lombardi, and S. Cerutti. Cardiovascular neural regulation explored in the frequency domain. *Circulation*, 84(2):482–492, 1991.
- [112] G. Mancia, R. Fagard, K. Narkiewicz, J. Redón, A. Zanchetti, M. Böhm, T. Christiaens, R. Cifkova, G. De Backer, A. Dominiczak, M. Galderisi, D. E. Grobbee, et al. 2013 ESH/ESC guidelines for the management of arterial hypertension: The

- task force for the management of arterial hypertension of the European society of hypertension (ESH) and of the European society of cardiology (ESC). *Journal of Hypertension*, 31(7):1281–1357, 2013. doi: 10.1097/01.hjh.0000431740.32696.cc.
- [113] E.-J. Marey. *La méthode graphique dans les sciences expérimentales et principalement en physiologie et en médecine*. G. Masson, 1878.
- [114] L. Marple. Resolution of conventional fourier, autoregressive, and special arma methods of spectrum analysis. In *Acoustics, Speech, and Signal Processing, IEEE International Conference on ICASSP'77.*, volume 2, pages 74–77. IEEE, 1977.
- [115] A. Martínez, R. Alcaraz, and J. Rieta. Detection and removal of ventricular ectopic beats in atrial fibrillation recordings via principal component analysis. In *Engineering in Medicine and Biology Society, EMBC, 2011 Annual International Conference of the IEEE*, pages 4693–4696. IEEE, 2011.
- [116] J. Martinez, R. Almeida, S. Olmos, A. Rocha, and P. Laguna. A wavelet-based ECG delineator: evaluation on standard databases. *Biomedical Engineering, IEEE Transactions on*, 51(4):570–581, Apr. 2004. ISSN 0018-9294. doi: 10.1109/TBME.2003.821031.
- [117] J. Mateo and P. Laguna. Analysis of heart rate variability in the presence of ectopic beats using the heart timing signal. *Biomedical Engineering, IEEE Transactions on*, 50(3):334–343, 2003. ISSN 0018-9294. doi: 10.1109/TBME.2003.808831.
- [118] J. Matschkal, C. C. Mayer, P. A. Sarafidis, G. Lorenz, M. C. Braunisch, R. Guenther, S. Angermann, D. Steubl, S. Kemmner, Q. Bachmann, C. Hauser, L. Nerl, M. Baumann, J. F. Mann, P. Moog, C. Kuechle, L. Renders, U. Heemann, S. Wassertheurer, and C. Schmaderer. Comparison of 24-hour and office pulse wave velocity for prediction of mortality in hemodialysis patients. *Am J Nephrol*, 49(4):317–327, 2019. ISSN 0250-8095.
- [119] G. Mauck, C. Smith, L. Geddes, and J. Bourland. The meaning of the point of maximum oscillations in cuff pressure in the indirect measurement of blood pressure—part ii. *Journal of biomechanical engineering*, 102(1):28–33, 1980.
- [120] C. Mayer, M. Bachler, M. Hörtenhuber, C. Stocker, A. Holzinger, and S. Wassertheurer. Selection of entropy-measure parameters for knowledge discovery in heart rate variability data. *BMC Bioinformatics*, 15(Suppl 6):S2, 2014. ISSN 1471-2105. doi: 10.1186/1471-2105-15-S6-S2.
- [121] C. Mayer, M. Bachler, A. Holzinger, P. K. Stein, and S. Wassertheurer. The effect of threshold values and weighting factors on the association between en-

- trophy measures and mortality after myocardial infarction in the cardiac arrhythmia suppression trial (CAST). *Entropy*, 18(4):129, 2016. ISSN 1099-4300. doi: 10.3390/e18040129.
- [122] C. C. Mayer, J. Matschkal, P. A. Sarafidis, S. Hagmair, G. Lorenz, S. Angermann, M. C. Braunisch, M. Baumann, U. Heemann, S. Wassertheurer, and C. Schmaderer. Association of ambulatory blood pressure with all-cause and cardiovascular mortality in hemodialysis patients: Effects of heart failure and atrial fibrillation. *Journal of the American Society of Nephrology*, 29(9):2409–2417, 09 2018.
- [123] K. McCullough, P. Sharma, T. Ali, I. Khan, W. C. Smith, A. MacLeod, and C. Black. Measuring the population burden of chronic kidney disease: a systematic literature review of the estimated prevalence of impaired kidney function. *Nephrology Dialysis Transplantation*, 27(5):1812–1821, 2012. doi: 10.1093/ndt/gfr547.
- [124] J. McNames, T. Thong, and M. Aboy. Impulse rejection filter for artifact removal in spectral analysis of biomedical signals. *Conf Proc IEEE Eng Med Biol Soc*, 1: 145–148, 2004.
- [125] Medical Netcare GmbH. Quality Assurance in dialysis care in Germany. <https://m-nc.de/en/qa-dialysis>, 2016. [Online; accessed 25-January-2019].
- [126] Medical Netcare GmbH. Jahresbericht Datenanalyse Dialyse für den Gemeinsamen Bundesausschuss, Berichtsjahr 2016. https://www.g-ba.de/downloads/39-261-3024/2017-07-20_QSD-RL_MNC-Jahresbericht-2016.pdf, 2017. [Online; accessed 23-Januar-2019].
- [127] S. Milborrow. *rpart.plot: Plot 'rpart' Models: An Enhanced Version of 'plot.rpart'*, 2018. R package version 3.0.6, Available at <https://CRAN.R-project.org/package=rpart.plot>.
- [128] S. Moeller, S. Gioberge, and G. Brown. ESRD patients in 2001: global overview of patients, treatment modalities and development trends. *Nephrology Dialysis Transplantation*, 17(12):2071–2076, Dec. 2002.
- [129] A. I. Moens. *Die Pulskurve*. EJ Brill, 1878.
- [130] H. Mølgaard. Evaluation of the reynolds pathfinder ii system for 24 h heart rate variability analysis. *European heart journal*, 12(11):1153–1162, 1991.
- [131] J. N. Morgan and J. A. Sonquist. Problems in the analysis of survey data, and a proposal. *Journal of the American statistical association*, 58(302):415–434, 1963.

- [132] J. P. Murgó, N. Westerhof, J. P. Giolma, and S. A. Altobelli. Aortic input impedance in normal man: relationship to pressure wave forms. *Circulation*, 62(1):105–116, 1980.
- [133] National Kidney Foundation. K/DOQI clinical practice guidelines for chronic kidney disease: Evaluation, classification, and stratification. *American Journal of Kidney Diseases*, 39(2 SUPPL. 1), 2002.
- [134] W. Nichols, M. O'Rourke, and C. Vlachopoulos. *McDonald's blood flow in arteries: theoretical, experimental and clinical principles*. CRC Press, London, 6th edition edition, 2011.
- [135] T. F. of ESC and NASPE. Heart rate variability: standards of measurement, physiological interpretation and clinical use. Task Force of the European Society of Cardiology and the North American Society of Pacing and Electrophysiology. *Circulation*, 93(5):1043–1065, Mar. 1996.
- [136] B. Olshansky, H. N. Sabbah, P. J. Hauptman, and W. S. Colucci. Parasympathetic nervous system and heart failure: pathophysiology and potential implications for therapy. *Circulation*, 118(8):863–871, Aug. 2008.
- [137] M. F. O'Rourke. Influence of ventricular ejection on the relationship between central aortic and brachial pressure pulse in man. *Cardiovascular Research*, 4(3):291–300, July 1970. ISSN 0008-6363.
- [138] Österreichisches Dialyse- und TransplantationsregisterGesellschaft. Nierenerersatztherapie in Österreich. https://www.nephro.at/JB_all.htm, 2017. [Online; accessed 04-February-2019].
- [139] J. Pan and W. Tompkins. A real-time qrs detection algorithm. *Biomedical Engineering, IEEE Transactions on*, (3):230–236, 1985.
- [140] B. Pannier, A. P. Guérin, S. J. Marchais, M. E. Safar, and G. M. London. Stiffness of capacitive and conduit arteries. *Hypertension*, 45(4):592–596, 2005. ISSN 0194-911X. doi: 10.1161/01.HYP.0000159190.71253.c3.
- [141] G. Parati, J. E. Ochoa, G. Bilo, R. Agarwal, A. Covic, F. W. Dekker, D. Fliser, G. H. Heine, K. J. Jager, L. Gargani, M. Kanbay, F. Mallamaci, Z. Massy, A. Ortiz, E. Picano, P. Rossignol, P. Sarafidis, R. Sicari, R. Vanholder, A. Wiecek, G. London, and C. Zoccali. Hypertension in chronic kidney disease part 1: Out-of-office blood pressure monitoring: Methods, thresholds, and patterns. *Hypertension*, 67(6):1093–1101, 2016. doi: 10.1161/HYPERTENSIONAHA.115.06895.

- [142] A. L. Pauca, M. F. O'Rourke, and N. D. Kon. Prospective evaluation of a method for estimating ascending aortic pressure from the radial artery pressure waveform. *Hypertension*, 38(4):932–937, 2001. doi: 10.1161/hy1001.096106.
- [143] T. G. Pickering, J. E. Hall, L. J. Appel, B. E. Falkner, J. Graves, M. N. Hill, D. W. Jones, T. Kurtz, S. G. Sheps, and E. J. Roccella. Recommendations for blood pressure measurement in humans and experimental animals. *Hypertension*, 45(1):142–161, 2005. doi: 10.1161/01.HYP.0000150859.47929.8e.
- [144] S. M. Pincus. Approximate entropy as a measure of system complexity. *Proceedings of the National Academy of Sciences*, 88(6):2297–2301, 1991.
- [145] S. M. Pincus and A. L. Goldberger. Physiological time-series analysis: what does regularity quantify? *American Journal of Physiology - Heart and Circulatory Physiology*, 266(4):H1643–H1656, 1994.
- [146] S. M. Pincus and R. R. Viscarello. Approximate entropy: a regularity measure for fetal heart rate analysis. *Obstet Gynecol*, 79(2):249–255, 1992.
- [147] S. M. Pincus, I. M. Gladstone, and R. A. Ehrenkranz. A regularity statistic for medical data analysis. *Journal of clinical monitoring*, 7(4):335–345, 1991.
- [148] A. Porta, T. Gnechi-Ruscone, E. Tobaldini, S. Guzzetti, R. FoptUlan, and N. Montano. Progressive decrease of heart period variability entropy-based complexity during graded head-up tilt. *Journal of Applied Physiology*, 103(4):1143–1149, 2007. ISSN 8750-7587. doi: 10.1152/jappphysiol.00293.2007.
- [149] R Core Team. *R: A Language and Environment for Statistical Computing*. R Foundation for Statistical Computing, Vienna, Austria, 2017. Available at <https://www.R-project.org/>, Accessed 2019-04-05.
- [150] U. Rajendra Acharya, K. Paul Joseph, N. Kannathal, C. Lim, and J. Suri. Heart rate variability: a review. *Medical and Biological Engineering and Computing*, 44: 1031–1051, 2006. ISSN 0140-0118. doi: 10.1007/s11517-006-0119-0.
- [151] M. Ramsey. Noninvasive automatic determination of mean arterial pressure. *Medical and Biological Engineering and Computing*, 17(1):11–18, 1979.
- [152] J. S. Richman and J. R. Moorman. Physiological time-series analysis using approximate entropy and sample entropy. *American Journal of Physiology - Heart and Circulatory Physiology*, 278(6):H2039–H2049, 2000.
- [153] M. T. L. Rovere, J. T. B. Jr, F. I. Marcus, A. Mortara, and P. J. Schwartz. Baroreflex sensitivity and heart-rate variability in prediction of total cardiac mor-

- tality after myocardial infarction. *The Lancet*, 351(9101):478 – 484, 1998. ISSN 0140-6736.
- [154] D. Rubinger, N. Revis, A. Pollak, M. H. Luria, and D. Sapoznikov. Predictors of haemodynamic instability and heart rate variability during haemodialysis. *Nephrology Dialysis Transplantation*, 19(8):2053–2060, 2004. doi: 10.1093/ndt/gfh306.
- [155] D. Saadi, G. Taney, M. Flintrup, A. Osmanagic, K. Egstrup, K. Hoppe, P. Jennum, J. Jeppesen, H. Iversen, and H. Sorensen. Automatic real-time embedded QRS complex detection for a novel patch-type electrocardiogram recorder. *Translational Engineering in Health and Medicine, IEEE Journal of*, 3:1–12, 2015. ISSN 2168-2372. doi: 10.1109/JTEHM.2015.2421901.
- [156] M. E. Safar, J. Blacher, B. Pannier, A. P. Guerin, S. J. Marchais, P.-M. Guyonvarc’h, and G. M. London. Central pulse pressure and mortality in end-stage renal disease. *Hypertension*, 39(3):735–738, 2002. doi: 10.1161/hy0202.098325.
- [157] A. H. Salans, L. N. Katz, G. R. Graham, A. Gordon, E. I. Elisberg, and A. Gerber. A study of the central and peripheral arterial pressure pulse in man. *Circulation*, 4(4):510–521, 1951. doi: 10.1161/01.CIR.4.4.510.
- [158] M. A. Salo, H. V. Huikuri, and T. Seppanen. Ectopic beats in heart rate variability analysis: effects of editing on time and frequency domain measures. *Ann Noninvasive Electrocardiol*, 6(1):5–17, Jan 2001.
- [159] P. Sarafidis, P. Georgianos, A. Karpetas, A. Bikos, L. Korelidou, M. Tersi, D. Divanis, G. Tzani, K. Mavromatidis, V. Liakopoulos, P. Zebekakis, A. Lasaridis, and A. Protogerou. Evaluation of a novel brachial cuff-based oscillometric method for estimating central systolic pressure in hemodialysis patients. *Am J Nephrol*, 40(3):242–250, 2014. ISSN 0250-8095.
- [160] P. A. Sarafidis, C. Loutradis, A. Karpetas, G. Tzani, A. Piperidou, G. Koutroumpas, V. Raptis, C. Syrgkanis, V. Liakopoulos, G. Efstratiadis, G. London, and C. Zoccali. Ambulatory pulse wave velocity is a stronger predictor of cardiovascular events and all-cause mortality than office and ambulatory blood pressure in hemodialysis patients. *Hypertension*, 70(1):148–157, 2017. ISSN 0194-911X. doi: 10.1161/HYPERTENSIONAHA.117.09023.
- [161] P. A. Sarafidis, A. Persu, R. Agarwal, M. Burnier, P. de Leeuw, C. J. Ferro, J.-M. Halimi, G. H. Heine, M. Jadoul, F. Jarraya, et al. Hypertension in dialysis patients: a consensus document by the european renal and cardiovascular medicine

- (EURECA-m) working group of the european renal association–european dialysis and transplant association (ERA-EDTA) and the hypertension and the kidney working group of the European Society of Hypertension (ESH). *Nephrology Dialysis Transplantation*, 32(4):620–640, 2017. doi: 10.1093/ndt/gfw433.
- [162] R. Saran, B. Robinson, K. C. Abbott, L. Y. Agodoa, P. Albertus, J. Ayanian, R. Balkrishnan, J. Bragg-Gresham, J. Cao, J. L. Chen, et al. US renal data system 2016 annual data report: epidemiology of kidney disease in the United States. *American journal of kidney diseases*, 69(3):A7–A8, 2017.
- [163] R. Saran, B. Robinson, K. C. Abbott, L. Y. Agodoa, N. Bhave, J. Bragg-Gresham, R. Balkrishnan, X. Dietrich, A. Eckard, P. W. Eggers, et al. Us renal data system 2017 Annual data report: Epidemiology of kidney disease in the United States. *American Journal of Kidney Diseases*, 71(3, Supplement 1):A7, 2018. ISSN 0272-6386. US Renal Data System 2017 Annual Data Report.
- [164] M. J. Sarnak, A. S. Levey, A. C. Schoolwerth, J. Coresh, B. Culleton, L. L. Hamm, P. A. McCullough, B. L. Kasiske, E. Kelepouris, M. J. Klag, P. Parfrey, M. Pfeffer, L. Raij, D. J. Spinosa, and P. W. Wilson. Kidney disease as a risk factor for development of cardiovascular disease. *Hypertension*, 42(5):1050–1065, 2003.
- [165] R. Sassi, S. Cerutti, F. Lombardi, M. Malik, H. V. Huikuri, C.-K. Peng, G. Schmidt, Y. Yamamoto, B. Gorenek, G. H. Lip, G. Grassi, G. Kudaiberdieva, J. P. Fisher, M. Zabel, and R. Macfadyen. Advances in heart rate variability signal analysis: joint position statement by the e-cardiology esc working group and the european heart rhythm association co-endorsed by the asia pacific heart rhythm society. *Europace*, 2015. ISSN 1099-5129. doi: 10.1093/europace/euv015.
- [166] J. D. Scargle. Studies in astronomical time series analysis. II-Statistical aspects of spectral analysis of unevenly spaced data. *The Astrophysical Journal*, 263:835–853, Dec. 1982.
- [167] J. Schläpfer and H. J. Wellens. Computer-interpreted electrocardiograms: benefits and limitations. *Journal of the American College of Cardiology*, 70(9):1183–1192, 2017.
- [168] C. Schmaderer, S. Tholen, A.-L. Hasenau, C. Hauser, Y. Suttman, S. Wassertheurer, C. C. Mayer, A. Bauer, K. D. Rizas, S. Kemmner, K. Kotliar, B. Haller, J. Mann, L. Renders, U. Heemann, and M. Baumann. Rationale and study design of the prospective, longitudinal, observational cohort study “rISk stratification in end-stage renal disease” (ISAR) study. *BMC Nephrology*, 17(1): 161, 2016. ISSN 1471-2369. doi: 10.1186/s12882-016-0374-8.

- [169] R. A. Sherman and R. Hootkins. Simplified formulas and nomograms for monitoring hemodialysis adequacy. In *Handbook of Dialysis Therapy (Fourth Edition)*, pages 310–318. Elsevier, 2008.
- [170] T. Shoji, M. Emoto, K. Shinohara, R. Kakiya, Y. Tsujimoto, H. Kishimoto, E. Ishimura, T. Tabata, and Y. Nishizawa. Diabetes mellitus, aortic stiffness, and cardiovascular mortality in end-stage renal disease. *Journal of the American Society of Nephrology*, 12(10):2117–2124, 2001.
- [171] E. Soria-Olivas, M. Martinez-Sober, J. Calpe-Maravilla, J. Guerrero-Martinez, J. Chorro-Gascó, and J. Espi-Lopez. Application of adaptive signal processing for determining the limits of p and t waves in an ECG. *IEEE Transactions on Biomedical Engineering*, 45(8):1077–1080, 1998.
- [172] V. S. Stel, A. Kramer, C. Zoccali, and K. J. Jager. The 2007 era-edta registry annual report—a precis. *NDT plus*, 2(6):514–521, 2009.
- [173] P. Stoica, R. L. Moses, et al. *Spectral analysis of signals*, volume 452. Pearson Prentice Hall Upper Saddle River, NJ, 2005.
- [174] M. Suzuki, T. Hiroshi, T. Aoyama, M. Tanaka, H. Ishii, M. Kisohara, N. Iizuka, T. Murohara, and J. Hayano. Nonlinear measures of heart rate variability and mortality risk in hemodialysis patients. *Clinical Journal of the American Society of Nephrology*, 7(9):1454–1460, 2012. doi: 10.2215/CJN.09430911.
- [175] L. Taback, E. Marden, H. Mason, and H. Pipberger. Digital recording of electrocardiographic data for analysis by a digital computer. *IRE Transactions on Medical Electronics*, (3):167–171, 1959.
- [176] V. Taviani, A. J. Patterson, M. J. Graves, C. J. Hardy, P. Worters, M. P. Sutcliffe, and J. H. Gillard. Accuracy and repeatability of fourier velocity encoded m-mode and two-dimensional cine phase contrast for pulse wave velocity measurement in the descending aorta. *Journal of Magnetic Resonance Imaging*, 31(5):1185–1194, 2010. doi: 10.1002/jmri.22143.
- [177] T. Therneau, B. Atkinson, and B. Ripley. *rpart: Recursive Partitioning and Regression Trees*, 2017. R package version 4.1-11, Available at <https://CRAN.R-project.org/package=rpart>.
- [178] T. M. Therneau. *A Package for Survival Analysis in S*, 2015. R package version 2.38, Available at <https://CRAN.R-project.org/package=survival>.
- [179] A. Thompson and T. Pickering. The role of ambulatory blood pressure monitoring in chronic and end-stage renal disease. *Kidney International*, 70(6):1000–1007, 2006. ISSN 0085-2538.

- [180] F. H. Van Bergen, D. S. Weatherhead, A. E. Treloar, A. B. Dobkin, and J. J. Buckley. Comparison of indirect and direct methods of measuring arterial blood pressure. *Circulation*, 10(4):481–490, 1954.
- [181] L. M. Van Bortel. Is arterial stiffness ready for daily clinical practice? *Journal of hypertension*, 24(2):281–283, 2006.
- [182] L. M. Van Bortel, S. Laurent, P. Boutouyrie, P. Chowienczyk, J. Cruickshank, T. De Backer, J. Filipovsky, S. Huybrechts, F. U. Mattace-Raso, A. D. Protogerou, et al. Expert consensus document on the measurement of aortic stiffness in daily practice using carotid-femoral pulse wave velocity. *Journal of hypertension*, 30(3): 445–448, 2012. doi: 10.1097/HJH.0b013e32834fa8b0.
- [183] L. W. Van Laake, T. F. Lüscher, and M. E. Young. The circadian clock in cardiovascular regulation and disease: Lessons from the Nobel Prize in Physiology or Medicine 2017. *European Heart Journal*, 39(24):2326–2329, Dec. 2017. ISSN 0195-668X. doi: 10.1093/eurheartj/ehx775.
- [184] C. Vlachopoulos, K. Aznaouridis, M. F. O’Rourke, M. E. Safar, K. Baou, and C. Stefanadis. Prediction of cardiovascular events and all-cause mortality with central haemodynamics: a systematic review and meta-analysis. *European Heart Journal*, 31(15):1865–1871, 2010. doi: 10.1093/eurheartj/ehq024.
- [185] C. Vlachopoulos, K. Aznaouridis, and C. Stefanadis. Prediction of cardiovascular events and all-cause mortality with arterial stiffness: A systematic review and meta-analysis. *Journal of the American College of Cardiology*, 55(13):1318 – 1327, 2010. ISSN 0735-1097. doi: <http://dx.doi.org/10.1016/j.jacc.2009.10.061>.
- [186] H. Wang, M. Naghavi, C. Allen, R. M. Barber, Z. A. Bhutta, A. Carter, D. C. Casey, F. J. Charlson, A. Z. Chen, M. M. Coates, et al. Global, regional, and national life expectancy, all-cause mortality, and cause-specific mortality for 249 causes of death, 1980–2015: a systematic analysis for the global burden of disease study 2015. *The Lancet*, 388(10053):1459–1544, 2016. doi: 10.1016/S0140-6736(16)31012-1.
- [187] C. Wanner, J. Zimmermann, S. Schwedler, and T. Metzger. Inflammation and cardiovascular risk in dialysis patients. *Kidney International*, 61:S99 – S102, 2002. ISSN 0085-2538. Proceedings of the First International Conference on New Insights in End-Stage Renal Disease.
- [188] R. A. Ward. Single-patient hemodialysis machines. In *Handbook of Dialysis Therapy (Fourth Edition)*, pages 157–167. Elsevier, 2008.

- [189] S. Wassertheurer, J. Kropf, T. Weber, M. Van der Giet, J. Baulmann, M. Ammer, B. Hametner, C. Mayer, B. Eber, and D. Magometchnigg. A new oscillometric method for pulse wave analysis: comparison with a common tonometric method. *Journal of human hypertension*, 24(8):498–504, 2010.
- [190] T. Weber, M. Ammer, M. Rammer, A. Adji, M. O'Rourke, S. Wassertheurer, S. Rosenkranz, and B. Eber. Noninvasive determination of carotid-femoral pulse wave velocity depends critically on assessment of travel distance: a comparison with invasive measurement. *Journal of hypertension*, 27(8):1624–1630, 2009. doi: 10.1097/HJH.0b013e32832cb04e.
- [191] T. Weber, S. Wassertheurer, M. Rammer, E. Maurer, B. Hametner, C. C. Mayer, J. Kropf, and B. Eber. Validation of a brachial cuff-based method for estimating central systolic blood pressure. *Hypertension*, 58(5):825–832, 2011. doi: 10.1161/HYPERTENSIONAHA.111.176313.
- [192] T. Weber, S. Wassertheurer, B. Hametner, S. Parragh, and B. Eber. Noninvasive methods to assess pulse wave velocity: comparison with the invasive gold standard and relationship with organ damage. *Journal of Hypertension*, 33(5):–, 2015. ISSN 0263-6352.
- [193] W. Wei, M. Tölle, W. Zidek, and M. van der Giet. Validation of the mobil-o-graph: 24 h-blood pressure measurement device. *Blood pressure monitoring*, 15(4):225–228, 2010.
- [194] N. Westerhof, F. Bosman, C. J. D. Vries, and A. Noordergraaf. Analog studies of the human systemic arterial tree. *Journal of Biomechanics*, 2(2):121–143, 1969. ISSN 0021-9290.
- [195] Wikimedia commons. Hemodialysis-en. <https://commons.wikimedia.org/wiki/File:Hemodialysis-en.svg>, January 2008. Accessed 2019-02-05, Creative Commons Attribution 3.0.
- [196] J. L. Willems, P. Arnaud, J. H. Van Bommel, P. J. Bourdillon, R. Degani, B. Denis, I. Graham, F. M. Harms, P. W. Macfarlane, G. Mazzocca, et al. A reference data base for multilead electrocardiographic computer measurement programs. *Journal of the American College of Cardiology*, 10(6):1313–1321, 1987.
- [197] B. Williams, G. Mancia, W. Spiering, E. Agabiti Rosei, M. Azizi, M. Burnier, D. L. Clement, A. Coca, G. de Simone, A. Dominiczak, et al. 2018 ESC/ESH guidelines for the management of arterial hypertension. *European Heart Journal*, 39(33):3021–3104, 2018. doi: 10.1093/eurheartj/ehy339.

- [198] F. N. Wilson, F. D. Johnston, A. G. Macleod, and P. S. Barker. Electrocardiograms that represent the potential variations of a single electrode. *American Heart Journal*, 9(4):447–458, 1934.
- [199] J. Womersley. Flow in the larger arteries and its relation to the oscillating pressure. *The Journal of Physiology*, 124(suppl):31–32, Dec. 1954. ISSN 1469-7793. doi: 10.1113/jphysiol.1954.sp005136.
- [200] J. R. Womersley. Method for the calculation of velocity, rate of flow and viscous drag in arteries when the pressure gradient is known. *The Journal of Physiology*, 127(3):553–563, Mar. 1955. ISSN 1469-7793.
- [201] World Bank, Health indicators. Population, total. <https://data.worldbank.org/indicator/SP.POP.TOTL>, 2017. [Online; accessed 04-February-2019].
- [202] M. N. Yang, T. & Levy. Effects of intense antecedent sympathetic stimulation on sympathetic neurotransmission in the heart. *Circ. Res.*, 72(1):137–144, Jan. 1993.
- [203] J. Yentes, N. Hunt, K. Schmid, J. Kaipust, D. McGrath, and N. Stergiou. The appropriate use of approximate entropy and sample entropy with short data sets. *Annals of Biomedical Engineering*, 41(2):349–365, 2013. ISSN 0090-6964. doi: 10.1007/s10439-012-0668-3.
- [204] T. Young. The croonian lecture. on the functions of the heart and arteries. *Philosophical Transactions of the Royal Society of London*, 99:1–31, 1809.
- [205] L. A. Zadeh. Fuzzy sets. *Information and control*, 8(3):338–353, 1965.
- [206] L. Zhao, S. Wei, C. Zhang, Y. Zhang, X. Jiang, F. Liu, and C. Liu. Determination of sample entropy and fuzzy measure entropy parameters for distinguishing congestive heart failure from normal sinus rhythm subjects. *Entropy*, 17(9):6270, 2015. ISSN 1099-4300. doi: 10.3390/e17096270.
- [207] G. Zuanetti, J. M. Neilson, R. Latini, E. Santoro, A. P. Maggioni, and D. J. Ewing. Prognostic significance of heart rate variability in post-myocardial infarction patients in the fibrinolytic era. *Circulation*, 94(3):432–436, 1996. ISSN 0009-7322. doi: 10.1161/01.CIR.94.3.432.

Curriculum Vitæ

Personal Information

Name Stefan Hagmair
Date of Birth January 17, 1988
Citizenship Austria
Email s_hagmair@gmx.at

Education

Since 2015 TU WIEN
Doctoral programme in Engineering Sciences - Technical Mathematics

2008 – 2015 TU WIEN
Bachelor's and Master's programme Technical Mathematics
Master thesis "Determination and Evaluation of Heart Rate Variability
Parameters with a Focus on Nonlinear Methods"
Graduated with honors as Diplom-Ingenieur

06/2016 UNIVERSIDAD POLITÉCNICA DE MADRID, SPAIN
Athens course: Time-series analysis in R

11/2014 UNIVERSIDAD POLITÉCNICA DE MADRID, SPAIN
Athens course: Nonlinear mathematical models and their applications

2013 – 2014 STOCKHOLM UNIVERSITY, SWEDEN
Erasmus Programme

2002 – 2007 HTL WELS
Technical College
Specialization in Mechatronics
Graduated with honors

Work Experience

Since 2015 AIT AUSTRIAN INSTITUTE OF TECHNOLOGY GMBH
Center for Health & Bioresources, Biomedical Systems
Research Fellow

2017 – 2018 TU WIEN
Lecturer at the Institute for Analysis and Scientific Computing
“Modelling and Simulation of the Heart Circulation”

2016 – 2017 TU WIEN
Lecturer at the Institute of Electrodynamics, Microwave and Circuit Engineering
“Biosignal analysis using Matlab”

2014 – 2015 AIT AUSTRIAN INSTITUTE OF TECHNOLOGY GMBH
Health & Environment Department, Biomedical Systems
Research Associate

2010 – 2015 MATH.SPACE
Verein für Mathematik als kulturelle Errungenschaft
Instructor of mathematic classes for children

08/2012 ALPEN-ADRIA UNIVERSITÄT KLAGENFURT
Synchronization by Pulse Coupling
Internship

04 – 08/2008 IMS NANOFABRICATION GMBH
Development and adjustments of the testbench for the CHARPAN project
Project Assistant

Research Skills

Mathematical modelling & simulation

Medical statistics

Programming/software skills for mathematical applications: Matlab, R, Maple, Mathematica

Language Skills

German (native language), English (fluent), Swedish (basic)

Selected Publications

- [1] S. Hagmair, M. Bachler, S. Wassertheurer, and C. Mayer. Nonlinear methods in heart rate variability: Can they distinguish between nonpathological and pathological subjects? *SNE Simulation Notes Europe*, 25(3-4):145–150, 2015.
- [2] S. Hagmair, M.C. Braunisch, M. Bachler, A.-L. Hasenau, A. Bauer, K. Rizas, S. Wassertheurer, M. Baumann, C. Mayer and C. Schmaderer. Differences of heart rate variability and augmentation index between dialysis and post-dialysis periods in patients with end-stage renal disease *Artery Research*, 16:75, 2016.
- [3] S. Hagmair, M.C. Braunisch, M. Bachler, C. Schmaderer, A.-L. Hasenau, A. Bauer, K.D. Rizas, S. Wassertheurer and C.C. Mayer. Implementation and verification of an enhanced algorithm for the automatic computation of RR-interval series derived from 24h 12-lead ECGs. *Physiological Measurement*, 38(1):1–14, 2017.
- [4] S. Hagmair, M. Bachler, M.C. Braunisch, G. Lorenz, C. Schmaderer, A.-L. Hasenau, L.v. Stülpnagel, A. Bauer, K.D. Rizas, S. Wassertheurer and C.C. Mayer. Challenging Recently Published Parameter Sets for Entropy Measures in Risk Prediction for End-Stage Renal Disease Patients *Entropy*, 19(11):582, 2017.
- [5] C.C. Mayer, J. Matschkal, P.A. Sarafidis, S. Hagmair, G. Lorenz, S. Angermann, M.C. Braunisch, M. Baumann, U. Heemann, S. Wassertheurer, and C. Schmaderer. Association of ambulatory blood pressure with all-cause and cardiovascular mortality in hemodialysis patients: effects of heart failure and atrial fibrillation. *Journal of the American Society of Nephrology*, 29(9):2409–2417, 2018.
- [6] C.C. Mayer, J. Matschkal, P.A. Sarafidis, S. Hagmair, G. Lorenz, S. Angermann, M.C. Braunisch, M. Baumann, U. Heemann, C. Schmaderer, and S. Wassertheurer. Central systolic blood pressure provides additional information in risk prediction in hemodialysis patients *Artery Research*, 24:70, 2018.